Ministry of Education and Sciences of the Russian Federation
Russian Academy of Sciences
Russian National Commission for UNESCO
UNESCO Institute for Information Technologies in Education
Government of Saint-Petersburg
Council of Rectors of Saint-Petersburg Higher Education Establishments
Russian Foundation for Basic Research
United National Aerospace University
Saint-Petersburg State University of Aerospace Instrumentation (SUAI)
UNESCO Chair «Distance Education in Engineering» of SUAI

ФОРМИРОВАНИЕ СОВРЕМЕННОГО ИНФОРМАЦИОННОГО ОБЩЕСТВА – ПРОБЛЕМЫ, ПЕРСПЕКТИВЫ, ИННОВАЦИОННЫЕ ПОДХОДЫ

XV Международный форум
1 – 5 июня 2014 года

MODERN INFORMATION SOCIETY FORMATION – PROBLEMS, PERSPECTIVES, INNOVATION APPROACHES

XV INTERNATIONAL FORUM
1 – 5 June, 2014

PROCEEDINGS OF THE FORUM
Volume 3

РОССИЯ, САНКТ-ПЕТЕРБУРГ 2014 SAINT-PETERSBURG, RUSSIA

ББК 001.9
УДК 72.4
Ф79

Ф79 XV International Forum «Modern information society formation – problems, perspectives, innovation approaches»: Proceedings of the Forum. Volume 3. St. Petersburg, 1–5 June / SUAI, SPb., 2014. 70 p.
ISBN 978-5-8088-0906-2

ISA District 12 (International Society of Automation) and SUAI (Saint-Petersburg State University of Aerospace Instrumentation) have organized the Tenth ISA European students paper competition (ESPC-2014). Papers of the best students were included into this volume of the proceedings of the XV International Forum «Modern information society formation – problems, perspectives, innovation approaches». Papers can be interesting for students, post-graduated students, professors and specialists.

ISBN 978-5-8088-0906-2

190000, St. Petersburg, st. B. Morskaya, 67

On behalf of ISA, I extend congratulations to the ISA Russia Section, ISA District 12, and the St. Petersburg State University of Aerospace Instrumentation (SUAI) on successfully completing the 10th ISA European Student Paper Competition.

Students are the future for our Society. We are excited about the potential of these talented students who will help "set the standard for automation" and shape the processes that will improve and make better our lifestyle in the years ahead. No matter which career path they choose, we hope ISA will have a place in their continuing education and professional development.

The papers published in this volume, selected by the advisory committee, represent the best contributions from among an excellent group of papers. I commend the students who committed their time to prepare a paper and on having their work selected for this publication.

Sincerely,

Peggie W. Koon, Ph.D.
2014 ISA President

On behalf of ISA, I extend congratulations to the ISA Russia Section and the St. Petersburg State University of Aerospace Instrumentation (SUAI) on successfully completing the tenth ISA European Student Paper Competition.

It is vital to the development of engineers that they have the oportunity to display there talents in competitions like this. These papers also display the level of these talented individuals who will be shaping the processes that will enhance our lifestyle in the future

The papers published in this volume, selected by the advisory committee, represent the best contributions from among an excellent group of papers. The students who committed their time to prepare a paper should be very proud to be selected for this publication.

To the lecturers you are also playing an important part in shaping the future and you should feel very proud of the standard that is visible in this publication. Whichever career path the students choose, we hope ISA will continue to play an important role in their continuing education and professional development

On behalf of ISA may I extend my best wishes to all students and attendees in the 2014 ISA European Student Paper Competition.

Sincerely,

Brian J. Curtis
ISA District 12 Vice-President

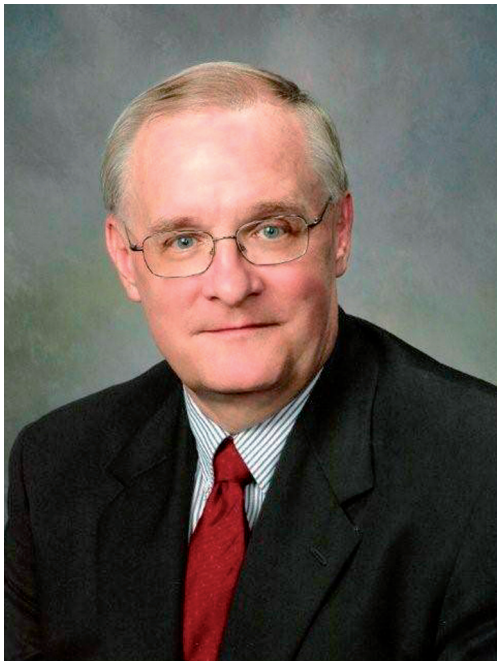

I would like to extend congratulations to the ISA Russia Section, ISA District 12, Indiana State University (ISU), and the St. Petersburg State University of Aerospace Instrumentation (SUAI) for successfully organizing the Tenth ISA European Student Paper Competition. This international forum has become one of the foremost conferences in the world.

As an education and member of ISA for almost 30 years, I continue to appreciate the sharing of technical information by students and faculty members. This global sharing will serve to help advance the technical knowledge base and help in the global collaboration of ideas. I always look forward to having the opportunity to share with students the amazing challenges and personal rewards that a life in automation can bring. ISA is honored to have the opportunity to nurture the next generation of automation professionals.

Indiana State University and the International Society of Automation look forward to our continued relationship between the Russia Section, District 12, and SUAI. Through distance learning classes on project management and ongoing international forums, we are developing new understandings in the technical, cultural, and personal arenas.

Congratulations to those who have developed papers for this volume and to the advisory committee who have the difficult task of making paper selections.

Sincerely,

Gerald W. Cockrell
ISA Former President (2009)
Professor Emeritus(ISU)

Gerald W. Cockrell

EXPERIMENTAL DETERMINATION OF THE OPTICAL FIBER SENSOR CHARACTERISTICS FOR DETERMINING THE LOADING OF FREIGHT CARS

Alexander Adadurov,
Associate professor, PhD
Roman Bushuev,
Graduate student
Alexander Kryacko,
Head of Department, Doctor of Science
Sergey Tyupin,
Associate professor, PhD

Saint-Petersburg State University of Aerospace Instrumentation,
Saint-Petersburg, Russia

Abstracts

The technique of an assessment of loading of freight cars on the basis of use fiber-optical sensors is considered. Techniques of calculation of normalizing parameters of the sensors depending on speed of movement of the car and its weight are given.

I. TECHNIQUE OF USE OF THE FIBER SENSOR AS THE MEASURING PANEL

Passage wagon wheels over optical fiber sensor (OFS) leads to a reduction of the laser luminous flux radiation passing through a OFS. Block diagram shown in Fig. 1.

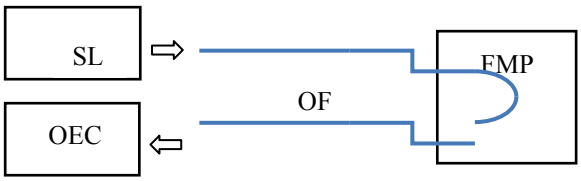

Fig. 1. Block diagram of the optical fiber sensor

Emission of semiconductor laser or LED (SL) passes through an optical fiber (OF), part of which is located in the Force Measuring Panel (FMP). FMP is an analogue of under-rail pad, inside it is located OF. A second end of OF connected to the optical-electronic converter (OEC) for generating an electrical signal whose amplitude is proportional to the light flux at the entrance of the OEC.

In general we can assume that the value of the output signal is determined by changes of coefficient OFS (U_{out}) transmittance of light flux OF (K_{OF}):

$$U_{OUT} = f\left(K_{OF}\right).$$

In this case K_{OF} value proportional to the force applied to the FMP and leads to a change in the optical properties of OF.

Sensor [3] gives the following dependence of the OFS output signal from the applied force (fig. 2).

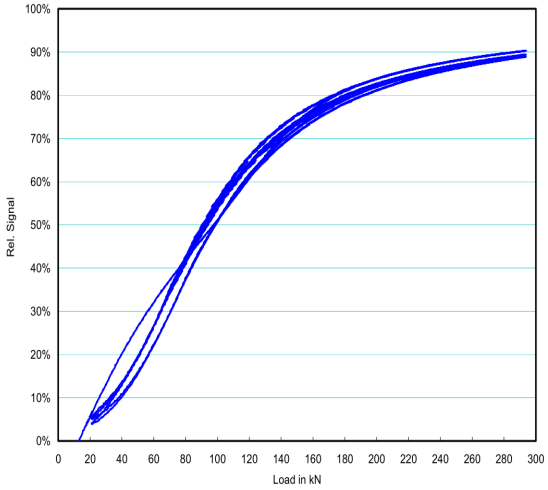

Fig. 2. Dependence of output voltage of the sensor from the applied force

It should be noted that the characteristics of OFS in figure 2 is illustrative, demonstrating the power of OFS, and cannot be used to calibrate OFS.

To determine the dependence of the OFS output signal from the attached static load was carried out laboratory experiments by applying a calibrated load to the FMP with using complex for force measuring sensors calibration (fig. 3)

a b

Fig. 3. Calibration complex of measuring sensors

Installation allows adjusting the force applied to the FMP in the range of 2 to 2000 kN with a relative error of 0.001. To calibrate OFS the force was varied discretely in the range from 50 to 450 kN. Figure 4 is a graph of OFS output voltage when loading and unloading FMP.

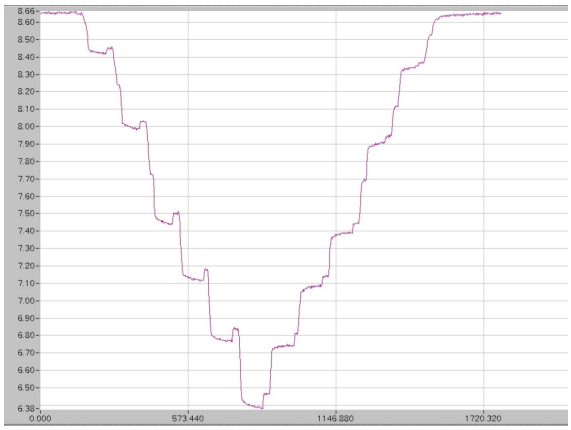

Fig. 4. Change of output tension under loading

The horizontal axis in figure 4 shows the time in seconds and the vertical – the output voltage of OEC OFS U_{OUT} in volts. The maximum deviation of the output signal at a load of 450 kN was 2.28 V. U_{OUT} dependence on the applied load is shown in figure 5.

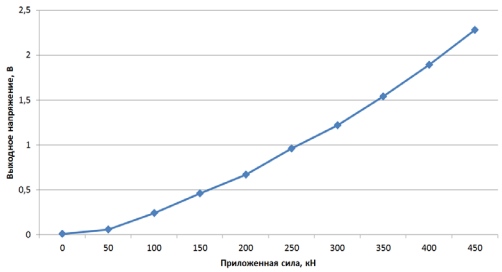

Fig. 5. Dependence of output voltage on the enclosed loading

The data obtained show almost linear dependence U_{OUT} in load range from 50 to 450 kN, which differs from the OFS manufacturer data according to which the linear portion of the output signal OFS ends with a load of about 100 kN.

It is noted that in experimental conditions force transmitted to OFS through a thick metal plate, and the sensor is lying on the solid support (Fig. 3b). Therefore, we can assume that the OFS was placed between two rigid bodies, which differs substantially from the use of the OFS at its finding between rail and sleeper.

One of the main characteristics of the railway track is stiffness. Under the stiffness understood the ratio corresponding force to the railhead (vertical, horizontal) to deflection at the point of application of force deflection in vertical or transverse horizontal plane. Stiffness influences the maximum amount of deflection of the rail under load, on the characteristics of the oscillations arising in the ballast bed, and the force acting from the sleeper to the OFS located between rail and sleeper.

Until the moment when the system “ballast bed – sleeper” will reach the limit of elasticity exist difference force acting on the OFS from rail side and the reaction force of support determined by the stiffness of the system “ballast bed – sleeper”. Whereby the output signal OFS in real conditions will almost always less than in experimental conditions. The less stiffness of the railway track the greater is the difference.

As part of this work was not intended research stiffness of railway track, so to calibrate OFS was selected method using a formulation with known axle load.

To calibrate the output OFS signals was carried out experiment by using the test railway equipment, which consisted of a locomotive TGM-4 (axles – 4, total weight – 78.6 tons, axle load – 19.65 tons, the average load on each wheel – 9.82 tons) and the empty car (axles – 4, total weight – 22.85 tons, axle load – 5.57 tons, the average load on each wheel – 2.29 tons).

Test railway equipment made four cycles of transits through the measuring section. Each cycle consisted of a drive in the forward direction with ve-

locities 20, 30, 40 and 55 km/h and travel in the opposite direction at a speed of about 30 km/h. And since when traveling in the opposite direction locomotive is moving behind the car, then the side of the locomotive relative to established OFS has not changed (each wheel was driving in the forward and backward direction through the same OFS).

As all wheelsets were out of wheel tread defects then the results of the experiment was supposed:

– to determine the ability of the total calibration of OFS for assess the weight of cars and axle load;

– to assess the possibility of using OFS for detecting uneven wagon load;

– to determine the dependence of the output signal OFS from the train speed.

Figure 6 shows the output signals of the seven OFS installed on successive sleepers when driving at a speed of about 30 km/h.

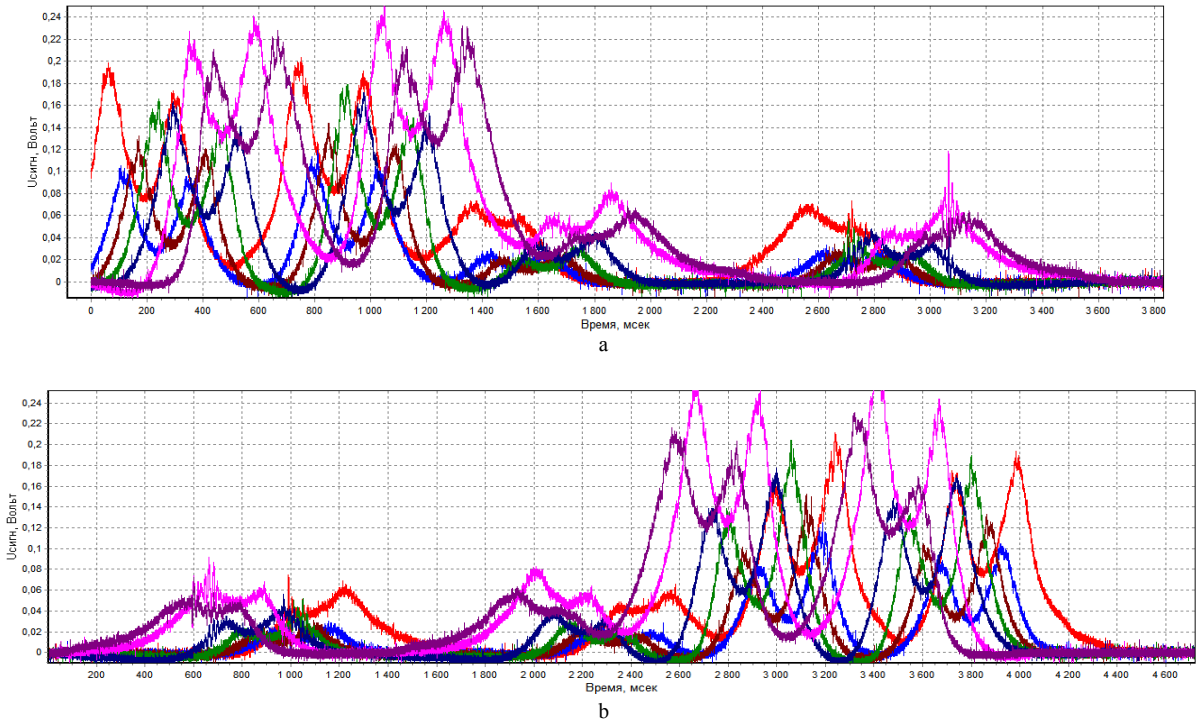

Fig.6. The output voltage of sensors at a speed of 30 km/h

In figure 6a moved in the forward direction (locomotive in front), and figure 6b – in reverse (car behind the locomotive).

The obtained dependences allow to allocate moments when axes passing through each OFS, and to evaluate the difference between the signals from the locomotive, which is comparable to the weight of the loaded car, and the empty car.

However it's clearly seen that the maximum values of the output signals of different OFS in corresponding to moment when axis passing directly over OFS differ in size by more than two times.

As OFS have identical characteristics tested in the laboratory on the absolutely rigid basis, so the reason for this signal difference amplitude can be only differences of stiffness parameters of the system "rail-sleeper-ballast bed" in the installation of each OFS. Indeed, it was visually noticeable elastic deflection of rail with the amplitude of tens of millimeters. The reason for such large fluctuations is the lack of rigidity of the rail ballast bed, leading to the OFS "hypersensitivity" relative to the value of maximum elastic deflection of the rail on each of the sleepers.

In accordance with "Requirements to the location of the system to control vertical dynamic loads (SCVDL) based on optical fiber sensors" tamping should be done as "deviations from the specified size in the profile railway track distances when moving trains do not exceed 10 mm, and in locations of floor units measuring devices less than 5 mm". Failure to meet these requirements leads to a significant difference between the amplitude of OFS.

At the same time we should recognize that to achieve the lack of variations in stiffness of the "rail-sleeper-ballast bed" under actual operating conditions of railway track is impossible. So one of the challenges of designing OFS signal processing algorithms is the introduction normalizing multiplicative coefficients for each OFS.

Figure 6 is clearly seen the presence of high-frequency noise signal from each sensor, so to eliminate their influence in the calculation of the normalizing coefficient was produced smoothing of signal by using the algorithm "sliding window" duration of 5 milliseconds. Maximum values of "smoothed" output OFS signals given in table 1.

Total number of OFS during the experiment was 18, of which 7 OFS numbered from 0 to 6 were installed under the left rail, and 11 numbered from 11 to 21 – under the right rail. Thus OFS numbers in one

and the same sleeper are differ on 11, i.e. OFS with numbers 0 and 11 are arranged on a sleeper ordinal number 0 under the left and right rails, respectively. In order to simplify the analysis in the table shows the average values of the maximum OFS signal, and averaging was performed to change the speed in increments of 10 km/h, regardless of the direction of motion.

Table 1 shows the maximum values of the output OFS signals for different axes.

Table 1

OFS number	Axel number							
	1	2	3	4	5	6	7	8
0	0,18	0,16	0,18	0,17	0,06	0,05	0,06	0,05
1	0,10	0,08	0,10	0,09	0,02	0,02	0,02	0,02
2	0,12	0,11	0,14	0,11	0,02	0,03	0,03	0,03
3	0,15	0,12	0,17	0,13	0,02	0,03	0,03	0,02
4	0,16	0,15	0,17	0,15	0,04	0,05	0,05	0,04
5	0,21	0,24	0,23	0,26	0,06	0,07	0,05	0,07
6	0,18	0,21	0,18	0,23	0,04	0,05	0,04	0,05
11	0,08	0,09	0,07	0,07	0,02	0,02	0,02	0,02
12	0,09	0,10	0,09	0,09	0,02	0,02	0,02	0,02
13	0,16	0,16	0,13	0,13	0,03	0,04	0,04	0,03
14	0,10	0,10	0,09	0,09	0,01	0,02	0,01	0,02
15	0,29	0,27	0,23	0,24	0,06	0,07	0,09	0,06
18	0,06	0,09	0,06	0,08	0,01	0,02	0,01	0,02
19	0,20	0,27	0,19	0,26	0,04	0,05	0,06	0,05
20	0,16	0,21	0,15	0,20	0,04	0,05	0,04	0,05
21	0,07	0,09	0,06	0,09	0,02	0,02	0,04	0,02
Maximal signal	0,29	0,27	0,23	0,26	0,06	0,07	0,09	0,07
Minimal signal	0,06	0,08	0,06	0,07	0,01	0,02	0,01	0,02
Dynamic range (max/ min)	4,42	3,38	3,83	3,71	6,00	3,63	9,00	3,50

Taking into account the same load of all the wheels each mobile unit of test railway equipment, will determine the dependence of the output OFS signal from the applied load

$$KU^{j}_{OUT}\left(F_l\right)=\frac{U^{j}_{OUTa}}{F_l};$$

where F_l – load applied to OFS, kN; U^{j}_{OUTa} – the average value of the output voltage of the j-th OFS.

For test railway equipment the value shown in table 2.

Shown in table 2 values $KU^{j}_{OUT}\left(F_l\right)$ calculated for two cases – the locomotive with a load on the wheel as 96.3 kN and empty wagon wheel load as 28.5 kN. Coefficient KU^{j} is calculated as the average of these values.

It should be noted that during the experiment condition of ballast bed on measuring section did not satisfy the requirements, which led to a significant deflection of rails during the passage. This explains the large difference in the amplitudes of the output OFS signals, which had a negative impact on the accuracy of the estimates.

Table 2

OFS num-ber	Locomotive		Car		
	U^{j}_{OUTa}	$KU^{j}_{OUT}\left(F_l\right)$	U^{j}_{OUTa}	$KU^{j}_{OUT}\left(F_l\right)$	
0	0,17	1,79	0,05	2,46	2,12
1	0,09	0,94	0,02	0,89	0,92
2	0,12	1,25	0,03	1,23	1,24
3	0,14	1,48	0,02	1,12	1,30
4	0,16	1,63	0,04	2,01	1,82
5	0,24	2,46	0,06	2,82	2,64
6	0,20	2,09	0,05	2,06	2,08
11	0,08	0,80	0,02	0,89	0,85
12	0,09	0,95	0,02	0,86	0,91
13	0,14	1,49	0,03	1,56	1,53
14	0,10	0,99	0,02	0,71	0,85
15	0,26	2,67	0,07	3,13	2,90
18	0,07	0,77	0,01	0,67	0,72
19	0,23	2,38	0,05	2,23	2,30
20	0,18	1,86	0,04	2,01	1,93
21	0,08	0,80	0,02	1,12	0,96

One of the objectives of the experiment was to determine the dependence of the output OFS signals from the speed of test train, i.e. representation coefficient K^j in the form

$$K^j = \frac{K^j_{place}}{K(v)},$$

where $K^j_{place} = KU^j$ – coefficient taking into account the placement options of OFS; $K(v)$ – coefficient reflecting the change in output OFS signal when adjusting the speed of wheel v.

Analysis of the output signal OFS showed that with increasing speed, the signal amplitude decreases. Thus table 3 shows the average values of the signals for all locomotive axes at various speeds.

Table 3

OFS	20	30	40	50
0	0,173	0,168	0,160	0,150
1	0,085	0,088	0,081	0,070
2	0,115	0,117	0,115	0,103
3	0,140	0,139	0,138	0,117
4	0,152	0,151	0,150	0,132
5	0,230	0,231	0,220	0,180
6	0,200	0,193	0,179	0,163
11	0,075	0,071	0,070	0,067
12	0,090	0,089	0,088	0,080
13	0,140	0,137	0,137	0,127
14	0,095	0,091	0,090	0,082
15	0,253	0,249	0,241	0,212
18	0,072	0,072	0,069	0,063
19	0,192	0,198	0,217	0,212
20	0,175	0,152	0,164	0,162
21	0,070	0,066	0,071	0,073

To determine the $K(v)$, was used the values 14 from 16 of OFS, since for OFS number 19 and number 21 were discarded because of the obvious differences depending on the nature of other OFS.

Because the speed 20 km/h is a minimum for trains on the measuring section, so for each OFS were calculated normalized output signals at first

$$U^j_{norm}(v) = \frac{U^j_{out}(v)}{U^j_{out20}},$$

where U^j_{out20} – the average value of the output signal of the j-th OFS at 20 km/h; $U^j_{out}(v)$ – the average value of the output signal of the j-th OFS at v speed.

The values of the coefficient $K(v)$, calculated as an average value $U^j_{norm}(v)$ for all OFS at a given speed, are shown in fig. 7.

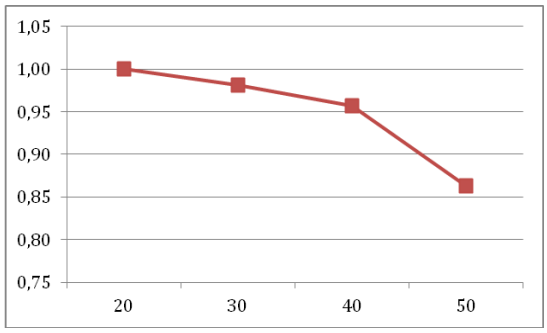

Fig. 7. Coefficient of proportionality K(v), considering change of an output signal from speed of a wheel

Reducing output OFS signal when wheel speed increases can be explained as follows. Reducing the time of loading force leads to the fact that the resilient deflection of the rail can not reach the limit value, while when the low speed rail flexes to large values, respectively, increasing the force exerted on the OFS from sleeper.

As seen on fig. 7 the change in slope of the curve K (v) takes place at a speed of 40 km/h,. I.e. at the value of the wheel load of about 100 kN at speeds of over 40 km/h the reaction force of the system "sleeper-ballast bed" has noticeably less important than at low speeds, which makes it advisable to use this ratio.

Using the test train for calibration of OFS is organizationally complex exercise, which it is advisable to conduct before the winter or summer, or after work to strengthen the ballast bed. Prolonged period between calibration using the test train can cause significant changes in stiffness of the system "rail- sleeper- ballast bed" that will lead to a substantial increase in the error OFS signal processing results and reduce the SCVDL characteristics.

As an alternative method is proposed to use calibration OFS signals when passing locomotives, especially electric, load changes on the y-axis relative to the nominal value of which is about 2 – 3%. The essence of the proposed method consists in that metering maximum value of OFS signals from each of the axles of locomotives (with 8 or 12) can significantly reduce the error in determining the average value of the signal and calculate the ratio of the nominal tire load to the average value of OFS signal from the maximum sufficient accuracy.

The advantages of this method are:

– coincidence of locomotives and wagons speed which eliminates the use of correction factors related to the speed of the car;

– capability of approximate weight of the locomotive (about 100 t) and loaded wagon (60 –96 t);

– regular passage through the measuring section with a known weight locomotives;

– traceability of changes in hardness of the ballast bed.

Algorithm for determining the wheel load using dynamic calibration of OFS consists of the following operations:

1. Determining the type of locomotive from the number of axes in the section, the distance between the wheels of the truck and distance in between the trucks.

2. Calculation of maximum envelope signal for each OFS when passing each axle locomotive – $U^j_{i\max}$, where j – number of OFS, and i=1, ..., N – serial number of the locomotive axis.

3. Calculate the average value for all locomotive axes for each OFS $\overline{U^j_{i\max}}$.

4. Calculating the ratio of nominal load locomotive wheels P_{nom} to the average OFS signal

$$K^j_{din} = \frac{P_{nom}}{\overline{U^j_{i\max}}}.$$

The magnitude of the coefficients obtained K^j_{din} can be divided into three groups:

– rejection OFS with abnormally high values $K^j_{din} > K^{\lim inal}_{din}$ (low OFS sensitivity to stress);

– calculating the load on each wheel of each OFS except discarded

$$P^j_i = K^j_{din} U^j_{i\max};$$

– calculating the average load on each wheel of train

$$\overline{P^j_i} = \frac{\sum_{j=1}^{M} P^j_i}{M},$$

where M – number of OFS after rejection.

Results of calculation K^j_{din} for three compositions, passed in September 2013 through SCVDL presented in table 4. Train number 1 passed 02.09.2013 at 11:48, train number 2 – 09.05.2013 at 12:07, train number 3 – 20.09.2013 at 13:44.

Table 4

Sleeper	OFS	Train №1		Train №2		Train №3	
		left	right	left	right	left	right
1	0/11	48,08	54,08	37,17	43,86	42,57	52,28
2	1/12	85,61	89,63	62,72	70,41	72,85	93,8
3	2/13	63,23	65,76	44,96	52,22	52,31	71,61
4	3/14	192,27	143,33	134,82	117,57	154,69	157,22
5	4/15	137,68	88,85	91,49	74,47	108,78	91,86
6	5/16	79,41	no	58,02	no	69,43	no
7	6/17	50,05	no	37,14	no	44,27	no
8	7/18	no	288,07	no	238,07	no	283,94
9	8/19	no	3700,86	no	4342,7	no	4206
10	9/20	no	3711,36	no	3702,6	no	3421
11	10/21	no	88,69	no	78,8	no	76,55

In the first two columns of table 4 are serial sleeper numbers and OFS installed on them. For each OFS given value K^j_{din} (t/V) during the passage of three trains.

OFS installed on 11 sleepers, and on 5 sleepers OFS installed under both rails (OFS number 0, 1, 2, 3, 4 and 11, 12, 13, 14, 15 – sleepers number 1 – 4), three OFS from the left side (OFS number 4, 5, 6 – sleepers number 5 – 7), and four OFS from right side (OFS number 18, 19, 20, 21 – sleepers number 8 – 11).

The magnitude of the coefficients obtained K^j_{din} can be divided into three groups:

– stable OFS with a value of coefficient always lower than the threshold (OFS number 0, 1, 2, 5, 6, 11, 12, 13, 15, 21);

– unstable OFS with coefficient which hovers around the threshold (OFS number 4);

– unreliable OFS with coefficient value is always higher than the threshold (OFS number 3, 14, 18, 19, 20).

For OFS rejection was chosen threshold $K_{din}^{\lim inal} = 100$, which corresponds to an output of 1V at a load of 100 tons per wheel.

A significant difference in the values K_{din}^{j} is not caused by the individual characteristics of OFS and ballast properties under the sleepers with OFA. This conclusion follows from the correspondence of the signal level (coefficient values K_{din}^{j}) from the OFS set to same sleeper from the left and right sides.

From the five sleepers which uses two OFS, on the first three on both sides go into the first group, both in the fourth sleeper OFS are unreliable, the fifth sleeper – on the left side OFS number 4 is unstable, and the right side OFS number 15 – stable, the values of all the coefficients of which are near the threshold.

It is also noteworthy the synchronicity change of the coefficients with time. Since September 5 all the coefficients were reduced in relation to the September 2 and September 20 increased relative to September 5.

High dynamics and multidirectional changes in the coefficients over time make it necessary to calibrate OFS at least once a day. The only way to do this is to use the information about the weight of the locomotive.

It should be noted that if the parameters of the locomotive axle load is unknown, possible to use the results of the last dynamic OFS calibration. At an average intensity of trains through SCVDL as 50 trains a day updating values $\overline{P_i^j}$ will be at least several times a day which allows us to construct an algorithm based on the tracking filter to reduce computation error $\overline{P_i^j}$.

Thus, even taking into account the error in determining the weight of the car can be argued that SCVDL based on OFS can be used to identify cars that are prone to outright because of uneven load placement or displacement of cargo during transportation.

According to the available information on the Internet for the safe movement of the car critical difference vertical load is 20%. Similar values among the considered wagons were not found.

II. CONCLUSIONS

1. The article analyzes the laboratory tests OFS to determine their characteristics for loads from 50 to 450 kN. Demonstrated that, on the basis of absolutely rigid output OFS signals is a linear function of the applied load.
2. The experimental study on the results of the calibration OFS by passing train with known axle load. The necessity of the introduction of multiplicative coefficients compensating differences in stiffness as a ballast bed between different OFS and the change in stiffness during operation.
3. According to experimental data and a procedure was developed the methodology and determined the coefficients with change of the output signal for various speeds of train.
4. Developed the algorithm for adaptive OFS calibration using data about type and weight of the locomotive. Using the developed algorithm got estimates of weight and uneven loading trains passing through SCVDL.

III. REFERENCES

1. Влияние ударных сил вибрации в балластном слое. Краснов О.Г., Акашев М.Г., Ефименко А.В., Сенча В.Н. // Путь и путевое хозяйство - 2013 - №3
2. Сладковский А.В., Погорелов Д.Ю. Исследование динамического взаимодействия в контакте колесо-рельс при наличии ползунов на колесной паре // Вісник Східноукраїнського національного університету. – 2008. – № 5
3. Гарипов Д.С., Кудюров Л.В. Динамика вагонного колеса, имеющего ползун // Вестник транспорта Поволжья - 2012 - №3(23)
4. НОРМАТИВЫ (КРИТЕРИИ ОЦЕНКИ) пороговых значений вертикальных сил взаимодействия колес подвижного состава с дефектами на поверхности катания и железнодорожного пути // РЖД, 2012

ESTIMATION EFFECTIVENESS OF INNOVATION PROJECT

Juli Kozlova,
Associate Professor
Michail Krichevsky
Doctor of Science, Professor

Saint-Petersburg State University of Aerospace Instrumentation,
Saint-Petersburg, Russia

juli_ko@list.ru, mkrichevsky@mail.ru

Abstracts

The paper discusses methods for assessing the effectiveness of innovative projects. Different approaches to assessment methodology are considered based mainly on foreign materials. Advantages and shortcomings of the approaches are discussed. The way of forming such evaluations is offered by use of fuzzy logic, which allows to obtain an estimate of efficiency in the form of scoring equation.

Keywords – innovation project, performance evaluation, fuzzy logic, scoring equation.

I. INTRODUCTION

Innovation is a major driving force for the economic growth and expansion of companies. The globalisation of markets has raised strong competitive pressures. The rapid evolving technology, the fast changing markets and the more demanding customers, require developing high quality new products more efficiently and effectively. Taken that every firm can be represented as a bundle of resources, skills and competencies, the effect of innovation is to transform a firm's inner capabilities, making it more adaptive, better able to learn, to exploit new ideas. This need to innovate has become clear by now [1].

Small- and medium-sized enterprises (SMEs) have shorter lines of communication, relatively informal decision making and more flexibility, which seems to give them an advantage for rapid innovation over large companies. Large companies have responded early to the need for the management of innovation. This was the only way to be competitive and remain in business, since most of those who failed to realise this need, didn't survive. They have examined their situation and in so doing have created a range of tools and techniques to help them adapt to changed circumstances and meet new market challenges.

Initiatives on improving the innovation have addressed ways of improving the product innovation process, through a wide spectrum of methods, techniques and tools without quantifying the degree of change of "innovativeness". The innovation process is iterative in nature and thus automatically includes the first introduction of a new innovation and the reintroduction of an improved innovation.

Innovation output is wide-ranging and differs from sector to sector. Measuring it entails quantifying the extent to which ideas for new products and services, stemming from innovative sectors, carry an economic added value and are capable of reaching the market [2].

At first the most commonly used measures of innovation are presented. Next the Innovation Union Scoreboard and the Summary Innovation Index are discussed. Then fuzzy logic is proposed for a new innovation indicator.

II. MEASURING INNOVATION

Many studies have focused on the importance of innovation, but the measurement of innovation is still clouded with statistical and conceptual problems. Innovation research often confounds innovation characteristics, innovation types and the hierarchical locus of the innovation. There is an emergence of a large number of conceptual activities, with many overlapping features [1]. Prior research on innovation measurement has not clearly distinguished between newness as unfamiliarity, as lacking fit with existing competences, or as implying new types of activity.

Earlier the most commonly used measures of innovative activities are: Research and Development (R&D) expenditures, patent counts and counts of major or minor innovations.

R&D data are usually collected in the Organisation for Economic Co-operation and Development (OECD) economies according to the definite procedures and categories. R&D statistics do not cover all aspects of technological change. R&D numbers measure only an input, which bears no real relation to innovation outcomes.

Patent data can be retrieved in the records of

US Patent Office and the European Patent Office. The main weakness of patent measuring is that each country has different patent legislation, not all inventions are patent or patentable and patents do not necessary represent a commercially exploited innovation. The study showed that two-thirds of firms had experienced attempts to copy their patented inventions, but only one in five actually used the courts to defend their patents.

There has been a huge increase in the use of innovation surveys over the last few years. Innovation surveys can be used as tools to analyse the innovative activities, assessing innovation of firms and explore their practices. In general there are two approaches to collect innovation data.

The first is the *object* approach and collects information on the level of individual innovation, i.e. information on the output of the innovation process. This approach may have the advantage of representing a direct measure of innovation due to the fact that only the significant innovations are recorded, but it is very difficult to develop comparable databases internationally.

The second approach, the *subject* approach, collects information at the level of the firm, i.e. information on the input of the innovation process, and can cover a wider range of issues. It can record information on the impact of innovation, on successful and unsuccessful innovative activities in innovating and non-innovating firms. This method usually utilises questionnaires or direct interviews. Although self-assessment measures may be prone to bias, they are the most commonly used form of performance assessment because more objective accounting measures and sources can also be biased.

Basic guiding lines for developing an innovation survey are included in the Oslo Manual [3]. The manual recommends the subject approach to use when conducting innovation surveys and this approach has since become dominant. The methodology suggested in the manual was used by Eurostat and the European Innovation Monitoring System within the European Commission. Surveys based on the Oslo Manual tend to be quite long, and require considerable resources within a firm to complete. Most such surveys are conducted under the terms of national statistics legislation, which generally contain legal provisions requiring the respondent to complete and return the questionnaire. Other surveys usually have poor response rates as firms get tired of the long lists of questions.

European Commission presents an indicator to measure performance in innovation output [2]. The rigorous measurement of the impact of innovation policies is key for evidence-based policymaking. Moreover, it bolsters the legitimacy of public action and the use of public funds.

III. INNOVATION UNION SCOREBOARD

At present Innovation Union Scoreboard (IUS) is a means to help monitor the implementation of the Europe 2020 Innovation Union flagship by providing a comparative assessment of the innovation performance of the EU27 Member States and the relative strengths and weaknesses of their research and innovation systems. The IUS includes innovation indicators and trend analyses for the EU27 Member States. It also includes comparisons based on a more reduced set of indicators between the EU27 and 10 global competitors [4].

The IUS 2011 distinguishes between 3 main types of indicators and 8 innovation dimensions, capturing in total 25 different indicators (fig. 1).

The Enablers capture the main drivers of innovation performance external to the firm and cover 3 innovation dimensions. Firm activities capture the innovation efforts at the level of the firm, grouped in 3 innovation dimensions. Outputs cover the effects of firms innovation activities in two innovation dimensions.

The 25 indicators better capture the performance of national research and innovation systems considered as a whole. While some of the indicators of the IUS can be more easily influenced by policy intervention than others, the overall ambition of the Innovation Union Scoreboard is to inform policy discussions at national and EU level, by tracking progress in innovation performance within and outside the EU over time.

The Enablers cover the main drivers of innovation performance external to the firm and it differentiates between tree innovation dimensions. “Human resources” includes tree indicators and measures the availability of a high-skilled and educated workforce. “Open, excellent and attractive research systems” includes tree indicators and measures the international competitiveness of the science base. “Finance and support” includes two indicators and measures the availability of finance for innovation projects and the support of governments for research and innovation activities.

Firm activities capture the innovation efforts at the level of the firm and it differentiates between tree innovation dimensions. “Firm investments” includes two indicators of both R&D and non-R&D investments that firms make in order to generate innovations. “Linkages & entrepreneurship” includes tree indicators and measures entrepreneurial efforts and collaboration efforts among innovating firms and also with the public sector. “Intellectual assets” captures different forms of Intellectual Property Rights (IPR) generated as a throughput in the innovation process.

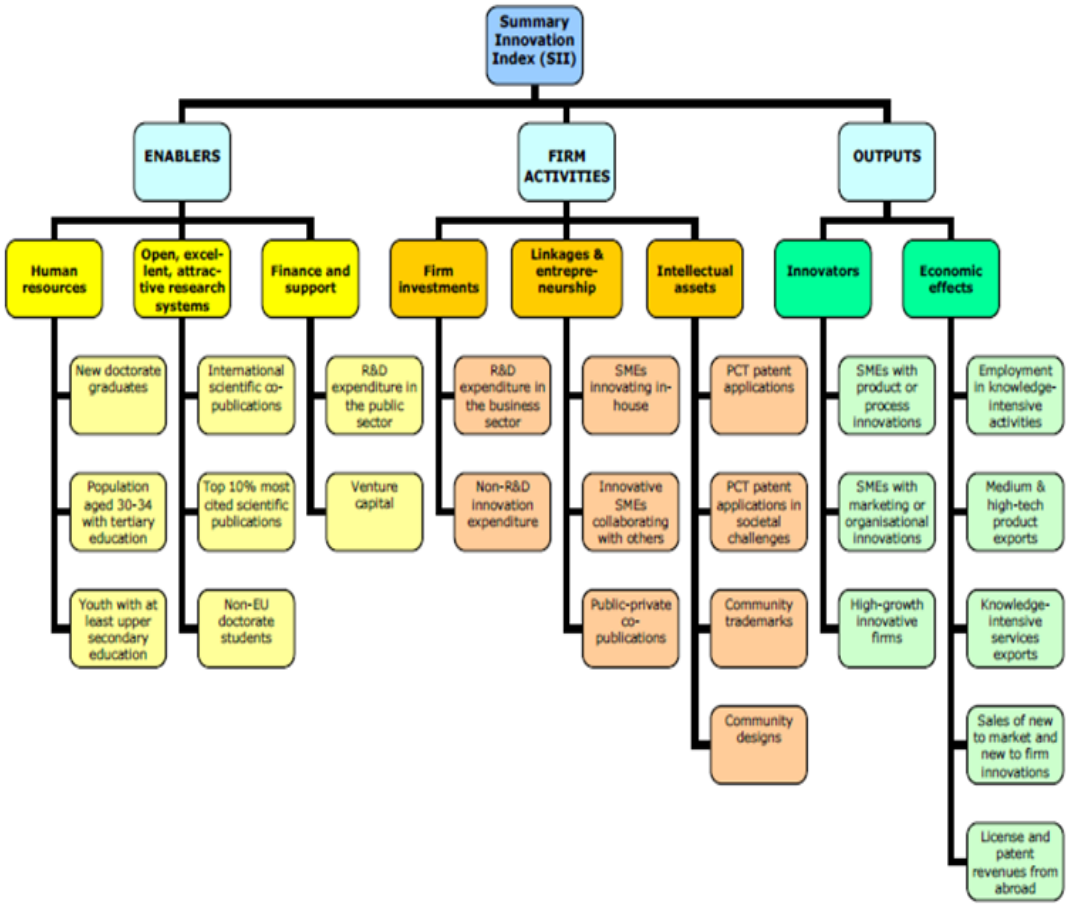

Fig. 1. Framework of the Innovation Union Scoreboard

Outputs cover the effects of firms' innovation activities and it differentiates between two innovation dimensions. "Innovators" includes tree indicators and measures the number of firms that have introduced innovations onto the market or within their organisations, covering both technological and non-technological innovations and the presence of high-growth firms. The indicator on innovative high-growth firms corresponds to the new EU2020 headline indicator, which will be completed within the next two years. "Economic effects" includes five indicators and captures the economic success of innovation in employment, exports and sales due to innovation activities.

The IUS uses the most recent statistics from Eurostat and other internationally recognised sources as available at the time of analysis. International sources have been used wherever possible in order to improve comparability between countries. The IUS 2011 may not fully capture the impact of the economic and financial crisis on innovation performance as there is a delay in data availability where data refer to 2009 or 2010 for 14 indicators and to 2007 or 2008 for 10 indicators. The current composite indicator consists of 24 individual indicators since the last indicator on "High-growth innovative enterprises as a percentage of all enterprises" is being developed.

The IUS 2011 largely follows the methodology of previous editions in distinguishing between tree main types of indicators and eight innovation dimensions, capturing in total 25 different indicators.

Based on their average innovation performance, the Member States fall into four performance groups:

– the performance of Denmark, Finland, Germany and Sweden is well above that of the EU27 average. These countries are the *Innovation leaders*;

– Austria, Belgium, Cyprus, Estonia, France, Ireland, Luxembourg, Netherlands, Slovenia and the UK all show a performance close to that of the EU27 average. These countries are the *Innovation followers*;

– the performance of Czech Republic, Greece, Hungary, Italy, Malta, Poland, Portugal, Slovakia and Spain is below that of the EU27 average. These countries are *Moderate innovators*;

– the performance of Bulgaria, Latvia, Lithuania and Romania is well below that of the EU27 average. These countries are *Modest innovators*.

The comparison of four performance groups is shown in figure 2.

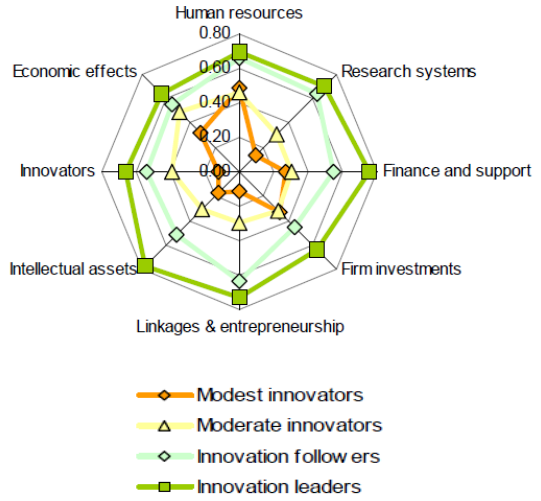

Fig. 2. Country groups: innovation performance

IV. SUMMARY INNOVATION INDEX

A summary picture of *innovation performance* is provided by the Summary Innovation Index (SII), a composite indicator obtained by an appropriate aggregation of the 24 IUS indicators. The methodology used for calculating this index consists of the following seven steps.

1. Identifying and replacing outliers.
2. Setting reference years.
3. Imputing for missing values.
4. Determining Maximum and Minimum scores.
5. Transforming data if data are highly skewed.
6. Calculating re-scaled scores.
7. Calculating composite innovation indexes.

The *growth in innovation performance* has been calculated for each country and for the EU27 using data over a five-year period. All countries except Luxembourg and the UK show an absolute improvement in the innovation performance over time (fig. 3). Bulgaria and Estonia have experienced the fastest growth in performance.

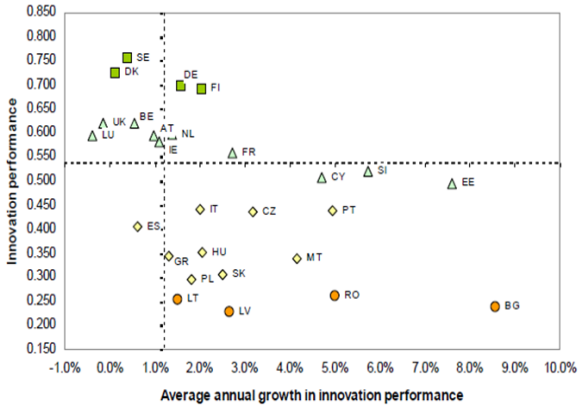

Fig. 3. Twenty-seven countries on plane "Average annual growth" and "Innovation performance"

Colour coding matches the groups of countries in figure 3 is the same as in the figure 2 and the following abbreviations for country names are used: AT – Austria; IS – Iceland; IT – Italy; BE – Belgium; BG – Bulgaria; LT – Lithuania; LU – Luxembourg; CH – Switzerland; LV – Latvia; CY – Cyprus; MT – Malta; CZ – Czech Republic; NL – Netherlands; DE – Germany; DK – Denmark; PL – Poland; EE –Estonia; PT – Portugal; ES – Spain; RO – Romania; FI – Finland; FR – France; SE – Sweden; GR –Greece; SI – Slovenia; SK – Slovakia; HU – Hungary; IE – Ireland; UK – United Kingdom.

For the calculation of the average annual growth rate in innovation performance we have adopted a generalized approach.

Step 1. Define growth for each country *c* per indicator, i.e. as the ratio between the non-normalised values for year *t* and year *t* - 1.

Step 2. Aggregate these indicator growth rates between year *t* and year *t* – 1 using a geometric average to calculate the average yearly growth rate.

Step 3. Calculate for each country *c* the average annual growth rate in innovation performance as the geometric average of all yearly growth rates.

Europe's main global competitors include Australia, the BRICS countries (Brazil, China, India, Russia and South Africa), Canada, Japan and the US. For these countries data availability is more limited than for the European countries (e.g. comparable innovation survey data are not available for many of these countries). Furthermore, the economic and/or population size of these countries outweighs those of many of the individual Member States and we thus compare these countries with the aggregate of the Member States or the EU27.

It is important to compare the innovation activities of the EU and Russia. The EU27 is performing better than Russia in most indicators (fig. 4). In "New doctorate degrees" and "Tertiary education" Russia is performing better. Overall there is a clear performance lead in favour of the EU27 and this lead is increasing, as Russia's innovation performance has grown at a slower rate than of the EU27.

Russia has been decreasing the performance gap in 2 indicators ("PCT patents in societal challenges" and "Knowledge-intensive services exports") and seen a decrease in its lead in "New doctorate degrees" and "Tertiary education". Only in Exports of medium-high and high-tech products has Russia increased its lead. The EU27 has increased its lead in the other 6 indicators for which data are available.

The dynamic performance of these key international competitors can also be grasped in a graph. Figure 5 shows the current performance lead or gap on the vertical axis and the change in this lead or gap on the horizontal axis. From figure 5 it becomes clear that Brazil and China are clearly catching-up to the EU27, that India's is only slowly catching-up, that Russia is faced with an increasing gap to the EU27 and the EU27 is neither catching-up to the US nor to Japan.

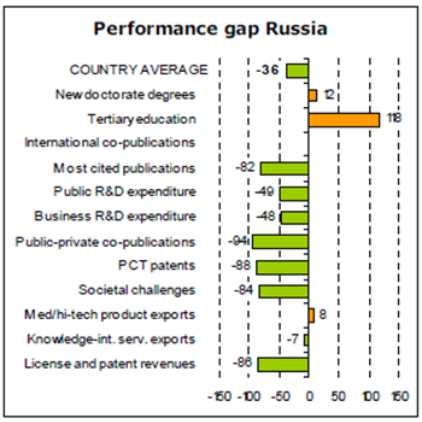

a)

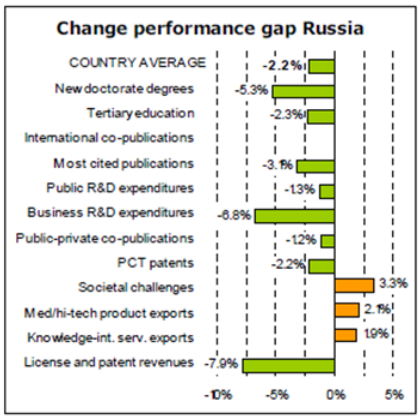

b)

Fig. 4. Comparison Russia – EU27
a) the indicators highlighted in orange reflect a performance gap for EU27; b) relative growth compared to that of EU27
Orange colored bars show that the country is growing faster than the EU27; green colored bars show that the country is growing slower than the EU27

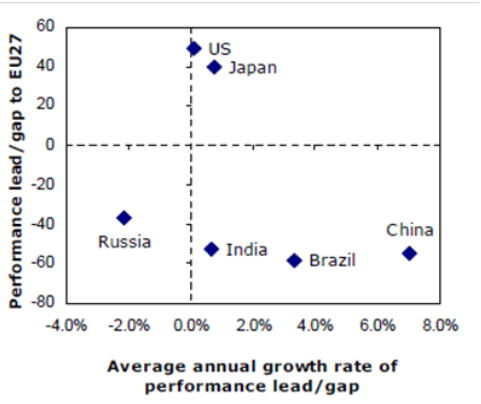

Fig. 5. Comparison of key international competitors

V. TOWARDS A NEW INDICATOR

Communication From The Commission To The European Parliament presents an indicator to measure performance in innovation output. The rigorous measurement of the impact of innovation policies is key for evidence-based policy-making. Moreover, it bolsters the legitimacy of public action and the use of public funds. [2]

The proposed indicator complements the Innovation Union Scoreboard (IUS) and its Summary Innovation Index (SII), which assess how the various strengths and weaknesses of Member States and the EU determine their overall performance, against a broad set of 24 innovation indicators, including inputs, throughputs and outputs. The proposed indicator will support policy-makers in establishing new or reinforced actions to remove bottlenecks that prevent innovators from translating ideas into products and services that can be successful on the market. Improved performance will contribute to smart growth, in line with Europe 2020 and its Innovation Union flagship initiative.

The indicator in this Communication zooms in exclusively on innovation output and monitors a reduced set of dimensions, including the contribution to job creation of fast-growing firms. Given its complementarity with the IUS, it is planned that the results of the proposed indicator are published simultaneously with those of the IUS.

Innovation output is wide-ranging and differs from sector to sector. Measuring it entails quantifying the extent to which ideas for new products and services, stemming from innovative sectors, carry an economic added value and are capable of reaching the market. Therefore, it can be captured by more than one measure. After exploring a broad set of options, the Commission opted for four IUS indicators, grouped into three components (patents, employment in knowledge-intensive activities (KIA), and competitiveness of knowledge-intensive goods and services), and a new measure of employment in fast-growing firms of innovative sectors.

The components of the innovation indicator:

The first component is technological innovation, measured by patents, as a crucial output of the R&D and innovation process, showing the ability of an economy to transform knowledge into technology. Therefore, policies improving the intellectual property rights (IPR) system and making it less costly benefit businesses deriving growth from own innovations. Measures such as the professionalization of access to IPR portfolios and tax reductions on patent profits can be instrumental for innovative business dynamics.

The second component focuses on how a highly skilled labour force feeds into the economic structure of a country. Investing in people is a challenge for Europe, as education and training provide workers with the skills for generating innovations. This component captures the structural orientation of a country towards KIA, by measuring the people it employs in KIA in business industries, where at least one third of the employees have a higher education degree, as a proportion of the total number of employees in that country.

The third component is the competitiveness of knowledge-intensive goods and services. In a well-functioning economy, it reflects its ability, resulting from innovation, to export innovative products and to

participate in global value chains. Competitiveness-enhancing measures and innovation strategies are mutually reinforcing for the growth of employment, export shares and turnover at the firm level. The component aggregates in equal weights the contribution of the trade balance of high-tech and medium-tech products to the total trade balance, and knowledge-intensive services.

Finally, the fourth component measures the employment in fast-growing firms of innovative sectors. Fostering the development of those firms is an integral part of modern research and innovation policy. Studies show that growth depends to a crucial extent upon fast-growing firms, which generate a disproportionally large share of jobs and can contribute to increased innovation investments during economic downturns. Therefore, some Member States strongly support easier access to finance for fast-growing firms, including for innovative projects and for risk capital at seed, start-up and early-growth stages.

We propose to form a new indicator to use fuzzy logic.

VI. FUZZY LOGIC FOR A NEW INDICATOR

Our understanding of most physical processes is based largely on imprecise human reasoning. This imprecision (when compared to the precise quantities required by computers) is nonetheless a form of information that can be quite useful to humans. The ability to embed such reasoning in hitherto intractable and complex problems is the criterion by which the efficacy of fuzzy logic (FL) is judged.

On the application level FL can be considered an efficient tool for embedding structured human knowledge into useful algorithms. It is a precious engineering tool developed to do a good job of trading off precision and significance. In this respect, FL models do what human beings have been doing for a very long time. As in human reasoning and inference, the truth of any statement, measurement or observation is a matter of degree. This degree is expressed through the membership functions that quantify (measure) a degree of belonging of some (crisp) input to given fuzzy subsets.

Fuzzy systems are universal approximators [5, 6]. These proofs stem from the isomorphism between two algebras – an abstract algebra (one dealing with groups, fields, and rings) and a linear algebra (one dealing with vector spaces, state vectors, and transition matrices) – and the structure of a fuzzy system, which comprises an implication between actions and conclusions (antecedents and consequents). The reason for this isomorphism is that both entities (algebra and fuzzy systems) involve a mapping between elements of two or more domains. Just as an algebraic function maps an input variable to an output variable, a fuzzy system maps an input group to an output group; in the latter these groups can be linguistic propositions or other forms of fuzzy information.

The classical control methodologies developed mainly for engineering are usually based on mathematical models of the objects to be controlled. Mathematical models simplify and conceptualize events in nature and human activities by employing various types of equations which must be solved. However, the use of mathematical models gives rise to the question how accurate they reflect reality. In complicated cases the construction of such models might be impossible.

Fuzzy models will become more and more popular as solution schemes, and it will make fuzzy systems theory a routine offering in the classroom as opposed to its previous status as a “new, but curious technology”. Fuzzy systems will be a standard course in any science or engineering curriculum. It contains all of what algebra has to offer, plus more, because it can handle all kinds of information not just numerical quantities.

Fuzzy logic system for our problem is the following. Figure 6 displays the fuzzy inference system (FIS) for four input variables and one output parameter. This system is destined for the assessment efficiency of the innovation project (EIP). The input parameters for this problem are patents, skills, competitiveness, employment. The output parameter determines the innovation output.

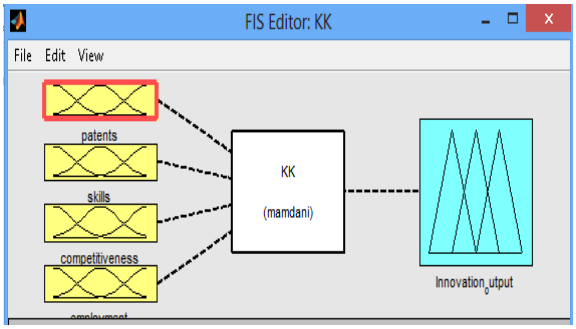

Fig. 6. Fuzzy inference system

The control objective is to find the output value for a particular set of input variables. Each of input parameters is the linguistic variable with three terms. Membership functions characterize the fuzziness in a fuzzy set in a graphical form for eventual use in the mathematical formalisms of fuzzy set theory. As example fig. 7 shows the membership functions for the input and output variables.

Next the rules of the FIS are defined. The number of the rules is the product of the number of terms in each input variable: 3*3*3*3 = 81. After the forming base of rules FIS gives the values of EIP as conditional units. We finally get a crisp value of the output which represents the values of EIP. Figure 8 displays the value of EIP equal 79 for given set of input variables.

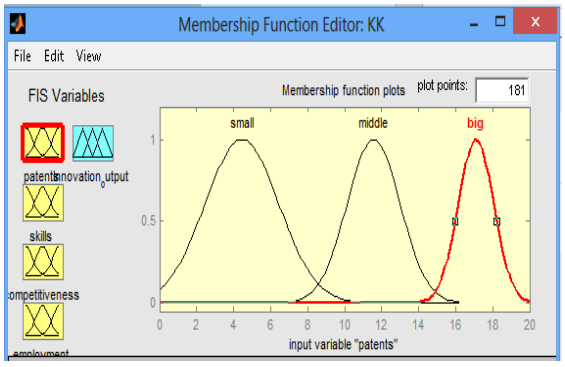

a)

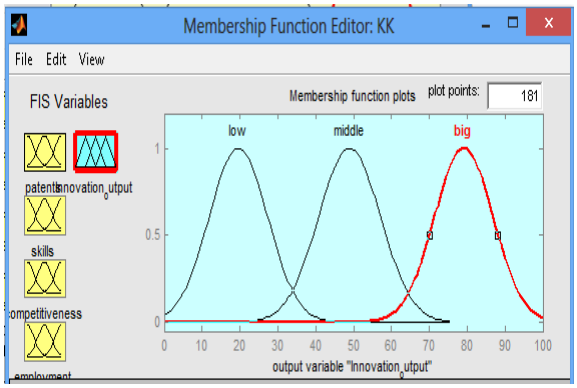

b)

Fig. 7. Membership functions
for the input (a) and output (b) variables

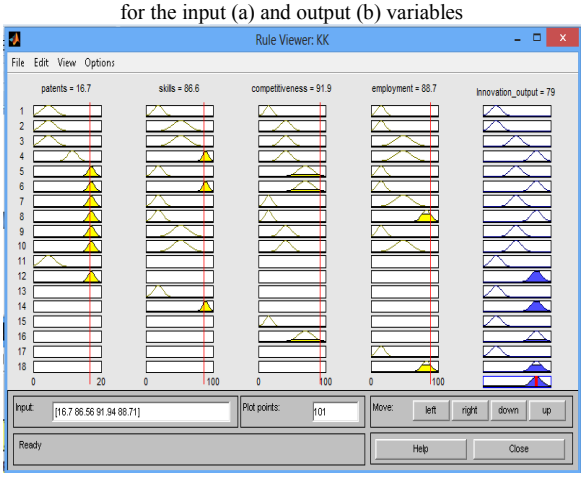

Fig. 8. Result of fuzzy inference system

The fuzzy approach of EIP assessing may be supplemented by conclusion of the regression equation. This equation will determinate value of EIP. Thus the authors propose a method of evaluating the effectiveness of an innovative project using fuzzy logic.

VII. REFERENCES

[1] E. Maravelakis Y. N. Bilalisz, A. Antoniadisy et al. Measuring and benchmarking the innovativeness of SMEs: A three-dimensional fuzzy logic approach. Production Planning & Control, Vol. 17, No. 3, April 2006, 283–292.

[2] Measuring innovation output in Europe: towards a new indicator. Communication from the Commission to the European Parliament, Brussels, 2013.

[3] Guidelines for Collecting And Interpreting Innovation Data. Oslo Manual, A joint publication of OECD and Eurostat, 2006.

[4] Innovation Union Scoreboard. The Innovation Union's performance scoreboard for Research and Innovation, 2012.

[5] V. Kecman. Learning and Soft Computing – Support Vector Machines, Neural Networks, and Fuzzy Logic Models. The MIT Press, London, 2001. - 576p.

[6] T. J. Ross. Fuzzy Logic with Engineering Applications. John Wiley & Sons Ltd, United Kingdom. 2010. - 607p.

A CO-OPERATIVE VEHICLE TO VEHICLE (V2V) COMMUNICATIONS SYSTEM TESTBED DEVELOPMENT

Giuseppe Avon, Erminio Agosta

University of Catania
Catania, Italy

Abstract

Modern societies depend on mobility and traffic is proportional to vehicle accidents. Sometimes human factor is determining, sometimes it totals up to adverse driving conditions. Security systems are introduced as technology advances, some of them are designed to assist driver, some other to intervene in order to avoid accidents or to mitigate effects. Technology aims to increase vehicle awareness, sensing systems and environment status, to inform and eventually replace driver on the strength of the situation. Increasing vehicle awareness brings in Vehicular Communications Systems (VCS) concept: vehicles communicate each other and with roadside units, solving problems in a cooperative manner, instead of trying to solve them individually. Vehicle and driver point of view becomes expanded, beyond the extent of any sensor can be locally installed. These systems are aimed at improving safety: driver is warned about imminent dangers as obstacles and abrupt changes in speed or course of neighbour vehicles. Side effects of these technologies are traffic congestion mitigation or law enforcing. V2V systems introduce network problems as vehicles and roadside unit become nodes of a fast changing, medium sized network. This paper presents a testbed for cooperative V2V communications systems.

I. INTRODUCTION

Active security systems are key to accident prevention, sometimes their effectiveness is comparable or even superior to passive security systems. Locating available vehicle data is the first step towards VCS. Vehicles are equipped with a multitude of sensors[1 – 3], some of them are not even presented to the driver, for example:

– single wheel speed sensors: used by ABS, TCS or ESP subsystems to deduce which wheels are locking (during emergency braking manuevers) or overrunning (accelerations on slippery surfaces);

– acceleration sensors: used by ABS, TCS or ESP to measure acceleration components and deduce vehicle movements;

– gyrometers: used by ESP to measure vehicle yaw (oversteer or understeer conditions) or rotation on other axes;

– steering angle: used by ESP to measure difference between driver input direction and effective vehicle rotation [4].

GPS receiver is always more integrated in cars and is easily available as optional. X-by-wire systems are increasingly used in modern vehicles: these systems require a multitude of sensors placed directly on driver input commands (gas throttle, braking pedal, clutch pedal, gear) and they become eventually available to the further processing needed by VCS. Data, conveniently formatted, coming from onboard sensors and from vehicles nearby is the key concept of VCS. A very detailed outline of the situation can be extracted by a dedicated onboard processing unit, far beyond any locally mounted sensor scope.

II. USE CASE

Presented VCS testbed was developed to demonstrate or evidentiate:

– needed data is already available from onboard sensors and ECU's;

– ease of algorithm to extract Collision Warning and Collision Detection alerts and their usefulness to the driver;

– communication challenges;

– other applications with same sensors data;

– problems and limitations.

III. COLLISION WARNING AND DETECTION

Using onboard accelerometer and gyroscope, collision warning and detection can be done, framing maximum vehicle acceleration, pitch, roll and yaw and setting thresholds. When data from sensors exceeds thresholds, a message is sent in broadcast and received by vehicles and roadside units in range. Vehicles directly receiving alerts will present a message to the driver, drawing alert on integrated navigation system cartography and, eventually, interacting by slowing down the vehicle or engage brake precharge, based on the target distance. Peaks in acceleration can be interpreted as abrupt braking manuevers or collisions, peaks in yaw can be, instead, interpreted as ab-

rupt evasive manuevers or vehicle loss of control. Alerts can be analyzed from the onboard computer to check if the alert has to be considered light (engine or vehicle keeps running) and can be acknowledged and cleared, or serious (engine cutoff, airbag and pretensioner engaged, system diagnosis failure) and other drivers must be warned about.

IV. COMMUNICATION CHALLENGES

To this day, there are no universally accepted standard protocols to support vehicle-to-vehicle communications [5, 6]. IEEE 802.11p seems to be the most promising communication standard, an amendment to 802.11 which deals with vehicular communication challenges. IEEE 802.11p is tailored to cope with:

– robust and fast connection setup for fast moving network nodes;
– halved bandwidth (20 to 10 Mhz compared with 802.11a) and halved symbol length to improve robustness;
– dedicated communication channels (Control channel – CCH and Service Channel – SCH) to send safety critical messages and two way general purpose communication.

While IEEE 802.11p standard is PHY – MAC/LLC oriented protocol, upper layers still remain outside the scope of the standard. Standard proposals are similar, more or less, by provided services and traffic separation (specific Vehicle-to-Vehicle or Vehicle-to-Infrastructure for safety related messages and general purpose data stream like mobile IP). Other challenges include message security, jam or denial-of-service avoidance and privacy issues[7, 8].

V. OTHER APPLICATIONS

Vehicles broadcasting current position in a periodical beacon can help onboard computer tracking traffic congestion in a particular area. Onboard navigator can reuse traffic data to re-route driver through alternative paths and avoid congestion. Roadside units along construction sites can warn drivers about reduced lanes or obstructions. Security or law enforcement vehicles can have special onboard units to signal their arrival, warn drivers and help in clearing up their pathway[9, 10].

VI. TESTBED DEVELOPMENT

Testbed was designed in order to model telemetry beaconing system and develop algorithms able to detect and issue collision warning and collision detection alerts to other driver, using a minimum or reduced set of data coming from onboard vehicle sensors. Testbed was initially implemented on two professional RC cars, normally used in races using STM32F4 Discovery and Raspberry PI as onboard unit and remote control replacement. Race cars remote control was replaced by a Bluetooth WiiMote controller connected to Raspberry PI and commands were filtered to improve car handling (acceleration curves and steering profiles were adapted to simulate normal driving). Filtered pilot input is then passed to STM32F4 Discovery microcontroller to control throttle and steering servos via PWM signals.

Real life environment	Simulated environment
Wheel speed sensors	GPS Speed output
Onboard accelerometer	ST iNEMO v2 / STM32F4 Discovery LIS302DL
Onboard gyrometer	ST iNEMO v2 / GPS course output
Onboard GPS	SkyTraq Venus 5 receiver
Telemetry	Not simulated
Onboard unit	STM32F4 Discovery / Raspberry PI
MAC/LLC IEEE 802.11p	Digi XBee / IEEE 802.11n adapter
Network Stack	Simple telemetry packet / Simple telemetry packet over IP + UDP
Vehicle HMI	Software running on standard PC

Base algorithm for dangerous maneuver or accident detection is implemented using only accelerometer data. Improvements are suggested by integrating data from iNEMO gyrometer and magnetometer. Testbed was then ported onto two real vehicles to verify data.

VII. ACCELEROMETER DATA

Axis are considered as listed below:

– X: from left side to right side;
– Y: from the rear side to the front side;
– Z: from bottom to the top.

Measurements were done to evaluate system performance in order to asses:

– system ability to detect a collision;
– system ability to detect an abrupt maneuver.

Accelerometer data must be filtered in order to become usable. Adopted filter chain comprises:

– low pass filter to remove noise generated from high frequency vibration induced in car (engine, road unevenness);
– high pass filter to remove DC (gravity);
– smoothing/rounding filter;
– Kalman filtering.

Filter parameters varies according to conditions and accelerometer type and were finely tuned with a test run on a smooth tarmac surface driving normally. Results evidence that accelerations between ± 0.3 g are normal and an emergency brake from 50 km/h to full stop produced a peak around 0.5 g. All things considered, it can be said that accelerations between ± 0.3

g can be considered inside safety frame. Samples exceeding these limits can be considered as critical maneuvers and an alert must be sent to nearby vehicles.

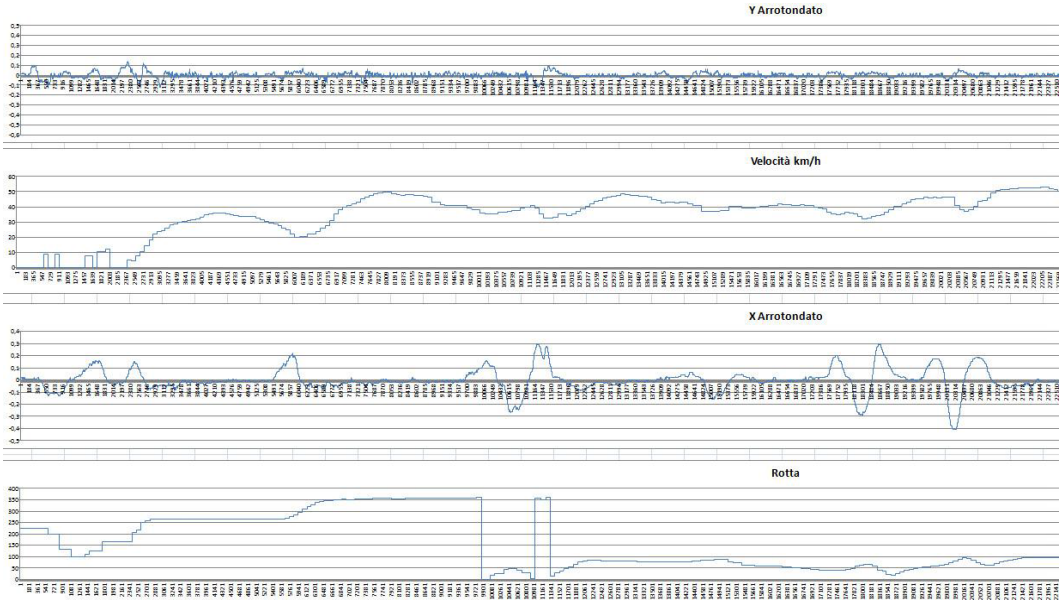

Fig. 1.

Graphs (fig. 1), in order, show (time series data):

- Y acceleration (filtered and rounded);
- Speed in km/h;
- X acceleration (filtered and rounded);
- GPS course.

While accelerometer data can be considered quite sufficient for ideal conditions (flat road, perfect tarmac surface), problems arise when accelerations combine on more than one axis (turning, ascending/descending road): acceleration dilutes on all three axis and thresholds become invalid. Accelerometer data must be integrated with gyroscope and/or compass data (IMU) to compensate vehicle inclination and steering.

VIII. GPS DATA

GPS positioning works well only when horizon is mostly visible [11 – 15]. Partially or completely occluded sky, as inside urban tunnels (tall building on the edges of narrow roads) degrade GPS positioning performance till compromising data. Mitigation can occur taking into account maps and data coming from IMU to integrate and improve GPS precision (dead reckoning, Kalman based sensor fusion).

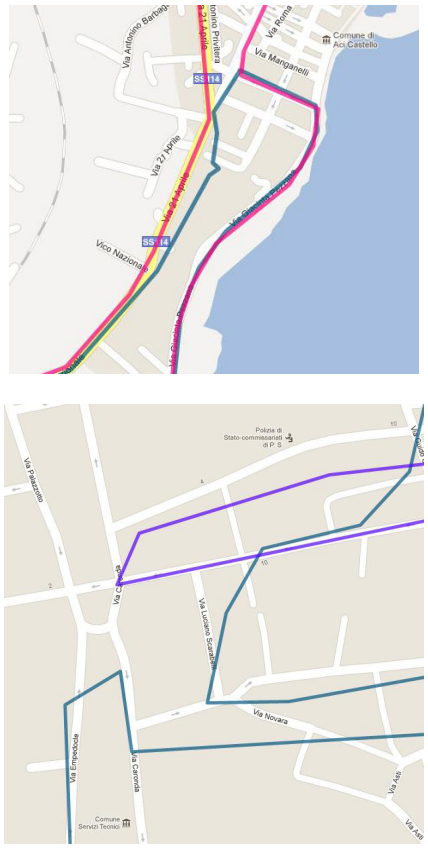

Fig. 2.

IX. COMMUNICATIONS

While RC cars where equipped with a Digi XBee (IEEE 802.15.4 ZigBee) unit, real vehicles where equipped with two 802.11n adapters. ZigBee works well up to 50 meters in line of sight, except when an obstacle is in the middle of the transmitters. 802.11n range is greater than ZigBee but continuos obstruction due to vehicles in the middle, fading due to trees and other obstacles made communication measurements very difficult. When in Line-of-Sight, a maximum distance of 400 m was recorded (using omni-directional roof mounted antenna), connection is abruptly lost if one of the two vehicles is behind a bend, obstructed by buildings or structures.

X. CONCLUSIONS AND FUTURE WORK

Testbed was developed mainly to highlight potential issues in vehicle to vehicle communication. While crash/abrupt maneuver detection algorithm can be easily implemented and improved using low cost hardware and data already onboard, still some problems about precise positioning and reliable, long distance communication occur.

XI. REFERENCES

[1] European Commission - Information Society and Media. (2007) i2010: Intelligent Car. Brochure.

[2] Gerhard Rieger, Joachim Scheef, Holger Becker, Michael Stanzel, and Robert Zobel. Active Safety Systems Change Accident Environment of Vehicles Significantly - A Challenge for Vehicle Design. PDF Document.

[3] Philip Grant et al., "Vehicle electronic control apparatus," 5,670,845, September 23, 1997.

[4] Friedrich Kost et al., Driving Stability Systems. Germany: Robert Bosch GmbH, 2005.

[5] Michele Weigle. (2008) Standards: WAVE/DSRC/802.11p.

[6] Rohde & Schwarz. WLAN 802.11p Measurements for Vehicle to Vehicle (V2V) DSRC. Application Note.

[7] M. Raya and J. Hubaux, "Securing Vehicular Ad-Hoc Networks," Computer Security, vol. 15, 2007.

[8] SAE International. (2010, February) DSRC Implementation Guide - A guide to users of SAE J2735 message sets over DSRC. Documento PDF.

[9] Thomas Strang and Matthias Röckl. (2008/2009) Vehicle Networks - V2X Communication Protocols. PDF Document.

[10] Hannes Hartenstein and Kennet Laberteaux, VANET Vehicular Applications and Inter-Networking Technologies, illustrata ed.: John Wiley and Sons, 2010.

[11] Survey Lab. GPS TTFF and Startup Modes. PDF Document.

[12] Klaus Betke. (2001, August) The NMEA 0183 Protocol. PDF Document.

[13] ASD (NII) / DASD (C3, Space and Spectrum). (2008, September) Global Positioning System Standard Positioning Service Performance Standard. PDF Document.

[14] Navigation Center - U.S. Department of Homeland Security. (1996, September) NAVSTAR GPS - User Equipment Introduction. PDF Document.

[15] Navigation Center - U.S. Department of Homeland Security. (1996, Settembre) NAVSTAR GPS - User Equipment Introduction. PDF Document.

IEEE 1588 AND DCCS PROTOCOL IMPLEMENTATION IN A SYSTEM COMPOSED BY TWO STM32F4 AND SPIRIT WIRELESS MODULES

Salvatore Cifalinò, Giuseppe Giuffrida

University of Catania,
Catania,Italy

Abstract

Time is a fundamental quantity, as well as the flow of time itself: it plays a central role in the project that we are going to present below. In fact we will see an application of the Precision Time Protocol (PTP), also known more commonly as 1588, that is the IEEE standard that outlines the rules of the communication protocol.

Such communication, in our case, has been established between two STM32F4 boards via two SPIRIT wireless modules.

The proposed objective is therefore to implement the communication of the two microcontrollers, synchronizing their clocks, with the help of the two SPIRIT modules and then build on the algorithm of the DCCS 1588 protocol, intended to improve the parameters of the communication.

I. INTRODUCTION

Time synchronization is an element that has often played a key role in many research studies. In addition it represents an important requirement in many applications.

There are many protocols and algorithms that make the time synchronization their ultimate goal: let's examine more precisely the IEEE 1588 protocol, developed for local systems for which high accuracy is required. It was released in November 2002 and based on the work done by John Eidson at the Agilent Labs. Its specifications for hardware and software allow network-connected devices (clients) to synchronize the clock of each of them to a clock network (master). The standard was initially developed for the industrial environment where it was not possible prior precise control using a Local Area Network (LAN). Only later, it aroused interest in telecommunications, energy and military fields. The standard is applicable to Local Area Networks that support multicast communication. Attempts by IEEE are ongoing to extend this protocol to the WLAN (Wireless Local Area Network), so they are developing implementations of IEEE 1588 on wireless sensor networks [1]. IEEE 1588 is a Master/Slaves protocol, which is based on the exchange of a series of packets between a master and several slaves. IEEE 1588 is able to synchronize heterogeneous systems (with clock varying in accuracy, resolution and stability) with higher accuracy within microseconds. To achieve this accuracy, it needs the "timestamp" of the shipping/incoming messages to be generated by a specific hardware or a component as close as possible to the physical means (as for the wireless sensors with the timestamp at the MAC layer), as opposed NTP acting only in software and does not require any special hardware. Detailed information on IEEE 1588 can be found in [2 – 4]. According to the IEEE 1588 protocol, devices synchronization requires two steps:

– determine which device will function as a master clock;

– measure and correct the divergence of the slave clock due to their offset and initial delay of the network.

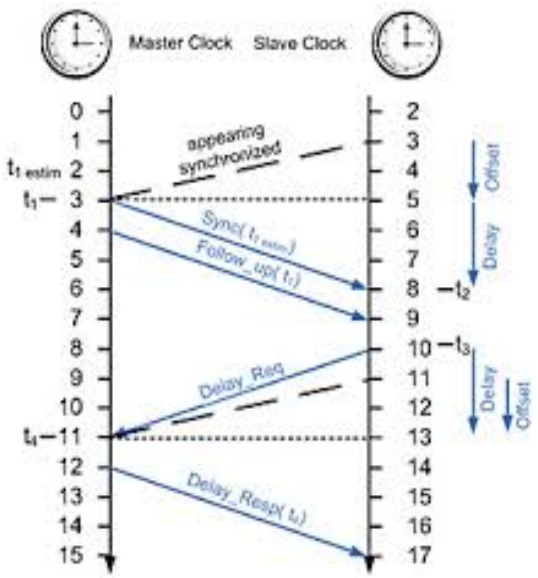

Fig. 1. Messages exchanged for the IEEE 1588 realization

When the system is initialized, the protocol uses the algorithm named Best Master Clock Algorithm (BMC) to automatically determine which clock in the network is the most accurate, and it will be named as master-clock.

The next step is the true PTP: firstly, a node (the master clock) sends a "Sync message" and records the exact instant of time in which such submission is made. This value is transmitted in a second message called "Follow-Up message". The receiver uses its own local clock to record the time of arrival of the "Sync messages" and compares it to the time value contained in the "Follow-up message". The difference between the two time values represents the offset of the slave-clock plus the propagation delay of the message.

This delay is calculated by the receiver node, which sends a message called "Delay-Request message" to the master-clock node and records the message shipping time.

When the master clock receives a "Delay-Request message", it records the arrival time and places it on a message called "Delay-Response message" that is forwarded to the slave clock.

Because of the divergence of the clock involved in the procedure, a periodic repetition of offset correction and propagation delay is needed to keep the clock in sync.

II. PROTOCOL IMPLEMENTATION

Let us now see how the 1588 protocol has been realized in terms of pseudo-code. All is inserted in a while cycle, in which the main body of the firmware, sending the messages provided by the PTP, is located. Time is fundamental for the sync and delay requests. In fact when code that directly involves them is written, then it is necessary to take into account the following assumption: that is the hypothesis, required by the protocol, that the time of propagation of the messages are symmetrical. In order to fulfill it, we need to be careful in trying to achieve the best possible similarity between the sending / receiving functions of two above messages. For example, the implementation of the function that handles the sync is the following:

Master node side

```
timestamp1.save();
timestamp2.insertqueue();
timestamp2.send():
```

Slave node side

```
timestamp2.receive();
t2=timestamp.convert+offset;
```

The master saves its current state before transmitting and the slave, after receiving the entire message from the Sync master, saves its state, too. After the sync, as the rules of the protocol implies, the Follow-up message is sent:

Master node side

```
insertQueue.timestamp1();
send.timestamp1();
```

Slave node side

```
timestamp1.receive();
timestamp1.saveInT2();
```

The Slave can now derive the sum of delay and offset by the relation:

$$\text{delay offset} + = (t2 - t1) \bmod . \quad (1)$$

The next message is the Delay Request, which is time critic:

Slave node side

```
t2.convert();
t2.insertqueue();
t2.send();
```

Master node side

```
t2.receive();
t3.save();
```

It is easy to see how the structure of the Delay Request is very similar to that of sync, to follow it and to realize the hypothesis of symmetry previously discussed.

The last message to be sent will be the Delay Response:

Master node side

```
t3.inserqueue();
t.send3();
```

Slave node side

```
t3.receive();
```

The Slave can now derive the difference of delay and offset by the relation (1). Having two equations relating the delay with the offset, it is possible to use systems theory of linear equations in order to calculate the offset, since this is our purpose. Indeed, this information will then be used by the slave to set the reference timer, subtracting the offset amount from the counter.

III. PERFORMANCE EVALUATION

An algorithm to measure and estimate the goodness of the synchronization has also been imple-

mented within the system. Then the code was modified on both the master and slave to build such a tool for performance evaluation.

The system is set to send the acquired data in a buffer via USB. By setting the buffer size to 1000, we will have a data monitoring 50 seconds long. The information collected can be plotted on a Microsoft Excel graph.

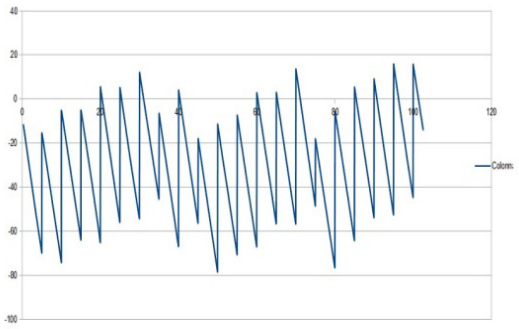

Fig. 2.

In the graph the instants of synchronization are represented by vertical lines. As you can imagine the synchronization occurs every 5 seconds and the accuracy is about 80 microseconds.

After each synchronization cycle, obviously synchronization accuracy is not constant and this is due to the variations that are introduced because of the variability of the wireless communication.

IV. DCCS ALGORITHM

The DCCS protocol (Dynamic Continuous Clock Synchronization) is a protocol used to synchronize the clocks, which is capable of correcting the clock drift and it is oriented to the use in the Wireless Sensor Networks. It is based on RBS (Reference Broadcast Synchronization) and CCS (Continuous Clock Synchronization) protocols, but it corrects some of their flaws. It is centered on the construction of a coefficient called α. Its purpose is to work on the relationship of calculating the offset to improve and smooth out the curve of the result, thereby also the drift between the two clocks will decrease.

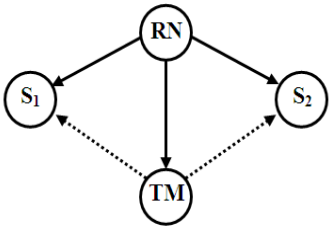

Fig. 3

The DCCS protocol aims to use the same mechanisms of CCS in scenarios where such measures are not possible, such as WSN, which are in fact composed most often from low cost devices and little configurable low level. DCCS introduces a new role in addition to the TM and the slave: the Reference Node, whose task is to send a Broadcast message Reference (similar to the message indication CCS) periodically. The only task of the TM becomes the value of the clock to record the arrival of each message RBM and subsequently transmit it to the slaves.

Not having a Reference Node, for the implementation of the algorithm is used an alternative solution in which the slave samples a value of its own clock at the end of each 1588.

The algorithm for the calculation of the virtual clock is simpler than those used by RBS and CCS, so as to be more easily usable on devices with low computational power. We define the instant *i*-th timestamp at the end of the *i*-th 1588, the slave can calculate a coefficient for correcting the drift αi :

$$\alpha i = \frac{CM(ti) - CM(ti-1)}{CS(ti) - CS(ti-1)},$$

whereas $CM(ti-1) = CS(ti-1)$, as a result of the 1588 protocol, the two clocks have been approximated, and that the offset $\Delta i = CM(ti) - CS(I)$, we can write:

$$\alpha i = \frac{\Delta + (CS(ti) - CS(ti-1))}{CS(ti) - CS(ti-1)}$$

We have thus obtained αi using only the values of the clock of the slave and the offset calculated through 1588. αi represents an approximation of the clock drift between the master and the slave, calculated based on the interval between the last two rounds of synchronization; to take account of the coefficients calculated at each synchronization, on each round is also calculated an average coefficient for the correction of drift α:

$$\alpha = \frac{k\alpha + \alpha i}{k+1}$$

The coefficient k has values in the range {0, ..., 9}; during the first 9 rounds is incremented by 1 for each round, then keeps the value 9 for the later rounds. This mechanism ensures that:

– in round j with $j \leq 10$, α is calculated as the arithmetic mean of αi with $i \leq j$;

– in round j with $j > 10$, α is calculated as a moving average, where the average coefficient (α) has weight 9/10 and the current coefficient (αi) has weight 1/10.

In this way the algorithm has a reliable value of the clock drift even during the first timings, and the initial value of the moving average is quite accurate. The weight of the initial value on the value of ϭ is 0.9 eleventh round of synchronization, but since each round its weight is multiplied by a factor 0.9, becomes negligible (less than 0.1) around the thirtieth round;

which allows eliminate the influence of possible initial values of αi imprecise in a relatively short time.

The value of the virtual clock at the generic time t is calculated as follows:

$$CVS(t) = \left(\frac{CS(t)}{\alpha} \right) + offset ,$$

where offset is the sum of the offsets calculated for each 1588. Let α to share because we have empirically found that the device used for the slave is faster than the one used for the master.

The results, for example, can be appreciated through the following graph (fig 4):

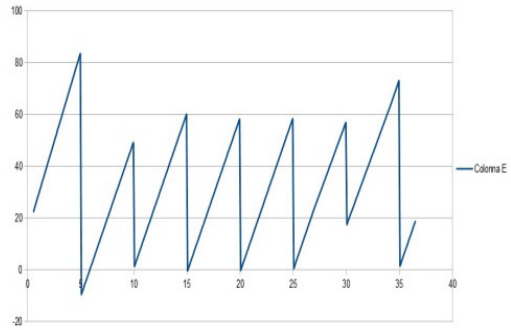

Fig. 4.

V. CONCLUSIONS

It was mainly of particular interest the programming of a system in which the timing constraints were of paramount importance and, consequently, also the type of programming had to adapt to them, taking into consideration the various instructions that have to be used to perform the required procedures. The following evaluation of the results allowed us to conclude saying that they are acceptable, since it is a protocol adapted to a wireless communication system, remembering of course that the results obtained through the implementation of the protocol in 1588 on a wired system had better performance.

It could be interesting a DCCS implementation on a wired system, so to compare the results with precision and analyze the discrepancy in performance between the two systems that would exploit on one hand the communication via USART and the SPIRIT modules on the other hand.

VI. REFERENCES

[1] A. Pakdaman, T. Cooklev. “IEEE 1588 over IEEE 802.11b for Synchronization of Wireless Local Area Network Nodes". San Francisco State University.

[2] National Institute of Standards and Technology, IEEE 1588 web site. http://ieee1588.nist.gov/..

[3] “Precision clock synchronization protocol for networked measurement and control systems". INTERNATIONAL STANDARD. IEC 61588. First edition 2004-09.

[4] A. McCarthy. “Special Focus: Understanding the IEEE 1588 Precision Time Protocol”. http://zone.ni.com/devzone/cda/pub/p/id/130.

[5] O. Mirabella, M. Brischetto, A. Raucea, P. Sindoni “Dynamic Continuous clock Synchronization for IEEE 802.15.4 based Sensor Networks” Department of Computer Engineering and Telecommunications – University of Catania, ITALY]

[6] O. Mirabella, M. Brischetto, A. Raucea “Evaluation of Clock Synchronization Protocols for Wireless Sensor Networks” Department of Computer Engineering and Telecommunications – University of Catania, ITALY]

[7] O. Mirabella, M. Brischetto, A. Raucea, F. Bannт, N. Caruso, “Improving the Dynamic Continuous Clock Synchronization for WSNs” Department of Computer Engineering and Telecommunications – University of Catania, ITALY]

[8] L. Lo Bello, A. Raucea, G. Patti, O. Mirabella “L-PTP: a Novel Clock Synchronization Protocol for Powerline Networks” Department of Electrical, Electronic and Computer Engineering – DIEEI University of Catania - Italy]

AIRLINES OF THE DEVELOPED AND THE DEVELOPING COUNTRIES

Denis Ikonnikov

Saint-Petersburg State University of Aerospace Instrumentation,
Saint-Petersburg, Russia
University of Applied Sciences,
Berlin, Germany

denis-ikonnikov@mail.ru

Abstract

More than one hundred years have passed since the first man's flight on plane. Today air travel has become an integral part of the transportation. Air companies of the developed countries dominate in this sector. However, recently there has been a strong rise of the aircraft industry in developing countries that do not experience serious economic consequences of the global crisis of 2008. In this situation, airlines of the developed countries should look for ways to keep the leading position on the market and reduce costs.

I. RISE OF THE DEVELOPING COUNTRIES

While the world is recovering from the global financial crisis that began in 2008 and airlines in developed countries suffer losses, developing countries are at the forefront, despite the difficult economic and market conditions.

According to the data of the International Air Transport Association the net profit of the air companies was just $7.6 billion (1.2% of revenues) in 2012. [1], that is two times lower than indicators in 2010. [2] The developed countries suffer the biggest drop in profits, while the airlines of the developing countries are gaining more and more profits. For example, in 2012 revenues of the Chinese airlines reached $22 billion that is three times more than in 2011.

Now the airlines of the Middle East, China and low-cost are coming at the forefront of the industry. According to research conducted by "The Boston Consulting Group" these airlines together will increase the market share of long-distance carriers from one-third to half of the world's share by the year 2020.

The reasons of such growth despite the harsh conditions:

– *cost advantages*. Costs are lower by 10–20% than in other Asian airlines and 30–40% lower than for the international carriers of the developed countries;

– *taxation*. This aspect is particularly noticeable in the Middle Eastern countries. Low corporate tax promote investment in new fuel-efficient planes. Consequently, these countries enjoy reduced fuel costs and service;

– *increased demand due to geographical advantages*. Middle Eastern countries may be involved in 60% of global flows, China – 45%, South Asia region – 30%.

Transportation of passengers in developing countries is growing rapidly. In 2005 – 2010 Middle Eastern airlines increased passenger traffic by 45 million people, having an annual growth of 11%. There are plans to increase passenger traffic in China from 1.1 billion to 2.5 billion per year in only ten years from 2010 to 2020. This will bring China to the second place after the United States. In India, this figure will increase three-fold – from 11 to 28 million people, in Indonesia it will quadruple – from 3.5 to 14 million people. [4]

Countries are actively engaged in increasing the frequency and the number of routes. Thus from 2009 to 2012 Middle Eastern airlines established 55 new destinations in Europe, Asia and Africa, and increased frequency of departures by 25%. China was noted by more modest rates – 21 new destinations (mainly in Europe and Asia). However, the frequency of departures increased by 40%. Whilst airlines of the developed countries added only 8 new destinations of flights, and increased the frequency by 17%.

On average, for each arriving aircraft in the Middle East there are 13 destination flights, in South-East region and China there are 9 destinations. However, this rate in China has the greatest tendency to increase.

Middle East and especially China are investing a lot of money in infrastructure for airports. China plans to build 50 new airports from 2010 to 2015. By 2020 in the three biggest airports in the Middle East the total passenger flow will be 160 – 220 million passengers per year, in China – 280 – 320 million passengers per year. New Beijing Airport will be the busiest in the world, with the capability to transport up to

400 million people per year (currently 74 million), that is more than the capacity of the airport in the USA Hartsfield-Jackson Atlanta International Airport, the busiest airport at the moment in the world.

II. REDUCING COSTS FOR MAINTENANCE

Aircrafts safely carry passengers over distances of 40 million miles every day. However, airlines cannot cope with, at first glance, trivial things such as maintenance costs and downtime.

Fuel costs are the highest costs in the aviation industry, whilst in second place, there are maintenance costs, on board services, call centers, and works on the ground that also have a significant portion in total costs.

There is a number of disadvantages in airlines' work, such as:

– passengers wait for 30 minutes to get their luggage because only one worker is occupied with such a procedure;

– skilled workers spend most of the time waiting;

– workers in maintenance shops are occupied mostly with searching for the repairing parts but not with the repair itself.

All that costs billions of dollars.

There are ways to reduce costs through the reduction of maintenance costs and downtime. In order to reduce costs it is obligatory to use labor, materials, and assets more efficiently. It is necessary to enhance reliability and improve safety measures.

One of the most striking examples is the company Toyota that uses efficient production technology without waste, where the whole working system works properly. There are standards of work and every employee is busy and knows what to do. This approach is based on four principles: waste disposal, control of deviations from the standard, flexibility and full use of human talent. This is not a company that produces aircrafts or provides services in aircraft industry but the technology can be used by the companies that work in the aircraft industry.

Table 1 shows the average time spent between the arrival and departure of aircraft, and saved time when the technology is used effectively, as well as ways to achieve effective use.

Table 1

The example of the effective use of time between flights for Airbus A320 [5]

	Time spent between flights (minutes)		Effective use
	Average time	Effective use	
Disembarking	6:14	4:38	Higher control over the passengers' luggage. Fewer passengers return back to find their luggage
Waiting till the cleaning crew enters the aircraft	0:24	0:18	Cleaning crew is ready to start working
Cleaning of the aircraft	11:48	9:40	The working process is standardized by time and cleaning processes. The equipment is always prepared in advance
Waiting till the permission to board passengers is transferred to the personnel	4:11	0	Visual signal from the cockpit to the personnel when the plane is ready to take passengers on board, for example, a bulb lights at the ramp
Waiting till the first passenger enters the airplane	4:06	0	Active work of the crew to bring passengers to the gangway
Passenger's boarding	19:32	16:00	The airplane crew helps passengers to put their luggage on the upper shelves, and also hints the direction to their seats.
Waiting for the list with the passengers' information	1:58	0:13	The person that is responsible for the list with the passengers' information follows the last passenger
Closing the doors of the aircraft	0:57	0:09	Hostess is ready to close the aircraft's door right after the last passenger
The ladder is moved away from the plane	1:39	0:43	It happens right after the closing of the aircraft's door
Total time spent	52:18	33:11	

Another clear example where the effective system can be applied is a maintenance shop.

If there is a system of effective use, then there is an efficient schedule and standardization. For example, everyone knows that, Airbus A320 will pass through the gate number 1 at a certain time, say, at three o'clock, and will leave 50 minutes later.

The plane moves along the special marks on the floor. Managers have made a list of routine tasks of what should be done. This list is immediately transmitted to mechanical engineers who will be engaged in repairing the aircraft. The details that are necessary for their work are delivered by the team responsible for the delivery. If there are non-routine tasks, the mechanical engineers instead of going down for details give a signal to the team responsible for the delivery, and that team delivers the necessary details. All data of the progress is displayed on the screen that helps the team to work effectively. The ultimate goal is to fix all the identified defects in 50 minutes.

This approach requires skillful management that could exercise control over the proceedings, each task, and the effective use of resources in real time. Senior Manager can perform short daily meetings before the work starts so that every worker could understand the task. Thus there will be a gradual improvement process.

Efficient technologies can also be applied in customer service during registration for the plane. The system can be based on the customers' segmentation: most of them will be serviced routinely; the other part will be serviced by the qualified personnel.

The application of effective technology is quite difficult and time consuming. However, the potential for their use is very large, and can lead to significant reductions in costs and increase in quality.

Recent attempts by European and American companies to use these technologies have led to a reduction in overall costs by 5 – 10%, which indicates the effectiveness of this technology.

III. CONCLUSION

In the ever-increasing global competition among airlines it is urgent to seek new ways to reduce costs and increase customer base. Now, despite the recent global crisis the airlines of the Middle East, China and low-cost get a huge increase in passengers flow, trying to win as many markets as it is possible. However, any company will be faced with a threshold of passengers flow, and therefore it should look for alternatives, such as efficient technologies, which have already been implemented by the developed European countries as well as by the United States. Developing countries should think about that, because in some time they will have to face this threshold. It is very important for the companies in developing countries to be ready when the time comes.

IV REFERENCES

[1] IATA Annual Review 2013.
[2] IATA Annual Review 2011.
[3] Surviving The Squeeze. Monica Wegner, Frank Budde, and Paul Tranter. Boston Consulting Group. October 2012.
[4] Middle Eastern Megacarriers: Gaining Altitude. Tom von Oertzen, Rend Stephan, Dale Schilling. Boston Consulting Group. September 2011.
[5] **The hidden value in airline operations**. Stephen J. Doig, Adam Howard, and Ronald C. Ritter. Mc Kinsey Quarterly, 2003.

ACOUSTO-OPTIC DEFLECTOR WITH ACOUSTIC LINE'S GEOMETRIC POSITION ANGLE AUTO-TUNING

Ruslan A. Khansuvarov

Saint-Petersburg State University of Aerospace Instrumentation,
Saint-Petersburg, Russia

E-mail: ruslan.hansuvarov@gmail.com

Abstract

The idea of acousto-optic self-tuning deflector, which automatically returns the position of the acoustic line, corresponding to the mode of Bragg diffraction feedback implementation is proposed. Features of sodium bismuthate's double molybdate grown by new technology – low gradient Czochralski process are illustrated.

I. INTRODUCTION

Acousto-optic deflectors are used in variety of optical systems and laser radiation controlling systems. These systems allow real-time optical signals' direction controlling and high-speed laser beam scanning.

There is one unsolved problem of deflector's operation in Bragg diffraction mode and this problem is preserving diffraction mode i.e. acoustic line's crystal position preserving despite external influences.

In this work one possible option of feedback implementation is considered. It allows preserving deflectors' position by piezoelectric rotators. Using piezoelectric rotators significantly simplifies mechanic scheme of self-tuning deflectors and piezoelectric rotators are much more inertialess than mechanical movers. Of course, one of the main criteria of such self-rotating systems operation is the initial setting of the deflectors in Bragg diffraction mode.

In additional, new material of acoustic line crystal was investigated as well; it is sodium bismuthate's double molybdate, grown by new technology – low thermal gradient method. As it turned, this crystal has a number of differences from the sodium bismuthate's double molybdate, grown by traditional Czochralski process, which makes it preferable for use in acousto-optical devices.

II. BRAGG DIFFRACTION MODE

If diffraction spectrum consists of two peaks, corresponding to values *m = 0* and *m = 1* (Fig. 1) it is Bragg Diffraction mode.

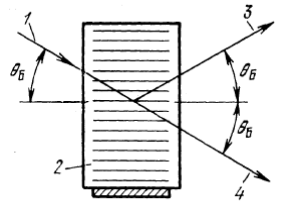

Fig. 1. Bragg Diffraction mode

First negative and higher order diffraction maxima are not available. The intensity of the first maximum is greater when the incident light is at an angle with the acoustic wave front, which satisfies the Bragg condition:

$$\sin\theta_Б = \lambda/2\Lambda \qquad (1)$$

where λ – the wavelength of optical radiation, Λ – the acoustic wavelength, $\theta_Б$ – the Bragg angle, i.e. diffraction occurs only with the formation of two peaks [1].

Bragg diffraction occurs at high frequencies at a large length of light and acoustic wave interaction. Before talking about the violation of the Bragg condition, the graphic dependence of reflection coefficient complex amplitude from the angle of light incidence θ should be given [2].

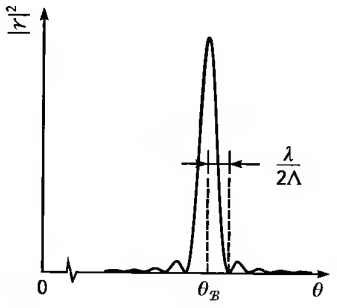

Fig. 2. Graphic dependence of reflection coefficient complex amplitude $|\gamma|^2$ from the angle of light incidence θ

As seen from the figure 2, the permissive variation is determined by the ratio of the wavelength of light to doubled elastic waves' length. For example, exploring the interaction of HeNe-laser with 630 nm

wavelength with an acoustic wave in the order of 50 microns in deflector, it appears that the varying quality of Bragg diffraction is observed only at an angle deviation less than 0.72 degrees.

Any external influence, whether shaking or vibration, can disturb the angle of light beam incidence on acoustic line at such small angles. So, we need to formulate the requirements for precision crystal corner self-tuning system.

III. FEEDBACK AND ACOUSTIC LINE CRISTAL ROTATION SYSTEM DESCTRIPTION

The author's analysis of the existing mechanical rotation systems found that the optimal choice to solve the existing problem is a piezoelectric system of angular offset. This system has a number of advantages (in comparing with mechanical motivators) – it has no mechanical parts, which is exposed by microdisplacements due to shaking. Piezoelectric system of angular offset is formed as a disk mounted on a piezoelectric motor with a passive rotor. The motor consists of several glued piezoelectric cylinders. Each cylinder is connected by sliding contacts. Radial oscillations, electrically excited in the disks, create a variable force F, normal to the surface of the disc in contact with the plate. Components of this force F_{long} and F_{bend} generate longitudinal and bending oscillations, which form the trajectory of the contact point (see Fig. 3) [4].

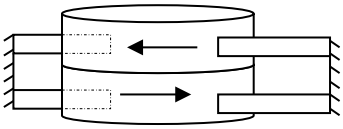

Fig. 3. Schematic drawing of the piezoelectric system of angular offset, consisting of two piezoelectric cylinders connected to the sliding contacts

Feedback for the acoustic line's geometric position angle auto-tuning can be implemented in the following way: fixing diffraction peak collapsing by two spaced photodetectors. Device's scheme that implements this method is shown on figure 4.

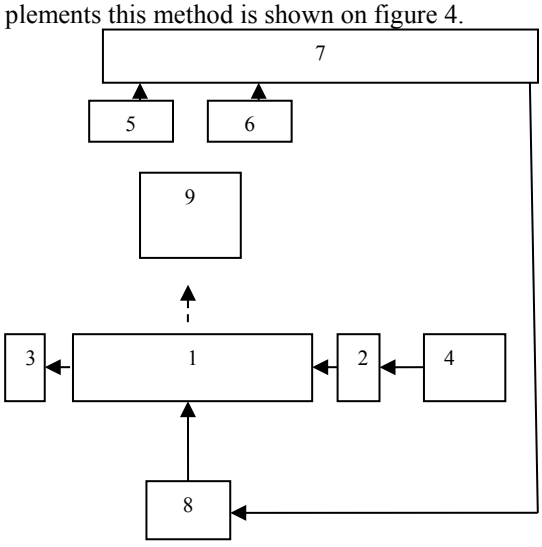

Fig. 4. Device's scheme

The following notations are used on the figure 4: 1 – Acoustic line; 2 – Piezotransducer; 3 – Absorber; 4 – Control voltage source; 5 – First photodetector; 6 – Second photodetector; 7 – The photodetector's signal processing unit; 8 – Piezoelectric system of angular offset; 9 – Semitransparent parabolic mirror.

Device that implements this method has already been set as patent's application basis and been sent to ROSPATENT on December 21, 2013.

IV. SODIUM BISMUTHATE'S DOUBLE MOLYBDATE CRYSTAL

Acousto-optic deflector, discussed in this paper, has an acoustic line, made of sodium bismuthate's double molybdate grown by new technology – low thermal gradient Czochralski process. $NaBi(MoO_4)_2$ has has substantially the same acousto-optic effective as crystal $PbMoO_4$. Lead ions replacement, causes a significant reduction of thermomechanical damage, and consequently, makes the $NaBi(MoO_4)_2$ crystal more technologically advanced with comparison to $PbMoO_4$ crystal, because of smaller ionic radius of sodium and bismuth in comparison to lead.

Sodium bismuthate's double molybdate is almost completely similar to the crystal lead molybdate PbMoO4, but in contrast to it $NaBi(MoO_4)_2$ can withstand large temperature changes during processing (cutting and polishing). Unlike developed crystal bismuth sodium molybdate, some crystals of lead molybdate destroyed right in glugs. They cannot be cut into shapes for acoustic lines. Elements require additional annealing, what complicates the manufacturing technology of acousto-optic devices.

Sodium bismuthate's double molybdate can be well sawn and polished and requires no additional annealing. Crystal can be grown large enough – 40 mm in diameter (see Fig. 5).

This crystal of sodium bismuthate's double molybdate was grown by new technology – it was grown by low thermal gradient method in Nikolaev Institute of Inorganic Chemistry, Siberian Branch, Russian Academy of Sciences. (Novosibirsk) [3]. This method allows to create crystals with high structural perfection, and this was not available formerly with using ordinary Czochralski process.

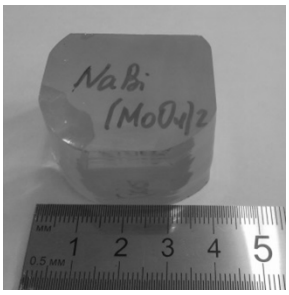

Fig. 5. $NaBi(MoO_4)_2$ crystal photo

Low gradient Czochralski process is significantly different from the traditional Czochralski process:

– the temperature variations in the melt which causes inhomogeneity of the crystal, becomes negligible;

– thermal tensions are reduced to a level, where they do not occur structure defects forming in crystals;

– ceed-holder rod input through the pipe, which plays the role of "diffuse gate", (and reduction of local overheating of the melt) suppresses the processes of decomposition and evaporation of the melt;

– gas inclusions do not result in increasing the density dislocation and tensions, and they often constitute a negative crystals (cavities that have faceting, equivalent to crystal matrix);

– layered growth mechanism becomes dominant, the crystallization front is almost always fully faceted.

It should be noted, that the gradient's reduction improves the working conditions of the heating element and increases its service life, since the same melt temperature of the heating element temperature in a low gradient is lower than for traditional version of Czochralski process. In addition, due to the suppression of melt evaporation, heater is well protected from interaction with the chemical elements that make up the melt, and the melt is protected with a cover and pipe from volatile compounds released from the heater.

For example, crystals of 4/m class, (it is double-bismuth molybdate class), the matrix of elasticity coefficients in the crystallographic axes XYZ has the form:

$$\begin{pmatrix} C_{11} & C_{12} & C_{13} & & & C_{16} \\ & C_{11} & C_{13} & & & -C_{16} \\ & & C_{33} & & & \\ & & & C_{44} & & \\ & & & & C_{44} & \\ & & & & & C_{66} \end{pmatrix}.$$

These elastic coefficients are: C11 = 10,674; C33 = 8,84; C44 = 2,57; C66 = 3,576; C12 = 5,197; C13 = 3,565; C16 = - 1,133.

Values are given in units of 10^{-10} N/m^2

X-ray analysis of two crystals $NaBi(MoO_4)_2$ – traditional and grown by the low thermal gradient Czochralski process was conducted.

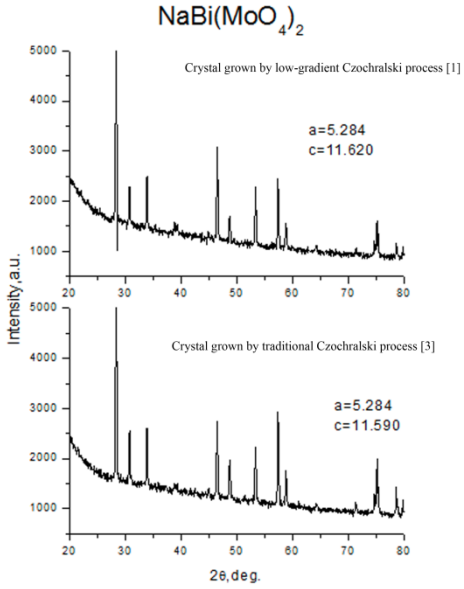

Fig. 6. X-ray structure analysis results

As follows from the X-ray analysis (see Fig. 6), the crystal grown by low thermal gradient Czochralski process has a larger index *c* of the crystal grating than the crystal grown by traditional Czochralski process [3].

V. ACOUSTO-OPTIC DEFLECTOR'S NUMBER OF RESOLUTION ELEMENTS CALCULATION

The main parameter of acousto-optic deflector is the number of resolution elements *N*. It corresponds either to the number of resolution frequency in the Fourier transform plane, or the number of resolution elements in the image plane. Number of resolved elements N can be defined as the ratio of the maximum deviation angle Δθ to the angular divergence of the optical beam λ/D, where D – diameter of the beam:

$$N = \frac{\Delta\theta D}{\lambda} \quad (2)$$

As

$$\Delta\theta = \frac{\lambda \Delta f}{V} \quad (3)$$

$$\frac{D}{V} = \tau \quad (4)$$

then

$$N = \tau \Delta f \quad (5)$$

i.e. *N* equal to the product transit time τ of the acoustic wave through the aperture of the optical beam *D* and bandwidth *Δf*. Therefore, it is necessary for deflector that the ratio of the angular divergence of the acoustic and optical waves was much smaller than one, i.e. $\alpha = \frac{\delta\theta_{opt}}{\delta\theta_{ac}} << 1$.

High-resolution devices require to have *N* as large as possible, but the value of *N* is limited by the

geometrical dimensions of the crystals and the acoustic damping. The first limiting factor is the geometric maximum permissible length of the acousto-optic deflector *D*.

Ratio $N = \tau\Delta f$, can be represented as

$$N = \frac{D}{2\Lambda} \tag{6}$$

where it is assumed that the relative band is maximum, i.e., $\Delta f = f0/2$.

Another restriction of the number of resolution elements can be set by considering the geometry of the beam divergence. The equation, which relatives the length L from the transducer in the near field distance (equivalent to D) to a point at half-power level (approximately 3 dB) – is

$$D = \frac{L^2}{2\Lambda} \tag{7}$$

Since the size of the acoustic beam in the scattering plane is

$$L = \frac{n\Lambda^2 Q}{2\pi\lambda} \tag{8}$$

number of resolution elements are defined as follows:

$$N = \left(\frac{n\Lambda Q}{4\pi\lambda}\right)^2 \tag{9}$$

The third principle restriction is the attenuation of the acoustic wave in the deflector, which can also be represented as a function of the acoustic wavelength Λ_0. If the attenuation at a frequency of 1 GHz, in decibels per unit of length is equal to γ, then the 3 dB attenuation corresponds to

$$D = \frac{3}{\gamma}\left(\frac{\Lambda}{\Lambda_0}\right)^2 \tag{10}$$

where Λ_0 – acoustic wavelength at 1 GHz. Substituting (9) into (5), we obtain the number of resolution elements

$$N = \frac{1{,}5\Lambda}{\gamma\Lambda_0^2} \tag{11}$$

Number of resolved elements, limited to these three independent parameters, is shown on figure 7 as an acoustic wavelength function.

The maximum number of resolvable beam's positions corresponding to the lower point of intersection of curves described by (6), (7) and (8). Plotting the dependence of the product of time bandwidth of the wavelength by choosing the material acousto-optical interaction in these expressions we can find operating frequency or length of the acoustic wave, and all other parameters.

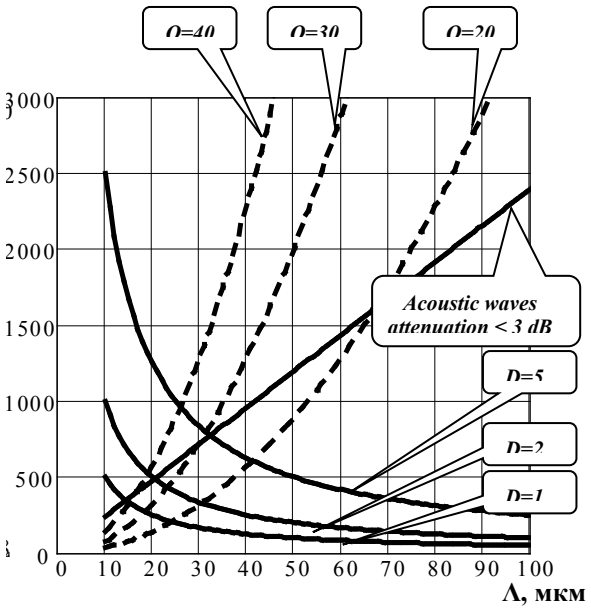

Fig. 7. Number of resolution elements N for $NaBi(MoO_4)_2$ crystal depends on wavelenth Λ

After a preliminary calculation we can define the requirements for the deflector's driver: the operating frequency or tuning range, output power and additional control functions of the output signal, served on an acousto-optical device.

VI. CONCLUSION

This paper shows what requirements limit Bragg diffraction mode preservation, which add-ons are necessary to make the optimal Bragg diffraction mode save as well as consider how they work. The most preferred system of crystal rotation was described.

Sodium bismuthate's double molybdate grown by new technology research allowed to find, that the crystal has a bigger index *c* of the crystal grating than the crystal grown by the traditional process.

Maximum number of resolvable beam positions calculated and shown, this important parameter of acousto-optic deflector may depend on

VII. REFERENCES

[1] Magdich L.N., Molchanov V. Ya. Akustoopticheskye ustroystva I ikh primeneniye. M.: "Sov. Radio" 1978, 112p

[2] Saleh B.E.A., Teich M.C. Fundamentals of Photonics, 2nd ed. - Wiley-Interscience, 2007, 1177 pages ISBN 978-5-91559-135-5

[3] Pavlyuk A.A., Vasiliev Ya.V., Kharchenko L.Yu., Kuznetsov F.A. Low thermal* *gradient technique and method for large oxide crystals growth from melt and flux // Proceeding of APSAM-92*. *Published in Japan. 1993. P. 164--171

[4] Petrenko S. F. P'ezoelektricheskiy dvigatel' v priborostroenii. – K. "Korshchuk", 2002.- 98p ISBN 966-7599-24-8

MATHEMATICAL AND SIMULATION MODELS OF ECHO SIGNALS OF ATMOSPHERIC INHOMOGENEITIES

George Kuyumchev

Imperial College Business School,
London, UK

I. INTRODUCTION

Development of devices used for detection of atmosphere inhomogeneities and tracking the movements of dense atmospheric meteorological formations, requires mathematical, in particular simulation models of these atmospheric processes. This include atmospheric formations caused by human activities – clouds of pollutants, dust clouds, etc.

This paper presents mathematical and imitational models of echo signals of atmospheric inhomogeneities in the centimetre range of electromagnetic waves. Dense meteorological formations of natural origin (rain, snow, hail, dense fog), and clouds (artificial harmful atmospheric emissions, smoke screens, etc.) are considered as inhomogeneities.

II. MATHEMATICAL AND SIMULATION MODELS OF ECHO SIGNALS OF ATMOSPHERIC INHOMOGENEITIES

In constructing mathematical model of fluctuations of the echo signals of atmospheric inhomogeneities we should take into account the fact that, the echo signals of inhomogeneities in the centimetre range are narrowband and spectrum of its fluctuations can be considered symmetrical with respect to the carrier frequency of probing signal. This fact allows us to consider two quadrature process defined, regarding the carrier frequency (taking into account the Doppler corrections), as two independent processes.

Thus, it is necessary to define and build a mathematical model of two quadrature random processes (processes or random fluctuations of the initial phase and of the envelope). In practice, often only statistical properties of the envelope process or its square are known. In this case, the experimental data allows us to determine the one-dimensional distribution law of the envelope of signal spectrum, width of spectrum fluctuations and the frequency corresponding to the spectrum mode, the rest of the characteristics are determined by the physical model adopted to describe the reflection of electromagnetic waves [1].

Based on the above, the observed echo signal of atmospheric irregularities can be written as

$$S(t) = A(t)\cos\left[\left(\omega_0 + \omega_g\right)t - \varphi(t)\right], \quad (1)$$

where $A(t)$ and $\varphi(t)$ – random processes, describe an envelope fluctuation and the initial phase of the echo signal, ω_0 – carrier frequency, also can be considered as an intermediate frequency of locator receiver) , and ω_g – the Doppler correction to the carrier, ω_g is proportional to the radial velocity of the wind v_R.

For modeling the device of optical observation of atmospheric inhomogeneities, we need to define quadrature of process $U(t)$ and $V(t)$ relative to ω_0. Then we get

$$\begin{aligned} S(t) &= A(t)\cos\left(\left(\omega_0 + \omega_g\right)t - \varphi(t)\right) = \\ &= A(t)\cos\left(\omega_g t - \varphi(t)\right)\cos\omega_0 t + \\ &+ A(t)\sin\left(\omega_g t - \varphi(t)\right)\sin\omega_0 t = \\ &= U^*(t)\cos\omega_0 t + V^*(t)\sin\omega_0 t, \end{aligned} \quad (2)$$

where * means that that quadrature $U^*(t)$ and $V^*(t)$ are defined not relative to the central frequency $\omega_0 + \omega_g$, but relative ω_0, when $v_R = 0$, $\omega_g = 0$, $U^*(t) = U(t)$, $V^*(t) = V(t)$.

Atmospheric inhomogeneities are volumetrically distributed objects, which can be represented as a large collection of independent elementary reflectors. Such a physical model leads to a normal distribution and quadrature, respectively, to the Rayleigh distribution of the envelope, this conclusion is confirmed by experimental data. As for the correlation and spectral characteristics, they were only research for envelope of echoes signals of atmospheric inhomogeneities. As a curve approximating the spectrum of the signal a variety of curves are usually used. Most often shifted Gaussian curve is used, where shift is determined by the Doppler frequency. Real spectre of reflected signals may differ from such an approximation. Therefore, to build simulation model we will take the Rayleigh law of the signal envelope and will not make any restrictive assumptions relative correlation and spectral properties. This will help to bring the results of the simulation of devices to the real conditions of their work. Simulation model of atmospheric inhomogeneities is determined by the modeling algorithm of fluc-

tuations of vector quadrature $\left(\mathrm{U}^*,\mathrm{V}^*\right)$ or amplitude-phase vector $\left(\mathrm{A},\varphi\right)$. We will construct quadrature simulation model. Conditional distributions $w\left(U_k,V_k/\mathbf{U}_{k-1},\mathbf{V}_{k-1}\right)$ are normal. Given a correlation function $R_u\left(\tau\right)=R_v\left(\tau\right)$ at a wind speed $v_R=0$, i.e. in the case of $\omega_g=0$. Then, because of the independence of the vectors U and V, correlation matrix $\left\|\mathbf{D}_{2k}\right\|$ of normal density distribution $w\left(\mathbf{U}_k,\mathbf{V}_k\right)$ when $V_R=0$ can be represented in the block form.

$$\left\|\mathbf{D}_{2k}\right\|=\begin{Vmatrix}\left\|D_k^{(U)}\right\| & \|0\| \\ \|0\| & \left\|D_k^{(V)}\right\|\end{Vmatrix}, \qquad (3)$$

where $\left\|D_k^{(U)}\right\|=\left\|D_k^{(V)}\right\|$ – matrix of correlation coefficients of echo signals quadrature.

Conditional distributions of random variables U_k and V_k are normal, and with the block matrix $\left\|\mathbf{D}_{2k}\right\|$, parameters of their conditional density of distribution are given by similar expressions given in [3]

$$\begin{cases}\bar{U}'_k=-\sum\limits_{i=1}^{k-1}\left(D_{i,k}^{(U)}/D_{k-1}^{(U)}\right)\cdot U_i,\\ \bar{V}'_k=-\sum\limits_{i=1}^{k-1}\left(D_{i,k}^{(V)}/D_{k-1}^{(V)}\right)\cdot V_i,\\ \sigma'_{U_k}=\sigma'_{V_k}=\sigma_{U_k}\sqrt{\left(D_k^{(U)}/D_{k-1}^{(U)}\right)}=\sigma_{V_k}\sqrt{\left(D_k^{(V)}/D_{k-1}^{V}\right)}.\end{cases} \qquad (4)$$

where $\bar{U}'_k,\bar{V}'_k$ – conditional means, $\sigma'^{\,2}_{U_k}=\sigma'^{\,2}_{V_k}$ – conditional dispersions of quadrature, $D_{i,k}^{(\cdot)}$ - cofactors of the corresponding elements of the matrices $\left\|D_k^{(U)}\right\|=\left\|D_k^{(V)}\right\|$. Hence, taking into account the independence of vectors $\mathbf{U}_k$ and $\mathbf{V}_k$, we get a simulation model of signals of atmospheric inhomogeneities when $v_R=0$.

$$\begin{cases}U_k=\bar{U}'_k-\sigma'_{U_k}\cdot\xi_i=\\ -\sum\limits_{i=1}^{k-1}\left(D_{i,k}^{(U)}/D_{k-1}^{(U)}\right)\cdot U_i+\sigma_{U_k}\sqrt{\left(D_k^{(U)}/D_{k-1}^{(U)}\right)}\cdot\xi_k,\\ V_k=\bar{V}'_k-\sigma'_{V_k}\cdot\eta_i=\\ -\sum\limits_{i=1}^{k-1}\left(D_{i,k}^{(V)}/D_{k-1}^{(V)}\right)\cdot V_i+\sigma_{V_k}\sqrt{\left(D_k^{(V)}/D_{k-1}^{V}\right)}\cdot\eta_k,\ k\ge 2,\end{cases} \qquad (5)$$

where ξ_k and $\eta_k, k=1,2,...,$ jointly independent normal random variables, each of which is normally distributed with zero mean and unit dispersion.

Taking into account that

$$\begin{cases}U_k^*=U_k\cdot\cos\left(\omega_g\cdot\Delta t\cdot k\right)-V_k\cdot\sin\left(\omega_g\cdot\Delta t\cdot k\right),\\ V_k^*=V_k\cdot\cos\left(\omega_g\cdot\Delta t\cdot k\right)+U_k\cdot\sin\left(\omega_g\cdot\Delta t\cdot k\right),\end{cases} \qquad (6)$$

where Δt – interval between samples of a continuous signal. After transformations we obtain a simulation model for $v_R\ge 0$

$$\begin{cases}U_k=-\sum\limits_{i=1}^{k-1}\left(D_{i,k}^{(U)}/D_{k-1}^{(U)}\right)\cdot\left[U_i\cdot\cos\left(\omega_g\cdot\Delta t\cdot k\right)-V_i\cdot\sin\left(\omega_g\cdot\Delta t\cdot k\right)\right]+\\ \quad+\sigma_{U_k}\sqrt{\left(D_k^{(U)}/D_{k-1}^{(U)}\right)}\cdot\left[\xi_k\cdot\cos\left(\omega_g\cdot\Delta t\cdot k\right)-\eta_k\cdot\sin\left(\omega_g\cdot\Delta t\cdot k\right)\right],\\ V_k=-\sum\limits_{i=1}^{k-1}\left(D_{i,k}^{(V)}/D_{k-1}^{(V)}\right)\cdot\left[V_i\cdot\cos\left(\omega_g\cdot\Delta t\cdot k\right)+U_i\cdot\sin\left(\omega_g\cdot\Delta t\cdot k\right)\right]+\\ \quad+\sigma_{V_k}\sqrt{\left(D_k^{(V)}/D_{k-1}^{V}\right)}\cdot\left[\eta_k\cdot\cos\left(\omega_g\cdot\Delta t\cdot k\right)+\xi_k\cdot\sin\left(\omega_g\cdot\Delta t\cdot k\right)\right].\end{cases} \qquad (7)$$

Expression (7) completely determines the quadrature simulation model of atmospheric inhomogeneities.p

III. REFERENCES

[1] Шепета Д.А. Разработка математических моделей и синтез алгоритмов моделирования входных сигналов бортовых систем обработки информации и управления. Автореферат диссертации на соискание ученой степени кандидата технических наук / Санкт-Петербург, 2000.

[2] Изранцев В.В., Шепета Д.А. Моделирование внешних сигналов бортовых приборных комплексов летательных аппаратов пятого поколения. Научное приборостроение. 2000. Т. 10. № 2. С. 14-19.

[3] Бессонов А.А., Сесин А.Е., Шепета А.П. Математические и имитационные модели морской поверхности. Аэрокосмическое приборостроение России. Серия 2. Авионика. СПб., 2005, с. 52-69.

MULTI-VARIABLES PROTOCOL FOR WSNS WITH TRANSMIT ONLY NODES

Maria Barbara Cristina Lombardo

Catania University,
Catania, Italy

Abstract

Wireless Sensor Networks (WSNs) with transmit-only nodes defines an attractive scenario due to their low cost production and deployment and energy efficiency. This kinds of networks need to transmit different type of data with low bit-rate, low power consumption and a simple protocol that support only transmit nodes. Due to the low price needs, the protocol must be simple, so it can be implemented into processor or microcontroller with limited computing resources. This study presents a WSN with pure transmit-only nodes and a simple protocol that allows transmission of different kinds of data in a compact frame to support a low bit-rate of wireless cannel. The scenario is a single-hop network that allows transferring different kinds of sensed data. This work also proposes an implementation of the protocol on a8-bit microcontroller (STM8S) and a really simple and cheap radio transceiver that provide a low bit-rate and low power transmission on 433 MHz ISM band.

Index Terms – Wireless sensor networks, transmit-only node, Internet of things, data communication, low power

I. INTRODUCTION

WSNs represent a very interesting scenario and it is a fundamental part of IoT [1]. The objects interconnection capabilities and their ability to measure environmental parameters and transfer them to sink node represent the main features of IoT. Wireless communication mechanisms support in a best way the interconnection capabilities of objects. In the last years wireless communication systems are grow up in number and types. The high diffusion level of wireless communication systems has cut down production cost of the transmission devices. WSNs scenario is useful for modern agricultural systems such as precision agriculture [2, 3] and Body Area Networks [4]. Generally, a wireless communication system needs a battery power supply, so it is necessary to identify a low power device and communication mechanisms that may be support energy harvesting [5]. It is necessary to pervasive distribute a large number of device in the environment, this involves that low power feature must be combined with the low devices cost. In order to support low price and power, the target devices for WSNs have a low computing capacity, so the communication mechanism must as simple as possible to easily implement it in a different kinds of devices.

The wireless scenario involves different kinds of problems:

– protocols and managements issues [6], it is necessary define right network mechanisms and protocols that support low bit rate, different devices and low computing capacity;

– systemic and electronics issues, the hardware of the system must provide a good combination of device's cost, power consumption and price;

– radio modulation, the radio physical level must be provide efficient modulation strategy to reduce power consumption and/or increase link budget.

The overall system cost affects the adoption of the technology. A good piece of cost depends on communication transceivers used to provide wireless communication channels. In order to reduce system cost transmit only nodes have received increased attention. This kind of node generally transmit data to a sink node in a single hop network topology. The transmit-only node provided data must be have low Quality of Service needs because it is impossible guarantee that data are delivered to the sink, the only way to define data reliability is retransmission. The transmit-only node allows defining simple mechanism, reducing power consumption and cost of device, so represent a good solution for WSNs.

Transmit-only node scenario is widely analysed from different point of view [7, 8] but in general, it is provide a mesh scenario with fully equipped node. This scenario allows a handshake between fully equipped nodes that allows a transmission schedule that optimize global network performance. Some study consider the transmit only node into the network topology [9, 10] but propose a mixed scenario in which there are transmit-only and fully equipped nodes. The mixed scenario generally defines two level of QoS, high level scheduled transmission between fully equipped nodes (in general there is a node master that schedule transmission when the channel is empty) and low level QoS transmission for transmit-only nodes. The protocol described in this study is implemented in a PURE transmit only scenario and provide an efficient mechanism that allows transferring of different kind of data for each node. Each node may communicate different kinds of data in the same communication with optimized overhead to respect the low bit rate constraint of the general WSNs wireless links.

The paper is organized as follow. Section II provide a description of proposed PulseNET protocols, the section provide a description of communication structure and a description of process to provide network management and data exchange. Section III presents a real world implementation with low-power, low-cost and low computing capacity hardware module. The implementation is deployed on 8-bit microcontroller (STM8S) and use a 433 MHz radio transceiver that provide AM-OOK modulation with low power consumption. Section IV provide a description of test and measure that validate the protocol features and functionality.

II. PULSENET

PulseNET is a transmission protocol that provide a single hop wireless communication and support pure transmit-only node networks topology. The protocol allows data transferring of short data (like sensor data) and provide a set of features to support different types of data. The supported data may be differ for the format and for the timing. The protocol has a target to define a efficient way to transfer sensor data.

A. Application Scenario

The network scenario is composed of a lot of transmit only nodes that acquire data from different wired connected sensors. Each sensor acquire environmental short data like temperature, pressure, etc. Fig.1 describes networks topology. The Sink node collects data from all transmit nodes inside its radio coverage. The sink node does following tasks:

- collects data from transmit node;
- evaluates collision probability;
- finds non reachable nodes.

B. Protocol

The PulseNet protocol provides following features:

- high protocol flexibility and extensibility;
- carry different kind of data together;
- high frame efficiency;
- payload with variable length.

To implement the above features PulseNET defines two protocol levels. DLL manges physical data format. Application layer that support data transferring.

PulseNET is a unidirectional protocol without confirmation. In this scenario the transport layer, internet layer and other ISO/OSI layers are not useful.

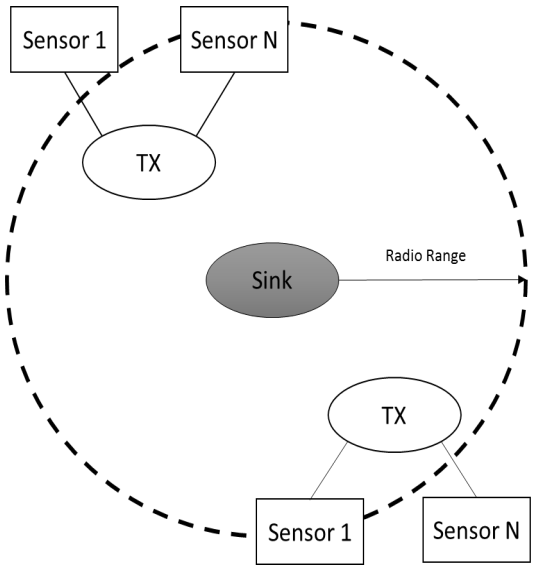

Fig. 1. Network Scenario

C. Data link layer

Data link layer provide a frame model that directly send to the radio channel. The frame consist of an header that identify the source node and carries node status informations, a variable length payload (1÷256) to transfer application data and a CRC to verify frame. Fig. 2 show the frame format. The frame header contains information about frame sequence and protocol version (CL).

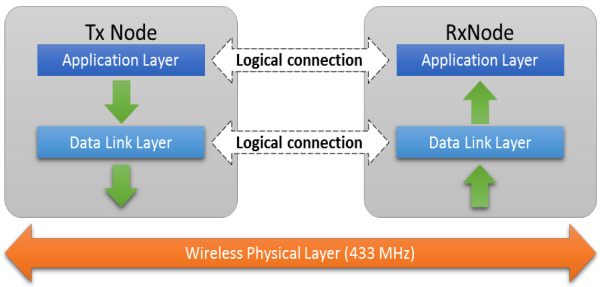

Fig. 2 Protocols Layers

D. Application layer

The application layer define all the functions to register and transfer data from sender to the sink node. Application defines two networks phase. Registration phase in which a transmission node send information about data format and timing of data collected. Data phase in which a transmit node produce data collected from the sensors.

A registration packet encapsulate some information about the data characteristics. The packet format define a packet header that define a packet type and the number of data variable that node want to register. After the header the protocol defines a variable number of registration record. Each registration record allows to describe a variable that node wants to transmit. Each variable is completely defined through this record that contains, a particular field (IL) that de-

scribe variable and information about variable scheduling. IL field (Fig. 3) contains information about data, in particular it provides a data identifier (5 most significant bit of IL) and the data size in byte with 1-8 range (3 less significant bit of IL). The TP field provide a transmission period instead TMR represent a maximum time deviation from TP, so a sender may be send a variable each TP but in order to decrease the collision probability it transmits with a random time between TP and TP + TMR.

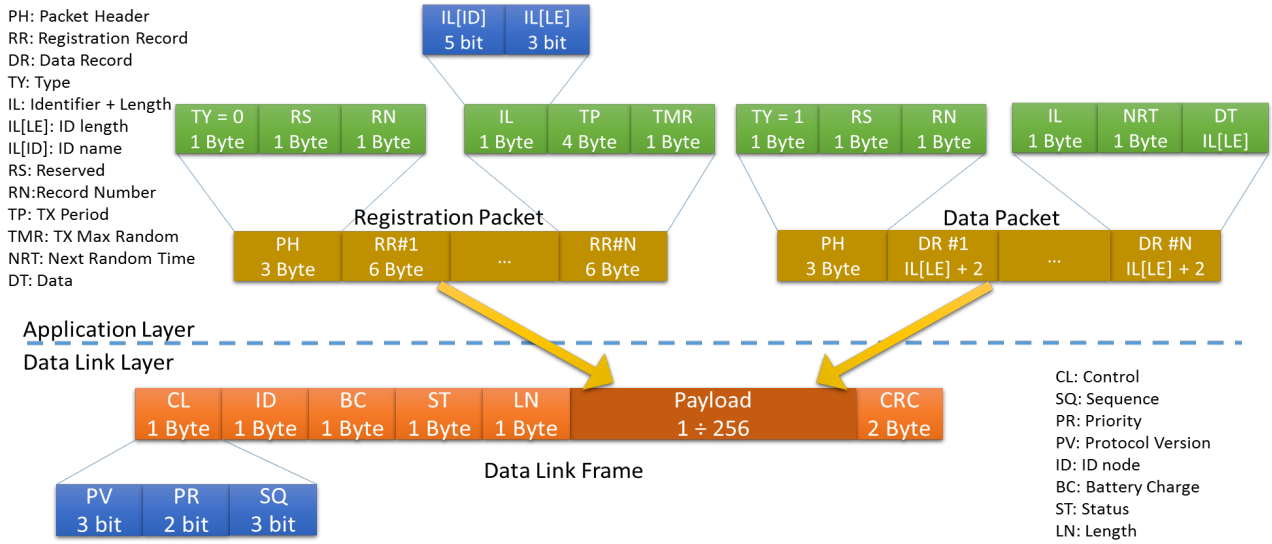

Fig. 3: Network Encapsulation Process

The data packet has same format of registration. It defines a packet header and a set of data record. A data record contains acquired sensors data in detail it carries a IL fields, a NRT that represent the pre-calculated time deviation of next packet that will carry this data, and the measured data. The NRT field provide a way to define a receiver sleep process, because the receiver know the next arrival time so it may be switch off itself to provide energy efficiency. The NRT also provide a useful information to estimate collision probability between packets from different nodes.

E. Transmit Process

The transmit process is really simple. Each node must provide two functionalities: variables registration and data communication. The switch between the two operational modes may be managed through external events generation like button pressure. In the data communication phase the transmit node will also provide a NRT for next packet randomly between 0 and TMR, this value must be encapsulate into data record.

Before each frame the transmit process send a preamble in order to synchronize the receiver. The last preamble byte is a start byte that define the start of the frame.

F. Receiver Process

The receiver process is more complex them the transmitter. The receiver must manage data from all transmit nodes and all variable for each node. It also verify the network status.

G. State diagram

In order to formalize frame receiver process PulseNET receiver defines a State Diagram shows in Fig. 4. Each state except wait_start implement a timeout mechanism. This timeout improve receiver robustness because allows to exclude data become from other source that transmit on the same wireless channel.

As described in state digram the receiver wait for start byte. When sink receive a start byte it goes to the receive_header state in which the wait for the header. When the header are completely received the process check the header correctness and if it is correct go to the receive_payload status. The sink persists on this state while receiving payload. When the payload become completed the receiver wait for the CRC. The last state verify frame CRC and send an indication to the upper layer.

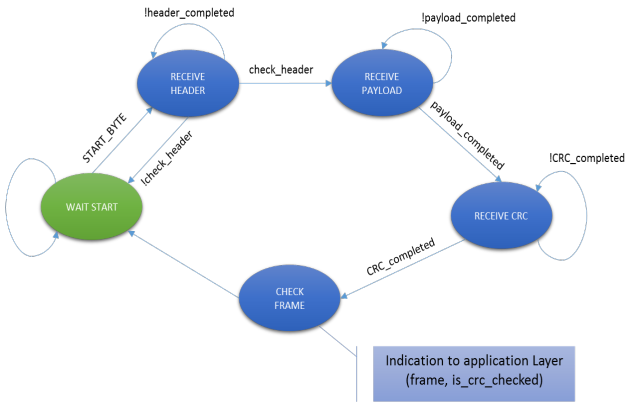

Fig. 2. Receiver State Machine

H. Application

Application level provide the packet data interpretation, after this it persist the extracted data. In order to store data the receiver define a specific structure that allows data storage.

Fig. 5 shows data memorization structure. The receiver needs to define a structure for each node that want to manage.

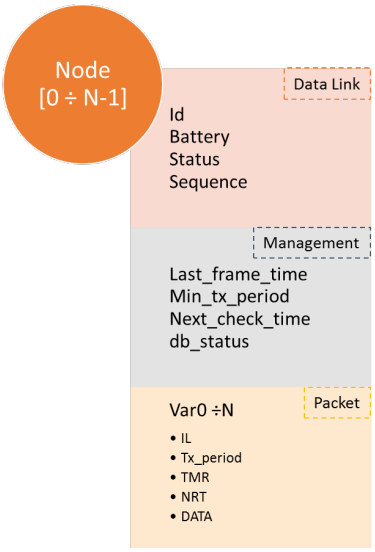

Fig. 3 Receiver, DB structure

Each DB elements maintain information about data and also management information. Db_status field define the data status on the DB of node with ID. The status can be EMPTY if the structure is unused, VALID if the structure provide a valid node's data and DEATH if the structure maintains data of non-reachable node. last_frame_time represent the last frame timestamp.

I. Node dead algorithm

The node status become DEATH when the sink node could not reach a node. A node become unreachable according the number of frame not received by the sink. In particular the sink define a parameter that represent the number of transmission lost before to set the node DEATH. The algorithm is based on time consideration. A node could be transfer different variables so receive process define the "node dead" when it wait for a time >= of minimum variable transmission period (min_tc_perido).

III. IMPLEMENTATION

This section presents an implementation of PulseNET protocol. The implementation's purpose is to show a real protocol's performance on low-power, low computing capacity hardware architecture. In detail this study describe a c-language implementation on really simple and cheap devices. The hardware implementation allows to check all protocol's features.

A. Hardware

The selected hardware respects following properties: low-power consumption, really simple processor's architecture and low-price of hardware components.

The hardware architecture consists of a two main modules: the transmitter and the receiver. In both hardware part the selected processors is STM8S, 8-bit microcontroller provided from ST Microelectronic. The selected transceiver are low-price modules that provides AM-OOK modulation on the ISM band of 433 MHz. The transmission transceiver supplies a radio power of 10 mW. Fig. 6 shows the implemented system.

The microcontroller is connected to the transceiver with a serial UART. The implementation use a UART bit rate of 600 bps.

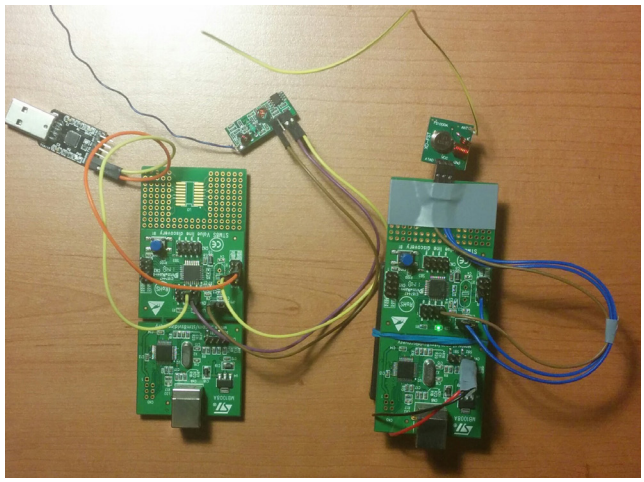

Fig. 6. Hardware

B. Software organization

PulseNET protocol can be easily implemented on different kind of devices. In order to provide software portability the protocols layers are developed as external library to integrate into platform dependent software. The library does not use platform dependent library. All library code respect ANSI C specification. All protocol's structures are declared on specific layer header files.

The implementation defines two header files one for each protocol layer. An interesting feature is the c union usage to map frame and packet field. The union is really useful for IL field and other bitmask field.

Following an example of union usage into the implementation:

```
/**
 * IL field of packet record.
 * This field allows identifying the variable
 * to send/register and its length in bytes.
 */
typedef struct PN_APP_IL_FIELD {
        union {
                unsigned char field;
                struct {
                        unsigned char length:3;    /**< Variable length in bytes */
                        unsigned char id:5;                /**< Variable identifier */
                };
        };
}pn_app_IL_field_t;
```

C. Death node implementation

Death node process is a platform dependent task. The software uses a timer based strategy to verify node status. The strategy adopts next_check_time parameter provided from the DB (Fig. 6). For each DB persisted nodes the parameter takes following value:

$$next_1 check_1 time = \min_1 tx_1 period * N \qquad (1)$$

where N – number of frames not received consecutively.

For each received frame the receiver calculates the next_check_time (NCT) according (1). After the first frame reception the NCT has a time period value that is N times the period of the most frequently node's variable. The software implement an interrupts based process that uses a timer to decrement the NCT value. If NCT assumes a 0 value then the receiver suppose that the transmitter does not send N frame consecutively so it set the node's status to DEATH.

D. Transmitter implementation

The transmitter can be send two types of packets: registration packet and data packet. The implementation suppose two transmission phase. A registration phase in which the node transmits only registration packets and a data phase in which the node transmits data packet according the variables period. The phases switch is controlled through the button pressure event.

Led of the STM8S development board is used to communicate the transmitter status. When the led are in blinking status the transmitter is in registration phase. When led is fixed the transmitter is in data phase.

E. Debugger

In order to debug the receiver functionality the software provide output on STM8S UART port. The receiver send on serial port following information: the right frame receptions, frame header error, frame CRC error, transmitter status change and DB status. The DB status are send on serial port when the STM8S receive a button event, other information are printed automatically.

IV. TEST AND MEASURES

This section show a set of test to verify protocol features and capability. The implemented protocol work right on the systems. The test performed check also node death routine that work well with the proposed solution.

To evaluate the radio performance the study present a set of measure that shows the protocol capabilities.

A. Radio performance

Scenario:

- 1 Transmitter
  - Data burst of 100 frames
  - Wait time between two frame 50 ms
  - Frame length 16 byte
  - Bitrate: 600bps
  - 2 preamble bytes
  - 1 start byte
- 1 Sink node

The test are performed at different distance to evaluate the radio performance. Fig. 7 shows the result. The system pro-vide a really short range transmission. In detail the transmission are reliable inside a 10 m of radius from the sink after this the system loss more than 30% of data. Over 20m of distance the performance rapidly decrease and after 30m the sink does not receive any packets. This performance are justified from the low radio transmit power and the low price of transceiver module. The performance may be improved through an impedance matching of antenna.

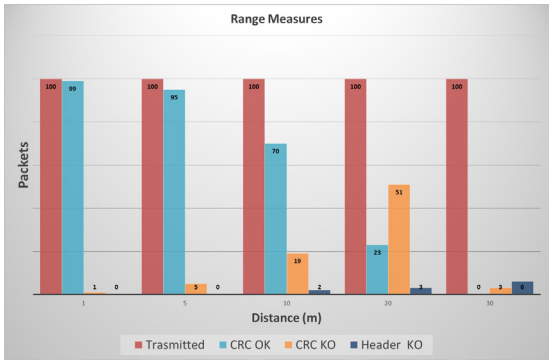

Fig. 7 Range Measure performance

V. REFERENCES

[1] L. Atzori, A. Iera, and G. Morabito, "The Internet of Things: A survey,"Computer Networks, vol. 54, no. 15, pp. 2787–2805, 2010.

[2] Z. F. Sun, M. K. Du and S. Y. Yin, "Development trend of Internet of things and perspective of its application in agriculture", Agriculture Internet Information, vol. 5(4), 2012, pp. 5-8.

[3] Liansheng Wang, Dongyan Xia, Wangyuan,Shujian Song. Study on modern water-saving irrigation based on the internet of things[J]. Science Technology and Engineering, 2011,11(10):7393- 395.

[4] Body Area Networks: A Survey. Chen, M., et al. 2011, Mobile Networks and Applications, Vol. 16, p. 171-193.

[5] HYPERLINK "http://ieeexplore.ieee.org/search/searchresult.jsp?searchWithin=p_Authors:.QT.Prasad,%20R.V..QT.&newsearch=true" Prasad, R.V. ; HYPERLINK "http://ieeexplore.ieee.org/search/searchresult.jsp?searchWithin=p_Authors:.QT.Devasenapathy,%20S..QT.&newsearch=true" Devasenapathy, S. ; HYPERLINK "http://ieeexplore.ieee.org/search/searchresult.jsp?searchWithin=p_Authors:.QT.Rao,%20V.S..QT.&newsearch=true" Rao, V.S. ; HYPERLINK "http://ieeexplore.ieee.org/search/searchresult.jsp?searchWithin=p_Authors:.QT.Vazifehdan,%20J..QT.&newsearch=true" Vazifehdan J, "Reincarnation in the Ambiance: Devices and Networks with Energy Harvesting", IEEE HYPERLINK "http://ieeexplore.ieee.org/xpl/RecentIssue.jsp?punumber=9739" Communications Surveys & Tutorials, Volume: 16 , HYPERLINK "http://ieeexplore.ieee.org/xpl/tocresult.jsp?isnumber=6734841" Issue: 1

[6] Improve Efficiency and Reliability in Single-Hop WSNs with Transmit-Only Nodes. Zhao, Jia, et al. 3, 2013, IEEE TRANSACTIONS ON PARALLEL AND DISTRIBUTED SYSTEMS, Vol. 24, pp. 520-534.

[7] A. Somasundara, A. Ramamoorthy, and M. Srivastava, "Mobile element scheduling for efficient data collection in wireless sensor networks with dynamic deadlines," in Proceedings of the 25th IEEE International Real- Time Systems Symposium, 2004, pp. 296–305.

[8] G. Fabeck, D. Bielefeld, and R. Mathar, "Power-aware sensor selection for distributed detection in wireless sensor networks," in IEEE Veh. Technol. Conf. Fall (VTC-Fall), 2009.

[9] B. Blaszczyszyn and B. Radunovic, "Using transmit-only sensors toreduce deployment cost of wireless sensor networks," in INFOCOM,2008, pp 1202–1210.

[10] B. Radunovic, H. Truong, and M. Weisenhorn, "Receiver architectures for UWB-based transmit-only sensor networks," in Proc. Int. Conf. Ultra-Wideband (ICU), 2005, pp. 379–384.

ALGORITHMS FOR SIMULATION OF THE SIGNALS REFLECTED BY THE SEA SURFACE

Vadim Nenashev

Saint-Petersburg State University of Aerospace Instrumentation,
Saint-Petersburg, Russia

nenashev.va@gmail.com

Abstract

Simulation algorithms of reflected by a sea surface the radar signals are considered in this paper. Such algorithms are necessary in design of onboard radio-electronic complexes case, especially in case of seminatural equipment simulation and in case of debugging the onboard computing systems software.

The characteristics of the multi-channel radio-electronic complexes, that contain difficult non-linear devices and instruments, are determined with the help of mathematical simulation computer methods. Thus it is necessary to construct simulation models of all input signals of devices, and implement algorithm of data handling. If simulation models are constructed on the basis of the experimental data, the method of mathematical simulation, in fact, is the machine experiment that allows to receive "experimentally" characteristics of quality of designed devices and instruments for situations which are close to real operating conditions of created equipment.

Methods of mathematical simulation have found a broad application in modern technical systems research, for example in case of sea surface observation for the purpose of timely detection of its pollution (oil spill, etc.). It has become possible due to the rapid development of electronic computing machine equipment, especially personal machines development, allowing to carryout the analysis of difficult systems for the rather short terms. The synthesis simulation algorithms tasks in the software of the modern computers, their inclusion in standard libraries and the connection of the appropriate software products to widespread application program packages, are the questions of exceptional importance.

The simulation with use of mathematical, seminatural and simulation models allows to carryout complex research of technical systems, impossible in case of full-scale tests to solve the exceptional complexity problems, unavailable to analytical methods [1]. For the modern difficult non-linear dynamic information measuring systems and management systems the similar problem is solved only by methods of statistical modeling with use of the modern computers.

Simulating complexes became a powerful and universal remedy of difficult information and measuring and controlling systems research. Nearly all types of simulation are applied practically on complexes. Complexes creation problems, the simulation process organization on them, task of analog-to-digital simulation are very difficult and knowledge-intensive, therefore in this paper authors were restricted to reviewing of sea surface simulation models. These models were used in case of mathematical and seminatural simulation of perspective onboard systems and had showed the efficiency in case of the solution of practical questions of engineering. Models allow define characteristics of considered options of creation of equipment before its real creation [2].

For a simulation model of a sea surface the set of parameters can be defined as a set of counting of the reflected signal envelope – vector $\mathbf{A}_L$, where L dimensionality of a vector (number of countings). For frequency distribution curve of a vector $\mathbf{A}_L$ we will accept multivariate normal logarithmic frequency $w(\mathbf{A}_L)$ curve which is most often used in case of the description of fluctuations of the signals reflected by a sea surface [2].

For algorithm of simulation of a vector $\mathbf{A}_L$ it is necessary to calculate the conditional frequency $w(A_L / \mathbf{A}_{L-1})$ curves, for $L = 2,3\ldots$. In general case for $L \geq 2$ $w(A_L / \mathbf{A}_{L-1})$ stated as [3].

$$w(A_L / \mathbf{A}_{L-1}) = \frac{w(\mathbf{A}_L)}{\int_0^\infty w(\mathbf{A}_L)\, dA_L} = \frac{1}{\sqrt{2\pi}\sigma'_L A_L} \cdot \exp\left(-\frac{1}{2{\sigma'_L}^2} \ln^2 \frac{A_L}{\overline{A}'_L} \right), \quad (1)$$

where

$$\begin{cases} \overline{A}'_L = \overline{A}_L \cdot \exp\left(-\sum_{l=1}^{L-1} \frac{\sigma_L D_{l,L}}{\sigma_l D_{L-1}} \ln \frac{A_l}{\overline{A}_l} \right), \\ \sigma'_{A_L} = \sigma_{A_L} \cdot \sqrt{D_L / D_{L-1}}. \end{cases} \quad (2)$$

Parameters $\overline{A}'_L$ and σ'_L are associated with energetic characteristics of the reflected signals and observation of a sea surface conditions of the expres-

sions given in [2, 3]. Values $D_{l,L}, D_{L-1}, D_L$ – matrices' determinants composed of logarithm coefficients correlation of signal envelope counting's. The elements of these matrices are defined by the empirical dependences given in [3].

The simulation model of a signal of a sea background is defined the same as in [3]

$$A_L = \overline{A}'_L \cdot \exp\left(\sigma_L \xi_L\right) = \\ = \overline{A}_L \cdot \exp\left[-\sum_{l=1}^{L-1} \frac{D_{l,L}}{D_L} \frac{\sigma_L}{\sigma_l} \ln \frac{A_l}{\overline{A}_l} + \sigma_L \cdot \sqrt{\frac{D_L}{D_{L-1}}} \cdot \xi_L \right], \quad (3)$$

in case $L = 1$ of it is necessary to suppose $\overline{A}'_1 = \overline{A}_1$ and $\sigma'_1 = \sigma_1$. The algorithm (3) allows to simulate envelope fluctuations in case of arbitrary spatially temporal correlative function, but complexity of algorithm increases in process of increase in the next estimated counting of an envelope. Except this shortcoming which is a consequence of universality of algorithm, practical difficulty of its usage consists as well in absence of reliable experimental data according to spatially correlative characteristics of signals.

For conditions of sea surface observation in case of small angles of sighting, it is possible to construct more effective (high-speed performance) algorithms of simulation of the countings that use only a sections of space-time correlative function. Thus it is necessary to use double-index recordings of a set of envelope countings of the reflected signal, i.e. vector $\mathbf{A}_L$ represents in the form of the matrix $\mathbf{A}_{N\times M}$. Matrix $\mathbf{A}_{N\times M}$ lines represent countings in a strobe of the receiving device of onboard system, and columns - the separate temporal line items of a strobe watched sequentially in time.

The signal model of a background simulation in case of these restrictions can be introduced in the form

$$\begin{cases} \eta_{i,j} = -\sum_{l=1}^{j-1} \left(D_{l,j}^{(\Pi)} / D_{j-1}^{(\Pi)} \right) \eta_{i,l} + \sqrt{D_j^{(\Pi)} / D_{j-1}^{(\Pi)}} \xi_{i,j}, \\ h_{i,j} = -\sum_{p=1}^{j-1} \left(D_{p,i}^{(B)} / D_{i-1}^{(B)} \right) h_{l,l} + \sqrt{D_i^{(B)} / D_{i-1}^{(B)}} \xi_{i,j}, \quad (4) \\ A_{i,j} = \overline{A}_{i,j} \cdot \exp\left(\sigma_{i,j}\right), \; j \in [1, M], \; i \in [1, N], \end{cases}$$

where $D_{i,j}^{(\Pi)}, D_{j-1}^{(\Pi)}, D_j^{(\Pi)}, D_{i,j}^{(B)}, D_{j-1}^{(B)}, D_j^{(B)}$ – the matrices' determinants composed of the correlation coefficients of the spaced along space and time coordinates signal envelope samples logarithms.
Relevant empirical relationships given in [4].

From the expressions (4) the algorithm for calculating the next value $A_{i,j}$ follows - line by line calculation of matrix elements $\mathbf{A}_{N\times M}$.

Step 1: Vector $\xi_1 = \left(\xi_{1,1}, \xi_{1,2} \ldots \xi_{1,M}\right)$ formation - vector of normally distributed independent random variables with zero mean and unit variance.

Step 2: Vector $\eta_1 = \left(\eta_{1,1}, \eta_{1,2} \ldots \eta_{1,M}\right)$ calculation.

Step 3: Vector $\mathbf{h}_1 = \left(h_{1,1}, h_{1,2} \ldots h_{1,M}\right)$ calculation.

Step 4: Vector $\mathbf{A}_1 = \left(A_{1,1}, A_{1,2} \ldots A_{1,M}\right)$ calculation.

Step 5: Vector $\xi_2 = \left(\xi_{2,1}, \xi_{2,2} \ldots \xi_{2,M}\right)$ is formation, and so etc

As a result of the random variables $A_{i,j}$, $j \in [1, M]$, $i \in [1, N]$ are given the average values given by the dispersion and given space and time correlation functions.

The resulting algorithm is rather complex, but here, in contrast to the algorithm defined by the expression (3). The number of operations during the next calculation $A_{i,j}$ decreases due to several causes. Firstly, the coefficients of the algorithm (4) for the vectors η_i, $i \in [1, N]$ calculation are computed only once. Secondly, the coefficients of the vectors $\mathbf{h}_j$, $j \in [1, M]$ are calculated from the matrices $\left\| \mathbf{D}_i^{(B)} \right\|$ that are larger than M times the size of the matrixes $\|\mathbf{D}\|$ used in the algorithm (3).

CONCLUSION

The proposed algorithm can accurately reproduce a section of space-time correlation function of the echo signals of the sea surface. This is not a significant limitation of this proposed algorithm in usage because in practice the usually function of the correlation section is only known. The proposed algorithm greatly reduce the amount of computation required to calculate the next frame of the echo envelope. This method can be used for modeling electronic systems in real time.

REFERENCES

[1] SEA PLANE LANDING CONTROL AT WAVE DISTURBANCES Nebylov AV, Nebylov VA, Panferov AI, Shepeta AP In the collection of : IFAC Proceedings Volumes (IFAC-PapersOnline) 17th IFAC Symposium on Automatic Control in Aerospace, ACA ' 2007.

[2] Izrantsev VV Shepeta DA Modeling external signals onboard instrument complexes aircraft of the fifth generation . Math. Universities. Priborostroenie. 2000 , № 2, p.76 -83.

[3] Bessonov AA, AE Cecina , Shepeta AP Mathematical and simulation models of the sea surface . Russian aerospace instrumentation. Series 2 . Avionics . St. Petersburg . , 2005, p. 52-69.

[4] Cecina AE, DA Shepeta Mathematical model echoes the sea surface observed airborne radars aircraft. Information management systems . 2010 . T. 45 . Number 2 . Pp. 21-25.

INFLUENCE OF INTERNAL HEAT SOURCE ON THE NATURAL VIBRATION FREQUENCY OF THE ELASTIC ELEMENTS OF MICROELECROMECHANICAL SYSTEMS

Artur Paraskun

Saint-Petersburg State University of Aerospace Instrumentation,
Saint-Petersburg, Russia

artur.paraskun@icloud.com

Abstract

The main functional elements of microelectromechanical systems (MEMS) usually attributed primarily their elastic elements, the operation mode which are longitudinal and transverse forced oscillations. Operating frequency range which ranges from tens of kHz to several MHz.

These elastic elements often represent a console or bridge beams, usually rectangular, rigidly connected to the body of MEMS.

I. MICROELECTROMECHANICAL SYSTEMS

When forced oscillations due to different mechanisms of internal friction in single crystals formed by heat is generated inside the elastic elements sources of thermal energy. Often, when the kinetic energy is consumed to commit work to change the microstructure of materials. The heat changes the temperature in single-crystal elastic suspensions to a stationary distribution of temperatures.

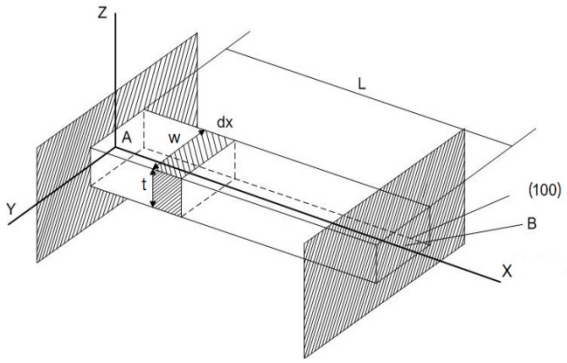

Fig. 1. Beam with rigidly clamped ends

Figure 1 shows the block diagram bridge beam, an example of which would be considered all the studied phenomenon. Here *w, t, L* – the dimensions of the beam; $L = 100*10^{-6}$ m, $w = 20*10^{-6}$ m, $t = 5*10^{-6}$ m; (100) - crystallographic direction ; A, B – the beam ends fixedly connecting it to the support.

In accordance with [1 – 3], the amount allocated in the volume element dv per unit time is equal to the thermal energy:

$$dP = \frac{\pi \cdot \sigma^2 \max \cdot \nu \cdot Q^{-1} \cdot w \cdot t\, dx}{\mathrm{E}} \quad (1)$$

wherein:

$wtdt=dv$;

σ – the maximum normal stress in the element dv for flexural vibrations of the beam;

$Q_{TY}^{-1} = \frac{\mathrm{E} \cdot \alpha^2 \cdot T}{C_p \cdot \varrho} \cdot \frac{\omega \cdot \tau}{1 + (\omega \cdot \tau)^2}$ – thermoelastic internal friction ;

$\mathrm{E}(100) = 1{,}3 \cdot 10^{11}\ Pa$ – modulus of elasticity of single-crystal silicon (crystallographic direction (100));

$\omega = 6{,}67 \cdot \sqrt{\frac{\mathrm{E}}{\varrho}} \cdot \frac{t}{L^2}$ – the fundamental frequency of oscillation of the beam;

$\tau = \frac{C_P \cdot \varrho \cdot h^2}{\lambda \cdot \pi}$ – relaxation time of the heat flux in the beam;

$\lambda = 150\ \frac{W}{m \cdot K}$ – thermal conductivity of silicon;

T – absolute temperature;

$Cp = 800\ \frac{J}{Kg \cdot K}$ – specific heat capacity mass Si (silicon);

$\varrho = 2{,}33 \cdot 10^3\ \frac{Kg}{m^3}$ – density of silicon ;

$\alpha = 2{,}3 \cdot 10^{-6}\ K^{-1}$ – coefficient of linear expansion of silicon.

Thermoelastic internal friction Q^{-1} – the main component of the internal friction in solids responsible conversion of kinetic energy into thermal fluctuations.

Besides Q_{TY}^{-1}, in kinetic energy dissipation takes place significant fluctuations component Q_M^{-1}, associated with structured changes in the single and the formation of defects. Its value depends on the

design and, according to [4], is calculated by the relation:

$$Q_M^{-1} = A \cdot \frac{W}{L} \cdot \left(\frac{t}{L}\right)^4 \qquad (2)$$

wherein *W, t, L* – dimensions beams, *A* – factor, $2 \le A \le 4{,}5$.

Since loss additive components, then for a constant $Q^{-1} = Q_{MY}^{-1} + Q_M^{-1}$, Q_{TY}^{-1} and Q_M^{-1} components are measured in a wide range, affecting the distribution of temperature in the elastic element.

In [5] it is shown that the distribution of heat from internal sources in the beam depends on the ratio of the primary natural frequency and frequency of forced oscillations.

In most MEMS devices operating frequency or equal to or less than the fundamental frequency of free oscillations , and the relaxation time $\tau \le T_0 = \frac{2\pi}{\omega_0}$ – the period of natural oscillations with frequency ω_0.

Under these conditions, the temperature gradient in the direction from the compressed to the stretched surface of the beam (fig. 2) disappears , the temperature inside the volume dv becomes constant, and the thermal process is isothermal.

Also under these conditions, the thermal power generated in the elastic element is integration of the expression (1) over the volume V.

$$\int_V dP_T = \int_0^l \frac{\pi \cdot \sigma^2(x) \cdot Q_{TY}^{-1} \cdot \nu \cdot w \cdot t}{\mathrm{E}}\, dx =$$

$$= \frac{\pi \cdot Q_{TY}^{-1} \cdot \nu \cdot w \cdot t}{\mathrm{E}} \int_0^l \sigma^2(x)\, dx \qquad (3)$$

To determine the dependence of $\sigma^2(x)$ construct diagrams of shear force F and bending moment for the beam shown in figure 1.

Pinching the ends of the beam makes it statically indeterminate, and to calculate the support reactions and reactive forces apply the method of moments [6].

In table 1 may be posted the data obtained by the calculation circuit and the values of the beams R_A, R_B, M_A и M_B.

Table. 1

The structure of the table for data posting

Design scheme	Support reactions A and B	Moment on the supports A and B	Moment in the span	Beam deflection

Since in some areas within the beam segments $\left(0 \le x_1 \le \frac{L}{2}\right), \left(\frac{L}{4} \le x_2 \le \frac{L}{2}\right), \left(\frac{L}{2} \le x_3 \le \frac{3L}{4}\right), \left(\frac{3L}{4} \le x_4 \le L\right)$ varies linearly with the bending moment and $\sigma_x = \frac{M_x}{W}$, where $W = \frac{w \cdot t^3}{6}$ – the moment of resistance of the cross section of the beam, $M_x = \frac{F}{2} \cdot \left(x - \frac{L}{4}\right)$, then the dependence of $\sigma^2(x)$ to participate $\left(0 \le x \le \frac{L}{2}\right)$ takes the form (fig. 2).

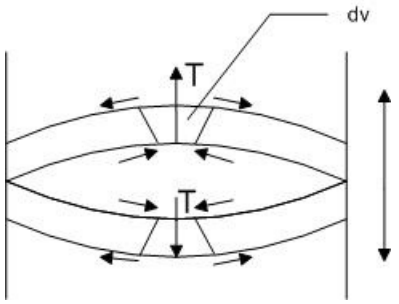

Fig. 2. The direction of heat flow in the beam for flexural vibrations

Analysis of this distribution shows that $\sigma^2(x)$ ranges portion $0 \le x \le \frac{L}{2}$ quadratically.

A similar pattern has this dependence on a plot $\frac{L}{2} \le x \le L$. Since the temperature distribution in each area of the same, the temperature of the beam will be aligned with the points x = 0 and $x = \frac{L}{2}$ point to $x = \frac{L}{4}$, and from the points $x = \frac{L}{2}$ and $x=L$ to the point $x = \frac{3}{4}L$ before reaching the isothermal state.

Steady temperature determined from the condition:

$$\int_V P_T\, dt = \int_S \mathrm{S} \cdot \chi \cdot \varepsilon \cdot \left(T^4 - T_0^4\right) ds \qquad (4)$$

Here:

$\int_S S \cdot \chi \cdot \varepsilon \cdot \left(T^4 - T_0^4\right) ds$ – the energy radiated from the surface of the heated beams per unit time;

$S=2(w+t)e$– lateral surface area of the membrane.

Given the previously mentioned relations for P_T and the values they heat balance equation beams corresponds to its isothermal as taking the form

$$\frac{F}{2} \cdot \frac{E \cdot \alpha^2}{C_p \cdot \varrho} \cdot \frac{\omega \cdot \tau}{1+(\omega \cdot \tau)^2} \cdot \frac{\pi \cdot \nu \cdot w \cdot t \cdot L^3 \cdot T}{w^2 \cdot t^4 \cdot 192} = 2 \cdot (\omega + t) \cdot L \cdot k \cdot \varepsilon \cdot \left(T^4 - T_0^4\right) \quad (5)$$

Amplitude of the external force F from the condition :

$$F_{max} = \frac{192 \cdot E \cdot Y}{S_{max} \cdot L^3} = 5{,}2 \cdot 10^{-2}\ N$$

when $f_{max} = 2 \cdot 10^{-6}\ m$, $Y = \frac{w \cdot t^3}{12}\ m^4$.

Coefficient ε is experimentally value ε depending on the wafer processing technology finishing – blank lies in the range (0.15–0.6). Assuming ε=0,5 , let (5) taking into account all of its constituent parameters to the form: $2*10^{-8}T = 1*10^{-16}(T^4 - T_0^4) \rightarrow T^4 - 2*10^8 T = T_0^4$, where T – absolute temperature desired beams in thermodynamic equilibrium with the environment. These values for T_0=300 K, T=600 K.

The value T is extremely high because calculated assuming that the entire heat generated in the beam energy is re-emitted through the side surface.

Considering the loss in the bearings, heat dissipation in the load bearing elements of MEMS due to heat conduction, the average temperature of the beams is set to be considerably lower. For the initial stages of designing MEMS close to making the article size and fixing scheme, the temperature of the elastic element will be about 450–500 K, which requires specification of design parameters of the oscillating system. When internal heating rigidly fixed beams it is compressed under the action of axial support reactions.

Carry out a rough estimate of changes in the primary oscillation frequency beams, using the approach described in [7].

The magnitude of the normal stress in axial compression does not depend on the geometry of the beam and is :

$$\sigma = \alpha \cdot E \cdot (T - T_0) = 2{,}3 \cdot 10^{-6} \cdot 1{,}3 \cdot 10^{11} \cdot 300 = 6 \cdot 10^7\ Pa$$

$$V = w \cdot t \cdot \sigma = 1 \cdot 10^{-10} \cdot 6 \cdot 10^7 = 6 \cdot 10^{-3}\ N$$

The fundamental frequency of vibrations of the beam without axial compression is:

$$\omega_0 = \frac{\beta}{L^2} \cdot \sqrt{\frac{E \cdot I}{\varrho \cdot F}} = 2{,}2 \cdot 10^7\ s$$

and under axial compression:

$$\omega_{0N} = \frac{\beta}{L^2} \cdot \sqrt{\frac{E \cdot I}{\varrho \cdot F}} \cdot \sqrt{1 - \frac{N \cdot L^2}{E \cdot I \cdot \pi}} = 1{,}84 \cdot 10^7\ s$$

where $I = 2{,}08 \cdot 10^{-22}\ m^4$

The value of the fundamental frequency oscillations generated at full conversion of thermal energy into thermal radiation is reduced compared with the value calculated at room temperature for about 50 %. You can suggest that, given the loss of kinetic energy fluctuations in the bearings. Frequency change will be in the range of 15–20 % ω .

II. CONCLUSION

As more accurate methods for calculating kinetic energy dissipation does not exist, it is obvious that the design of MEMS high accuracy requires mandatory subdivision of experimental studies that achieve the required performance of a product destination.

III. REFERENCES

[1] Работнов Ю.Н. Механика деформируемого твердого тела / Ю.Н. Работнов. – М.: Наука, 1988.

[2] Постников В.С. Внутренне трение в металлах / В.С. Постников. –

[3] М.: Металлургия, 1974.

[4] Балалаев Ю.Ф., Постников В.С. Об ультразвуковом нагреве металлов / Ю.Ф. Балалаев. - Физика и химия обработки металлов №9, 1968

[5] Митрофанов В.П. Колебательные системы с малой диссипацией / В.П. Митрофанов - М.: МГУ, 2010.

[6] Candler R. Impact of slot location on thermoplastic resonators / R. Candler – Solid-State sensor, Actuators and Microsystems, 2005, transducers'05. The 13th international Conference. p. 597-600 Vol. 1.

[7] Феодосьев В.И. Сопротивление материалов / В.И. Феодосьев – М.: Наука, 1974.

[8] Тимошенко С.П. Колебания в инженерном деле / С.П. Тимошенко – М.: Машиностроение, 1985.

THE SOURCE CODE QUALITY VALUATION METHODS

Nikita Petrin

Saint-Petersburg State University of Aerospace Instrumentation,
Saint-Petersburg, Russia

nikitapetrin@gmail.com

Abstract

This article contains review of factors influencing on the software quality and three methods of building source code models for further using in the auto systems aimed on nonfunctional source code quality assessment.

I. INTRODUCTION

In today's development values of the software development it's getting harder and harder to monitor the quality of that software. It is necessary to develop new and improve previous source code quality assessment auto systems, not only in the performance case but in the source code design compliance, source code compliance to the designed software architecture etc., especially this is necessary in a big program systems, who's lifecycle can rich tens of years. Source code of such systems can be evolutionary changed during lifecycle; some parts of such system could be used in other products etc. Such conditions impose additional requirements to the code readability and code compliance to the programming qualifying standards.

II. SOURCE CODE QUALITY

Software, just like any other human developed product has its quality grade, other words any software has its own grade of compliance to the qualifying standards: functional and nonfunctional.

Functional requirements consist of customer's requirements to the system functionality, functions' time execution, user's interface etc., other words these requirements consist of everything that customer or user have a deal with while using a software. The nonfunctional requirements are:

– source code architecture compliance to the developed architecture;
– source code compliance to in company's qualifying standards;
– architectural errors and anti-patterns absence in a source code etc.

Talking other words nonfunctional requirements are aimed to reduce costs of software improvement, recurring using, soft accompany and integration with other products.

The main errors' source in the developing system are experts, those who adapt customer's informal requirements to the formal state, who design system's architecture based on the formal requirements, who at last write source code and test it. [1]

Software state is not constant through its lifecycle. The main cause of this is that developing system's object model is often seriously difficult to understand and also it is hard or even impossible to predict changes in a technological process after its automation. In most cases changes are introduced to the source code for bringing new functionality into the developing system or improvement of old ones, also for correction of unpredictable and accidental cases of software errors. Errors are always accidental, while code improvements can be predicted. The conception of the software quality is introduced to define degree of the system's availability for release to the market. It is incorrect to release that works unstable and can stop working in any time; developer company should stabilize the state of software till qualifying standards' level. Quality grades are consist of two types: positive and negative. Positive grades are used more frequently than negative – with the positive quality grade developer has more wide understanding of the software's quality, then with the negative, because positive grade gives appreciation to the similarity of developed system with the abstract standard system, while negative grade talks only about count of software errors.

As was mentioned previously the software's quality types can be divided into two principal components [2]: functional (external) and nonfunctional (internal). In most cases the functional component is evaluated by software testing with the previously designed unit-tests base on the software specification. Nonfunctional errors are detected by expert's code inspection and static source code inspection. Within such detection probability of leaving some architectural and programming errors is pretty big. To reduce the amount of architectural and programming errors it is necessary to develop systems for auto testing source code.

III. METHODS OF THE DESCRIPTION OF MODEL OF THE SYSTEM'S SOURCE CODE

The main methods of the description of model of the system's source code for the program of the analysis of source code are [3]:

– creation of the focused count on the basis of an source code;

– creation of a tree of roles of an initial code on the basis of special identifiers of the roles described in a code;

– calculation of numerical metrics on the basis of an source code.

IV. FOCUSED COUNTS

Focused counts – most intuitively clear description of the source code, both reference, and defective. For an example we will consider the focused count constructed on the following source code:

```
int b;
int a;
a = a – b;
```

Though this code also isn't works, for an example it is enough. In figure 1 the focused count constructed on this code is represented.

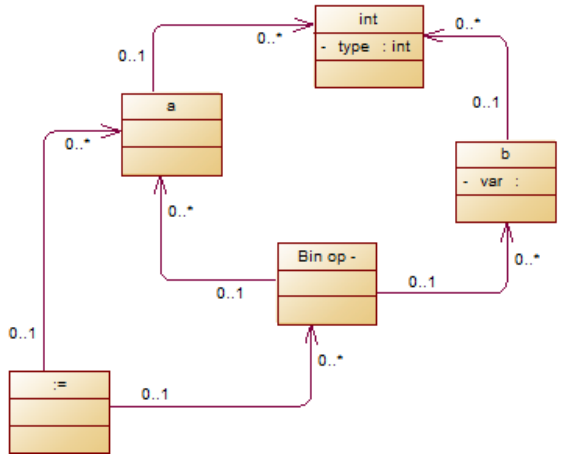

Fig. 1. Focused count

However simplicity of the focused count is not only its positive, but also negative property. Because of simplicity, focused counts it is inconvenient to describe architectural templates. The description of non-functional requirements to style of programming is the best application of focused count:

– compliance of source code to programming standards (standard, intra corporate);

– compliance of source code to the accepted programming paradigm;

– relevance of using these or another designs of language in a certain context, for example lock using assignment in conditional operators of languages C, C++.

In other words, focused counts best of anything are suitable for the description of simple structures of language in a reference or defective look. Using roles and metrics of source code is suitable for the description of architectural concepts more.

V. ROLES OF A SOURCE CODE

By means of the description of roles of entity of a source code it is convenient to describe the architectural concepts used in system, for example, patterns of design. Use of roles results in need of a special name of entity of a source code, or input of special text inserts (comments) with the description of a role of this or that essence, for example:

```
/// <roles>
///     domainObject,
///     subject
/// <roles>
```

The essence of automatic reviewing of a source code on the basis of roles consists in constructing logical communications between roles and if these logical communications don't correspond to reference communications – to report about detection of an architectural mistake. For example, we will consider a structural template bridge (fig. 2).

Apparently from figure 2, six classes are used in a template:

– Client – class directing inquiries to the class Abstraction;

– Abstraction – stores the link to object of Implementor, redirects inquiries to the class Implementor;

– RefinedAbstraction – expands the interface determined by the class Abstraction;

– Implementor – the class defining the interface for concrete classes offtakers. The interface of a class cannot correspond to the class Abstraction interface, often described interface of lower level, than in the class Abstraction;

– ConcreteImplementor – the class realizing the interface of the class Implementor.

Apparently from the scheme of classes, at correct realization of a template the class client has access only to the class Abstraction interface, according to this expression it is possible to write logical expression which will be checked when viewing a source code:

$$\text{for } \forall w{:}va(w)\in\{implementor, concreteImplementor\}\ IVG(w)\cap\{v\in VG : va(v)\notin\{abstraction, refinedAbstraction\}\} = \varnothing.$$

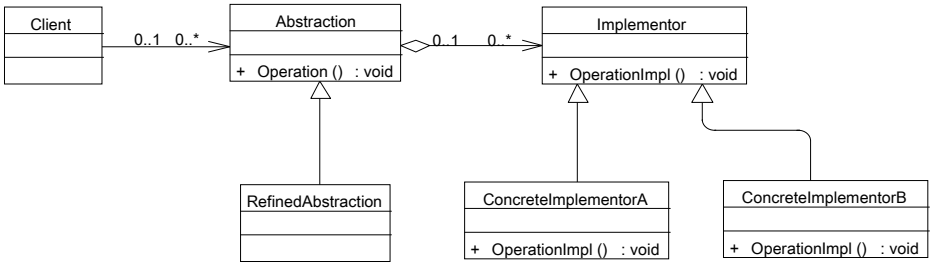

Fig. 2. Structural template – the bridge

VI. SOURCE CODE METRICS

The assessment of quality of a source code with using of metrics differs from considered earlier. Here the result of check of a source code on compliance to the reference will give not the binary answer ("corresponds" and "doesn't correspond"), but numerical. Considering that the assessment will be numerical, when developing metrics it is necessary to set admissible values for results which will speak about compliance or discrepancy of an estimated code to the reference. In fact process of an assessment of quality with use of metrics of a source code looks as follows:

– determination of basic and derivative metrics on the basis of which quality of the source code will be estimated;

– determination of intervals of values of a set of metrics in case of which observance, the source code meets qualifying standards;

– creation of derivative metric space for a reference code on the basis of analytical expression over a set of metrics;

– determination of intervals of values of the metrics corresponding to a reference and defective prototype solution.

The main scope of metrics is tracing of execution of architectural requirements recommendations to the source code, such as increase in coupling; connectivity reduction; absence of data classes; absence of monster classes.

We will consider, for example, as it is possible to describe increase in coupling by means of metrics.

Coupling is a level of use by methods of a class of methods and attributes of the same class. In other words, more class linked, more it is monolith, more it uses its attributes and methods instead of attributes and methods of third-party classes. In [3] the following calculation formulas of metrics of level of a class for coupling determination are given:

– number of couples of methods which don't use the general fields of a class (PP) – $\mu_{PP} = \sum_{\substack{m_1,m_2 \in \{s(e) \in IV_G(v):\\ vt(s(e))=Me\} \wedge \\ |OV_G(m_1) \cap OV_G(m_2)|=1}} |\{m_2\}|$, with an admissible interval [0.000, 1.000];

– number of couples of methods which use the general fields of a class (QP) – $\mu_{QP} = \sum_{\substack{f \in \{s(e) \in IV_G(v):\\ vt(s(e))=Va\}}} \frac{ivec(f, Me, ac)!}{2!(ivec(f, Me, ac)-2)!}$, with an admissible interval [0.333, ∞];

– quantity of methods of a class which don't use a class field (NMWA) – $\mu_{NMWA} = \left| \begin{matrix} \{m \in \{s(e) \in IV_G(v) : vt(s(e)) = Me\} \\ \wedge |OV_G(m)| = 1\} \end{matrix} \right|$, with an admissible interval [0.000, 0.333];

– number of couples of methods which don't use the general fields of a class minus number of coupleps of methods which use the general fields of a class (LCOM) – $\mu_{LCOM} = \mu_{PP} - \mu_{QP}$, with an admissible interval [0.000, ∞].

Also for estimation of a level of compliance of the source code to a prototype solution "increase in coupling" the formula is entered $\mu_1 = \frac{3\mu_{LCOM} + \mu_{NMWA}}{4}$.

The admissible interval determined an interval [0.100, ∞]. Respectively, in case of an assessment of quality of the source code the program can easily calculate the marked metrics and to compare result to a reference interval.

VII. CONCLUSION

On the basis of the provided valuation methods of nonfunctional quality of a software it is possible to construct system capable to exempt experts from manual inspecting of the source code. Such system will be easy to be set up under needs of corporation since all rules of an assessment of quality are described not by internal program entities, and changeable mathematical models. Having written once such system, the corporation will exempt itself from need of manual inspecting of the source code, and also will manage to force programmers to make refactoring of the source code for the purpose of increase in density of comments and coercion of readability of the source code to the accepted intra corporate standards.

VIII. REFERENCES

[1] В.В. Липаев Программная инженерия. Методологические основы, М.:ТЕИС, 2006 г., 608 стр.

[2] Galin D. Software Quality Assurance: From Theory to Implementation, Harlow, Addison-Wesley, 2003, 616 pp.

[3] В.В. Бураков Управление качеством программных средств, СПБ.:ГУАП, 2008 г., 287 стр.

RUSSIAN INNOVATIVE PROJECT FOR RADIOPHYSICAL AND GEOPHYSICAL EXPLORATION

Alexandra Petrova

Saint-Petersburg State University of Aerospace Instrumentation,
Saint-Petersburg, Russia

sandra17060791@mail.ru

Abstract

Geophysical methods are used in solving such problems as identification of favorable placement of mineral structures, heterogeneity structural and qualitative of the geological section, obtaining information on the availability and quality of mineral resources, the contour and size of deposits, state and features of rock masses.

Selecting the most effective methods of electrical prospecting for polymetallic ores is an actual issue nowadays. In this regard, the Russian Institute for Powerful Radiobuilding and the St. Petersburg State University developed and tested in practice, theory, techniques, equipment and software for magnetotelluric (MT), audio-magnetotelluric (AMT), controlled source audio-magnetotellurics (CSAMT), radio-magnetotelluric (PMT), and radio-controlled source magnetotelluric (PMT C) methods.

I. METHODS OF ELECTRIC PROSPECTING

Electric prospecting methods are based on the difference in density, magnetic, electrical and other properties of rocks of different mineral composition.

Electromagnetic research uses electromagnetic fields of different nature. By origin they can be divided into:

– natural – magnetotelluric fields resulting from interaction the Earth with eddy currents in the ionosphere and thunderstorm;

– artificial – fields created by using grounded lines connected to an AC[1] or DC[2], ungrounded circuits powered by alternating current, as well as antennas.

Frequency sounding is the method of prospecting variables harmonically changing field. It is used for exploration of both deep (a few kilometers) and skin-deep sections (up to a few hundred meters). In the case of deep sections exploration the soundings are carried out at the frequency range of 10^{-1}-10^{3} Hz (low frequency (LF) sounding). And in case of skin-deep exploration the soundings are carried out at the range of 10^{3}-10^{6} Hz (high frequency (HF) sounding). The penetration depth of electromagnetic field into the Earth can be determined by its frequency. This penetration depth increases while frequency decreasing.

The method of LF electromagnetic field includes all: the method of magnetotelluric sounding (MTS), electrical inductive methods, electromagnetic soundings and the method of natural alternating magnetic field.

Method of magnetotelluric sounding. This method has a high efficiency, a wide range of exploration depths, a large number of informative characteristics and relatively low cost research. These advantages are based on the use of the natural electromagnetic field of the Earth with a wide frequency range and a high spatial homogeneity as an excitation source.

Inductive methods. In this case ungrounded circuits powered by alternating LF harmonic or stepwise alternating current are used as excitation source.

Electromagnetic sounding. This one represents a method of vertical geoelectric exploration of section through the research of electromagnetic fields. They are based on the components measurement of the electromagnetic field on the condition of changing the distance between the source of the field and the receiver or the frequency of the exciting field.

The figure 1 shows the heterogeneity within the crust that create various anomalies of electromagnetic, gravitational and other fields of the Earth, fixed by using geophysical equipment.

For radio physical and geophysical exploration the most promising innovative project is the generating and measuring complex (GMC) with “Kola” source of electromagnetic radiation of ULF[3], ELF[4], VLF[5] range.

[1] AC- alternating current
[2] DC- direct current

[3] ULF – ultra low frequency
[4] ELF – extremely low frequency
[5] VLF – very low frequency

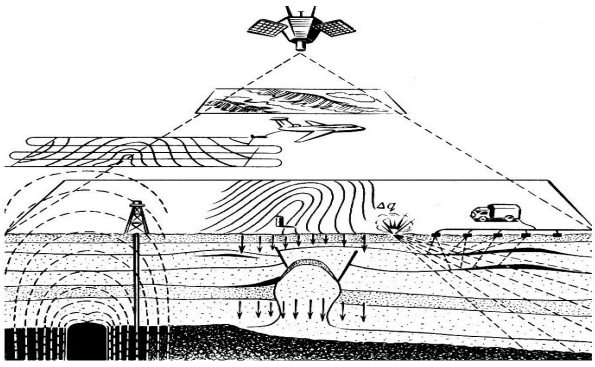

Fig. 1: Methods of studying the Earth's subsoil [3]

II. SUMMARY OF THE PROJECT

This GMC (fig. 2) is achieved for geophysical (electromagnetic) research and functioning in connection with special communication systems. Functioning practice of GMC has shown that the best source of the electromagnetic field is low lying horizontal antennas, such as power lines (fig. 3).

Fig. 2: "Kola" generating and measuring complex ULF, ELF, VLF range for radio physical and geophysical exploration [1]

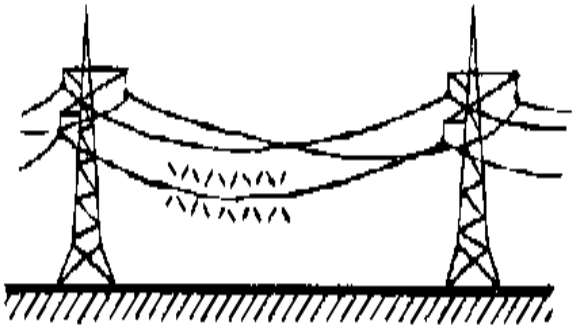

Fig. 3: Lying horizontal antennas, such as power lines [3]

This project is achieved for conducting fundamental and applied research in the areas of Radio Physics and Geophysics, the study of the propagation of ULF, ELF, VLF radio waves, near-Earth plasma structures, deep crustal structure, mineral exploration, including the provision of electric exploration at the shelf of the Arctic Ocean, including:

– research of mineral deposits (hydrocarbons, geothermal, mineral deposits);

– monitoring of electromagnetic precursors of earthquakes in earthquake-prone areas;

– determining of the site for critical facilities, including nuclear power plants;

– choosing the placement for disposal of radioactive waste.

III. UNIQUE PROJECT

The project is an innovative technology in the mineral exploration, including oil, gas and geothermal sources. Exploration with "Kola" source has high efficiency confirmed in practice. The figure 4 shows an accuracy comparison of the measurements using MTS with both natural field and controlled source.

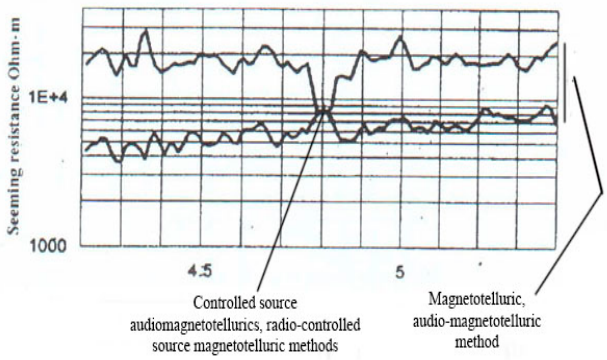

Fig. 4: Accuracy comparison of the measurements using MTS with both natural field and controlled source [5]

The similar equipment is manufactured in Germany (Metronix), the USA (ZongeEngineering) and Canada (Phoenix Geophysics), but the Russian one has unique characteristics[6]. The main of them is an ability of functioning in ULF range that makes advantages as depth and accuracy of the research simultaneously. The GMC provides a significant range of operations (up to 2000 km), while analogs allow operation at much smaller distances from the source (generally up to 15 – 20 km) with lower productivity.

It should be mentioned that GMC has a lack, which is bulkiness; nevertheless, it can be justified by technical capabilities. Moreover, the propagation theory of electromagnetic waves in layered strata affecting the interpretation of the results nowadays reveals underdeveloped.

Currently, the global market of marine electromagnetic research services is approximately $ 200 million per year. The stock value of the Norwegian EMGS company, which is the world leader in marine controlled source soundings, exceeds $ 1 billion. Successful marine electric prospection with a help of controlled source promises the success of such studies on land.

IV. PROJECT RELEVANCE

[6] Main characteristics of "Kola" GMC are shown in this article (Section V)

Receiving hardware-software systems are successfully applied to solve geoscience problems in Russia and abroad. The results of research are reflected in numerous publications in national and international journals and presented at various international conferences held by organizations such as IAGA, EAGE, SEG, AGU, EMSEV etc.

Since 1998, experimental studies of the propagation of ULF ELF VLF fields were performed in the Earth-ionosphere waveguide on routes of up to 1,500 km. Also, there were conducted experiments on comparing the accuracy of the measurement of seeming resistance of the Earth based on the analysis of the natural electromagnetic field of the Earth with the same use of a generator.

This equipment is implemented in the Kola Peninsula and successfully used by the scientists of the Polar Geophysical Institute in Kola Science Centre. Also it is functioning in the framework of various geophysical programs.

Geophysical studies have been already performed at searching geothermal sources on Kamchatka Peninsula, structure research for pumping drainage water (Yakutia), the study of the deep areas (Kola Peninsula and Peninsula Ribachii), work on regional profiles (Chukotka), exploration of the area before paving the tunnel for high-speed trains (Spain), exploration the structure of the lithosphere through the propagation of VLF radio waves in a waveguide "Earth-ionosphere" (Fennoscandian shield) [4], searching of ore deposits, gold Zabaikalie deposit (Sukhoi Log Tabornoye Uryah), polymetallic Hajar deposit (Morocco), copper mine (Chile), nickel Mount Keith deposit (Australia, operating with the company BHP Billiton), kimberlite pipes research (Yakutia and Archangelsk region.), uranium research (Northwest Region). [5]

V. TECHNICAL SPECIFICATIONS OF GMC [1]

Generator

Frequency range	0.01 –1000Hz (ULF,ELF,VLF)
Power	0.5 – 50 kW
Output current	up to 100 A
Supply voltage	380 V, 50 Hz
Coverage	up to 2,000 km

Recorder

Number of channels	4
ADC, bits	24
Frequency range	0.01–1000 Hz
Link with PC	Ethernet
Integrated accumulator	5 A * h, 12 V
Operating temperature range	20 …+ 50° C
Dimensions and weight of measuring unit	410 x 290 x 180 mm, 5 kg

Has the ability to synchronize measurements with GPS or GLONASS.

Magnetic Antenna

Frequency range	0.01-1000 Hz
Conversion factor – the frequency range 0.5-1000 Hz 0.1-0.5 Hz	Sensitivity of conversion 80 mV / nT* 160 mV / (nT × Hz)
Noise level at 10 Hz 1000 Hz	Spectral density of magnetic noise 12 fT** / √ Hz 2.5 fT / √ Hz
Dimensions and weigh	70 x 1110 mm, 5 kg

*nT=10−6 T
**fT =10−15 T

Additional options are:

– automated system for monitoring and recording of generator output;
– automated control measurements;
– controlled software monitoring.

VI. THE PROSPECTS

1. Prediction and research of gold deposits; holding exploratory geophysical work on root gold in southern Central Siberia.
2. Formation of optimization proposals for geophysical research in order to find root gold in Russian regions, including searching of new deposit types.
3. Receiving information about the internal structure Kingashsky mafic-ultramafic massif and defining there the most promising ore-blocks.
4. Participation in Strategic Plan of the State Committee of the Republic of Sakha (Yakutia) at Geology and Subsoil Use.
5. Studies on Alfven resonance in the ionosphere.
6. Studies on pearl auroral radiances in the ionosphere.

VII. CONCLUSION

The unique combination of accuracy and depth of exploration with the complex, developed by the Russian Institute for Powerful Radiobuilding and the St. Petersburg State University, this project has enormous potential not only in the field of mineral exploration. It also can be used for drinking water search, geothermals, deep seismic areas research, environmental monitoring (in particular, soil pollution), for various engineering projects such as e area studying for the future construction of nuclear power plants, research monoliths for waste disposal.

But it is worth mentioning that the theory of propagation of electromagnetic waves in layered strata is still imperfect, hence it prevents the possibility of

increasing the accuracy of the results interpretation of physical research.

VII. REPFERENCES

[1] www.rimr.ru
[2] geo.web.ru
[3] V.K. Khmelevskoy Electromagnetic sounding (International University of Nature, Society and Man “Dubna”)
[4] 1st Russian (with international participation) scientific workshop “Interaction of electromagnetic fields controlled sources ELF range with the ionosphere and the Earth's crust”). G. Apatity, February 17-22, 2014.)
[5] Belyaev P.P., Polyakov S.V., Ermakova E.N., Isaev S.V., Yakunin M.N., Sobchakov L.A., Vasilyev A.V., Astakhova N.L., Vladimirov D.N., Volosevich V.S., Protopopov L.N, Gordyushkin S.M., Savitsky A.P., Red'ko G.V., Eliseev A.A., Fedorov A.B., Ratnikov K.D.) First experiments on generating and receiving artificial ULF (0.3-12 Hz) emissions at a distance of 1500 km. // Radiophysics and Quantum Electronics, Vol. 45, No. 2, 2002

HYDROBIOLOGICAL MONITORING OF WATER BODIES USING REMOTELY SENSED DATA

Mark Polyak

Saint-Petersburg State University of Aerospace Instrumentation,
Saint-Petersburg, Russia

markpolyak@gmail.com

Abstract

In this article water quality monitoring using remotely sensed data is reviewed. Some main objectives of such monitoring are considered. Satellites capable of ocean color monitoring are listed. Mathematical models for remotely sensed data analysis are described. Two approaches to data analysis are proposed: a random field model and stochastic neural networks such as a Boltzmann Machine.

Keywords: remote sensing, chlorophyll a, ocean color, monitoring, hydrobiology, mathematical model.

I. INTRODUCTION

One of the most complex systems we are dealing with in everyday life is the natural environment. It has great impact on the course of human events, so the need of predicting environmental changes is evident. The predictions are mainly made by mathematical models which are based on scientific research and verified on longterm monitoring data.

Environmental monitoring consists of three branches: air quality monitoring, soil monitoring and water quality monitoring. The monitoring methods can be divided in two categories: *in-situ* methods and remote sensing methods. The former means direct measuring of physical or biological parameters in the exact area where the environmental process being measured is taking place, while the latter is based on indirect measurements such as airplane of satellite multispectral images.

Air quality monitoring deals with such problems as emission of different gasses in the atmosphere. Concentrations of oxygen, carbon dioxide and other gasses are measured. This also includes monitoring of greenhouse gas and emission of potentially life-threatening substances in the atmosphere.

Soil monitoring is concerned with problems like erosion control, soil contamination with metals and pesticides, remediation of contaminated soils, restoration of wetlands, soil degradation, nutrient management, movement of viruses and bacteria in soils and waters, bioremediation and so on.

Water quality monitoring deals with pollution of water by pesticides, heavy metals, oil film, toxic substances, bacteria and so on. It is also concerned with monitoring biological groups of species as they act as robust indicators of the quality of the environment that they are experiencing or have experienced in the recent past [1]. The problems which are solved by water quality monitoring are described in more detail in the next chapter.

II. OBJECTIVES OF ENVIRONMENTAL MONITORING OF WATER BODIES

The history of consistent *in-situ* water bodies monitoring goes back for at least as far as the XIX century. For example, hardly explored ocean color databases of Forel-Ule scale records [2 – 4] cover all seas and oceans (like modern satellites do) already since 1889.

Water quality monitoring is formed by monitoring hydrochemical, biological and hydrometeorological parameters. These parameters are deeply connected with each other. For example the ocean color depends on salt content, which is a hydrochemical parameter. Ocean color is also affected by concentration of chlorophyll *a* and other pigments, which are produced by phytoplankton and are thus biological factors. Finally weather conditions (hydrometeorological parameters) such as a storm or a calm sea influence the ocean's color as well.

Hydrochemical monitoring of bodies of water is mainly concerned with water pollution by toxic substances, maximum allowable concentration checks, etc.

Hydrobiological monitoring is usually divided into several areas: fish monitoring, birds and mammals monitoring, phytoplankton, zooplankton and zoobenthos monitoring. Changes in biological populations may indicate ongoing invisible processes such as eutrophycation (pollution by nutrients), noise pollution (from ships), and changes in sea bottom contour

and so on.

Finally hydrometeorological monitoring is used for weather forecasts.

All groups of monitored parameters described above belong to *in-situ* observations. A slightly different approach is based on using remotely sensed data as the data source for monitoring water bodies [23]. Remote sensing methods have greatly evolved in the last decade and became comparable with *in-situ* measurements and in many cases are considered even a better tool for both short term and long term monitoring.

The classification code of problems that may be assessed with remotely sensed data [5] contains 66 individual case studies which are grouped in 15 research themes from two general fields. The two main research areas are surface waters and aquatic bioresources.

Surface waters research includes hydrography and hydrometry of rivers, lakes, water storage basins, seas and oceans; river bed evolution, ice situation, high water and flooding analysis; glaciers monitoring; monitoring of ecological situation near pipeline river crossing.

Hydrobiology studies include the research on plankton, fish and mammals as well as watching over fishing vessels location.

As an example of real life monitoring objectives, the Gulf of Finland (GoF) committee [6] demanded combating eutrophication caused by nutrient loading as well as climate change the main problems of the water body. Monitoring programs of GoF include such topics as “Marine bio- and geodiversity”, “Pollution and ecosystem health”, “Fish and fishery” and “Maritime safety”.

Phytoplankton is one of the most important biological organisms living in every body of water. Aquatic food web is based on organic compounds created from carbon dioxide by phytoplankton. It accounts for half of all photosynthetic activity on Earth [7].

Phytoplankton can be easily detected because it produces chlorophyll *a* – green pigment needed for photosynthesis. Chlorophyll *a* concentrations in water depend on the phytoplankton quantity, making it easy to estimate phytoplankton biomass and its growth.

Determination of chlorophyll *a* concentrations in water samples is based on spectrophotometric analysis. One of the formulas used for *in-situ* chlorophyll *a* concentration estimation is the following [8]:

$$C_a = 11.85A_{664} - 1.54A_{647} - 0.08A_{630}, \quad (1)$$

where C_a is the chlorophyll *a* concentration in the solution (mg/L); A_X – solution absorbance values at X nm, produced by spectrophotometer. Chlorophyll *a* concentrations based on remotely sensed data are calculated in a similar manner as will be shown later.

III. SOURCES OF REMOTELY SENSED DATA

A description of satellites used to measure ocean color is given in Table 1. The ocean-color products obtained from these satellites define the optical properties of the water for a wide range of applications [9].

Table 1.

Some satellite remote sensing systems used to measure ocean color.
NASA denotes the National Aeronautics and Space Administration; ESA denotes the European Space Agency

Sensor	Satellite	Agency	Operating dates	Spatial resolution (m)	Number of bands	Spectral coverage (nm)	Repeat coverage (days)
CZCS	Nimbus-7	NASA	1978–1986	825	6	433–12,500	6
SeaWiFS	OrbView-2 (SeaStar)	NASA	1997–2010	1100	8	402–885	1-2
MODIS-Terra	Terra	NASA	1997–…	250/500/1000	36	405–14,385	0,5
MODIS-Aqua	Aqua	NASA	2002–…	250/500/1000	36	405–14,385	0,5
MERIS	Envisat	ESA	2002-2012	1150	15	412–1050	3

As of March 2014 the only remaining satellites capable of hydrobiological monitoring and providing open access to the data are Aqua and Terra, both carrying MODIS instrument and both operated by NASA. There are also projects Landsat 7 & 8 but they are oriented towards cartography tasks and are not well suited for monitoring phytoplankton.

Nevertheless there is a huge archive of remotely sensed data from previous missions. One of the longest sea and ocean monitoring space missions was SeaStar with SeaWiFS (Sea-viewing Wide-Field-of View Sensor) onboard. SeaWiFS operated for more than 13 years, collecting data from 1997 till 2010. Its predecessor Coastal Zone Colour Scanner (CZCS) on Nimbus – 7 satellite operated from 1978 to 1986.

Another mission – Envisat (ESA) with Medium Resolution Imaging Spectrometer (MERIS) onboard operated for 10 years from 2002 till 2012.

The Ocean Color project conducted by NASA [10] provides a single place access to all freely open remotely sensed data of water bodies. It combines SeaWiFS, CZCS, MERIS, MODIS and some other data archives.

IV. INFORMATION EXTRACTION FROM REMOTELY SENSED DATA

Remote sensing techniques can be used to monitor water quality parameters, i.e. chlorophyll [9], salinity [12], temperature [13], suspended sediments (turbidity) [11] and some other parameters and indexes [27].

There are many ocean color algorithms for determining chlorophyll *a* concentrations. Most of them depend upon blue-to-green ratios of water-leaving radiance or remote-sensing reflectance. The blue waveband is traditionally located near the phytoplankton absorption peak (440 nm) where chlorophyll *a* absorbs maximally. The green waveband is typically located in a region of minimal phytoplankton absorption (550 to 555 nm). For Coastal Zone Color Scanner (CZCS) data, chlorophyll concentrations were estimated using ratios of $L_w(443)/L_w(550)$ [14], where $L_w(\lambda)$ is the water-leaving radiance – the quantity and spectral quality of light reflected by the ocean's surface. This algorithm provides accurate pigment concentrations to ±40% accuracy in optically deep waters where phytoplankton dominates the optical properties. An algorithm for chlorophyll *a* determination in shallow waters is described in [15].

A measure of photosynthesis on land can be estimated by calculating so called Normalized Difference Vegetation Index (NDVI). It is a simple remote-sensing indicator which gives information whether the observed target has any vegetation or not. The formula is straightforward [16]:

$$NDVI = \frac{NIR - VIS}{NIR + VIS}, \qquad (2)$$

where NIR and VIS are spectral reflectance measurements acquired in the visible (red) and near-infrared regions.

V. MATHEMATICAL MODELS

There are different approaches to modeling hydrobiological processes. Classical mathematical approach is based on differential equations [17]. Stochastic models may be used as well [18 – 20].

Remotely sensed images can be thought of as a random field with X- and Y-axis denoting coordinates and Z-axis showing the value of a parameter (pixel intensity of the image, chlorophyll *a* concentration, sea surface temperature, etc). An example of such random field is shown on figure 1.

With this approach it is possible to use remotely sensed data for approximating parameter values in locations outside of a network of land monitoring stations. A network of water quality monitoring stations in Neva Bay is shown on figure 2. Information about chlorophyll *a* concentrations is being collected on this chain of ground stations since 1982. This information is a valuable source of ground trust data for analyzing remotely sensed data and developing mathematical models [21].

Neural networks such as stochastic Boltzmann Machine can be used to model and analyze complex remote sensing data [22]. Such networks allow extracting features from remote sensing data without supervised learning procedure. Boltzmann machine can be used for classification or just as a feature extractor together with other image recognition algorithms.

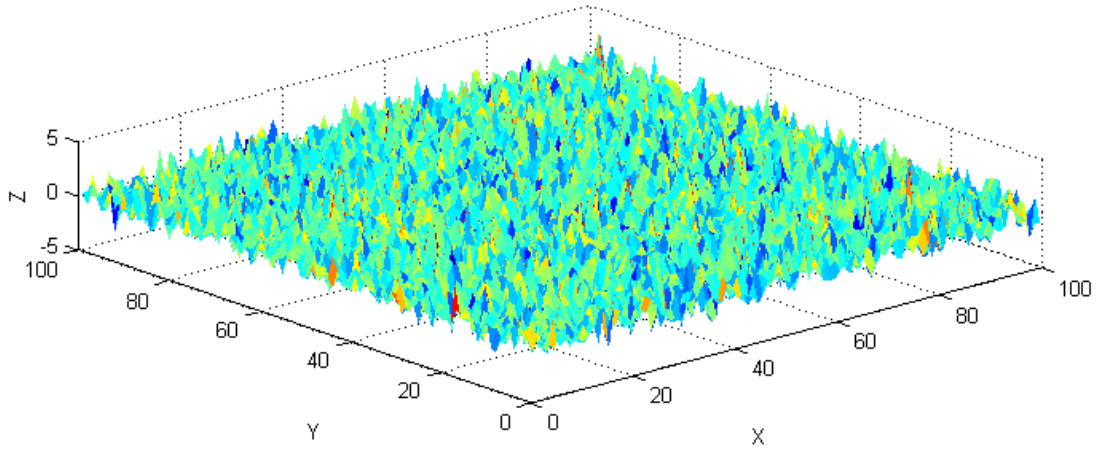

Fig. 1. Random field with Gaussian distribution of Z-axis values

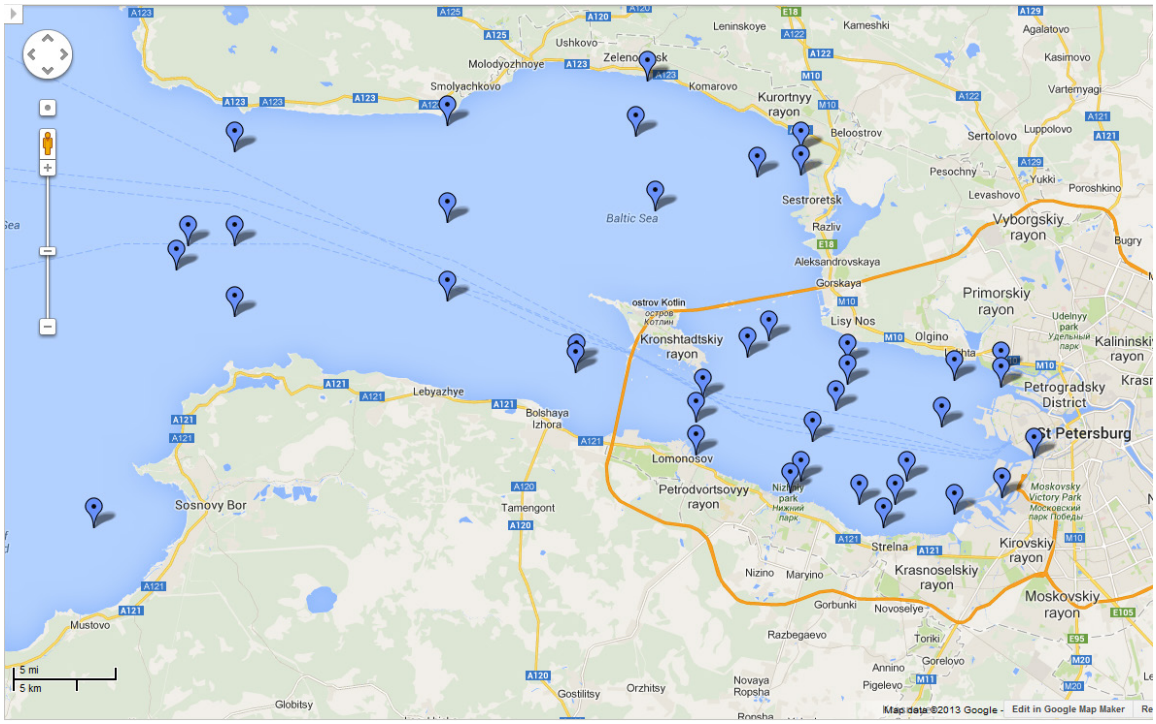

Fig. 2. Ground monitoring stations location in Neva Bay in Russian part of Gulf of Finland

VI. CONCLUSION

Remotely sensed data allows monitoring hydrobiological parameters such as phytoplankton quantity through chlorophyll *a* concentration.

Long-term ground monitoring data such as Forel-Ule ocean color observations or chlorophyll *a* concentrations can be compared with remote sensing data to provide more robust algorithms of estimating water quality parameters from remotely sensed data.

There are many practical examples of using remotely sensed data for efficiently monitoring bodies of water [24 – 26]. The future of monitoring of water bodies is behind remote sensing methods.

VII. REFERENCES

[1] Hart, C.W.; Fuller, Samuel F.J. Pollution Ecology of Freshwater Invertebrates. New York: Academic Press. 1974

[2] Wernand, M.R.; van der Woerd, H.J. & Gieskes, W.W.C. Trends in Ocean Colour and Chlorophyll Concentration from 1889 to 2000, Worldwide PLoS ONE, Public Library of Science, 2013, No 8.

[3] Wernand, M.R. & van der Woerd, H.J. Spectral analysis of the Forel-Ule ocean colour comparator scale. Journal of the European Optical Society - Rapid publications, 2010, No 5

[4] Wernand, M.R.; Hommersom, A. & van der Woerd, H.J. MERIS-based ocean colour classification with the discrete Forel–Ule scale. Ocean Science (OS), 2013, No 9, pp. 477-487

[5] Classification code for thematic problems of evaluating natural resources and environmental hazards by means of remotely sensed data, 7th Edition. Irkutsk: "ScanEx", 2008. / Классификатор тематических задач оценки природных ресурсов и окружающей среды, решаемых с использованием материалов дистанционного зондирования Земли. Редакция 7. – Иркутск: ООО «Байкальский центр», 2008.

[6] Gulf of Finland Year 2014. URL: http://www.gof2014.fi (verified on 23.03.2014)

[7] "NASA Satellite Detects Red Glow to Map Global Ocean Plant Health" NASA, 28 May 2009. URL: http://www.nasa.gov/topics/earth/features/modis_fluorescence.html (verified on 24.03.2014)

[8] Arar, Elizabeth J. In Vitro Determination of Chlorophylls *a*, *b*, $c_1 + c_2$ and Pheopigments in Marine And Freshwater Algae by Visible Spectrophotometry. National Exposure Research Laboratory, Office of Research and Development, U.S. Environmental Protection Agency, Cincinnati, Ohio. 1997

[9] Klemas, V. Remote sensing of algal blooms: an overview with case studies. Journal of Coastal Research, 28(1A), 2012. pp. 34-43

[10] Ocean Color Web. NASA. URL: http://oceancolor.gsfc.nasa.gov/ (verified on 24.03.2014)

[11] Klemas, V. Remote sensing of coastal plumes and ocean fronts: Overview and case study. Journal of Coastal Research, 28(1A), 2012. pp. 1-7.

[12] Klemas, V. Remote sensing of sea surface salinity: an overview with case studies. Journal of Coastal Research, 27(5), 2011. pp. 830-838

[13] Ritchie, Jerry C.; Zimba, Paul V. and Everitt James H. Remote Sensing Techniques to Assess Water Quality. Photogrammetric engineering and remote sensing. 2003. pp. 695-704.

[14] Gordon, H.R.; Clark, D.K.; Brown, J.W.; Brown, O.B.; Evans, R.H.; et al. Phytoplankton pigment concentrations in the Middle Atlantic Bight: Comparison of ship determinations and CZCS estimates. Applied Optics, vol. 22, 1983, pp. 20-36.

[15] Cannizzaro, J.P.; Carder, K.L. Estimating chlorophyll *a* concentrations from remote-sensing reflectance in optically shallow waters. Remote Sensing of Environment, vol. 101, 2006, pp. 13-24.

[16] Normalized Difference Vegetation Index (NDVI). Earth Observatory, NASA. URL: http://earthobservatory.nasa.gov/Features/MeasuringVegetation/measuring_vegetation_2.php (verified on 24.03.2014)

[17] Polyak, M. Evolutionary Predator-Prey Model with Stochastic Disturbance. XIV International Forum «Modern information society formation — problems, perspectives, innovation approaches»: Proceedings of the Forum. St. Petersburg, 2-6 June / SPb.: SUAI, 2013, pp. 59-63.

[18] Polyak, M. Smoothing interval estimation for a random process in real time. International Forum «Information and communication technologies and higher education – priorities of

modern society development»: Proceedings of the Forum. St. Petersburg, May 26-30 / SUAI, SPb., 2009, pp. 72-75.
[19] Polyak, M. Analysis of phase trajectories of a random process. International Forum «Modern information society formation – problems, perspectives, innovation approaches»: Proceedings of the Forum. St. Petersburg, June 6-11 / SUAI, SPb., 2010, pp. 75-80.
[20] Polyak, M. Phase-plane method: a practical approach. XII International Forum «Modern information society formation — problems, perspectives, innovation approaches»: Proceedings of the Forum. St. Petersburg, 30 May – 3 June / SUAI, SPb., 2011, pp. 55-59.
[21] Polyak M. Computer-based information system for monitoring the Neva Bay. Gulf of Finland Trilateral Cooperation Forum, 16-17 October 2013, Tallinn.
[22] Polyak, M. Data Processing Using Boltzmann Machines. XIII International Forum «Modern information society formation — problems, perspectives, innovation approaches»: Proceedings of the Forum. St. Petersburg, 5-10 September / SUAI, SPb., 2012, pp. 44-50.
[23] Dan G. Blumberg. Processing remote sensing data for solving environmental problems. Ben-Gurion University of the Negev, 2009.
URL: http://www.slideshare.net/beniamino/processing-remote-sensing-data-for-solving-environmental-problems-dang-blumberg-bengurion-university-of-the-negev (verified on 23.03.2014)
[24] Rango A. Application of remote sensing methods to hydrology and water resources. Hydrological Sciences-Journal-des Sciences Hydrologiques, Vol. 39, No 4, 1994. pp. 309-320
[25] Weiqi HE, Shan CHEN, Xuehua LIU, Jining CHEN. Water quality monitoring in slightly-polluted inland water body through remote sensing — A case study in Guanting Reservoir, Beijing, China. Front. Environ. Sci. Engin. China, 2008.
[26] Mouchot, Marie-Catherine; Alfoldi, Thomas; De Lisle, Daniel and McCullou, Greg. Monitoring the Water Bodies of the Mackenzie Delta by Remote Sensing Methods. Arctic. Vol. 44, Supp. 1, 1991. pp. 21-28
[27] NOAA AOML Physical Oceanography Division. Satellite Ocean Monitoring.
URL: http://www.aoml.noaa.gov/phod/data.php (verified on 24.03.2014)

MODELING OF IDENTIFICATION SYSTEMS SAW TAGS

Alexander V. Sorokin

Saint-Petersburg State University of Aerospace Instrumentation,
Saint Petersburg, Russia

ultramagnus88@gmail.com

Abstract

This paper gives an overview of mathematical models of the main elements of SAW tags, such as counter pin converter, on-chip grating reflectors. A model surfactants tags using a chirp signal.

I. INTRODUCTION

Work of surface acoustic wave (SAW) tags based on the phenomenon of the piezoelectric effect. The main structure of the SAW tags applied to the piezoelectric base (substrate). The most commonly used substrate material using lithium niobate (LiNbO3). Radio frequency identification (RFID) in the general form shown in figure 1.

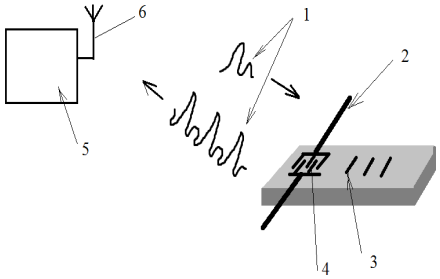

Fig. 1. Generalized form of an RFID system

Reader 5 sends a signal 1 through an antenna 6. Coming to the antenna 2 passive tags SAW IDT excites surface acoustic wave that propagates along the surface of the label. Part SAW reflected from the reflectors 3, and returning to the IDT, the response signal is turned on, consisting of time-delayed pulses. Time delay between the pulses is proportional to the distance between the reflectors. [1]

The coding information may be implemented as time-domain and frequency. Consider the time domain.

To work in this area, must have a zero pulses. In such labels used start and stop reflector. As shown in figure 2, the identification code of the label is determined by the position of the reflectors in the time slot .

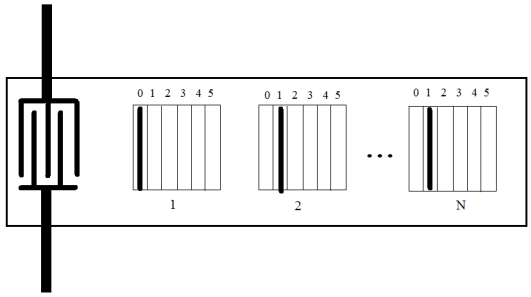

Fig. 2. Reflectors tags placed in the slots

Thus, the total number of codes is determined as N^m, where N – number of installations of the reflector in a single slot, m – total number reflectors.

II. MATHEMATICAL MODELS OF THE MAIN ELEMENTS OF THE LABEL

The main elements are tags SAW IDT (interdigital transducer) and reflectors set in the slots. Because the system is linear, it is possible to consider separately each reflector. Model reflection grating [2] is shown in figure 3.

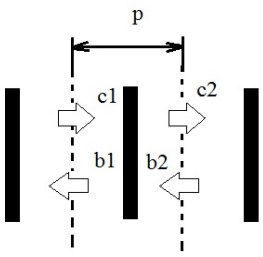

Fig. 3. Grating reflectors

It is assumed that at a fixed frequency w, an analytical description of the perturbations in the gaps between the electrodes using factors of the type exp (± jk0x), where k – wave number of the free surface. Based on the fact that the system is linear, considering a single electrode. Here, the complex amplitudes of the electrode extending from the left -b1, b2, c1 to the right, respectively, c2. Since the amplitudes are related

linearly, the outgoing wave from the electrode can be expressed by using the scattering matrix Sij:

$$\begin{bmatrix} b_1 \\ c_2 \end{bmatrix} = \begin{bmatrix} S_{11} & S_{12} \\ S_{12} & S_{11} \end{bmatrix} \begin{bmatrix} c_1 \\ b_2 \end{bmatrix} \quad (1)$$

In the simplest case, the SAW tag can be represented as a delay line.

Calculation of reflectors can be made using the methods described in the V. Novikov and V. Dmitriev [3]. The method of calculation is based on the consideration of the structure of the device two homogeneous plane waves propagating in opposite directions z:

$$R(z,k) = R(k)\exp(-jkz) \quad (2)$$

$$S(z,k) = S(k)\exp(+jkz) \quad (3)$$

where $R(k), S(k)$ – the complex amplitudes of the surface potentials c wave number k and angular frequency ω, the corresponding surface electric potentials.

The equations relating the complex amplitudes at the input of SAW $R_k(k), S_k(k)$ and output $R_{k+1}(k), S_{k+1}(k)$ k-th element of the structure, and the equation for current through a second electrode $l_k(k)$ have the form:

$$S_k(k) = r_k \eta_k \exp(-jkp_k) R_k(k) + \\ + \overline{r_k} \eta_k \exp(-jp_k k) S_{k+1}(k) + \tilde{\varphi}_{\overline{v}k}(k) \quad (4)$$

$$R_{k+1}(k) = r_k \eta_k \exp(-jkp_k) R_k(k) + \\ + r_k \eta_k \exp(-jp_k k) S_{k+1}(k) + \tilde{\varphi}_{v^+k}(k) \quad (5)$$

$$I_k(k) = \eta_k \exp\left(-\frac{jkp_k}{2}\right) * \left[\left\{ \xi_{k0}^+(k) + r_k \xi_{k0}^-(k) \right\} R_k(k) \right.$$

$$\left. + \left\{ \xi_{k0}^- + r_k \xi_{k0}^+(k) \right\} * S_{k+1}(k) \right] +$$

$$\eta_k * \left[\gamma_k^+(k) + \gamma_k^-(k) + \frac{iwW_k C_2}{2} \right] * U_0 \quad (6)$$

where $\tilde{\varphi}_{v\pm k}(k)$ – potentials generated by the exciting wave; U_0 – voltage applied to the IDT; r_k – complex reflection coefficient of k-th electrode; $\overline{r_k} = \sqrt{1-|r_k|^2}$; $\xi_{k0}^{\pm}(k)$, $y_{k0}^{\pm}(k)$ – parameters of the equations that determine the effectiveness of SAW excitation; $\eta_k = \frac{W_k}{W_0}$, W_0 – maximum aperture, W_k – overlapping k-th and the k+1 electrodes. The wave number in the reflection gratings in equation assumes the form $k = \frac{\omega}{V} - jy_k$, where the V – speed surfactant structure.

From these equations we can calculate the input conductivity RFID and its complex transmission coefficient. RFID response when applying to the input RF pulse is determined by the inverse Fourier transform.

II. SIMULATION MODEL OF SURFACTANT TAG

Passive tags can present the SAW delay line. On the label comes a linear frequency modulated signal at a frequency of 2.4 GHz .

The model label is shown in figure 4.

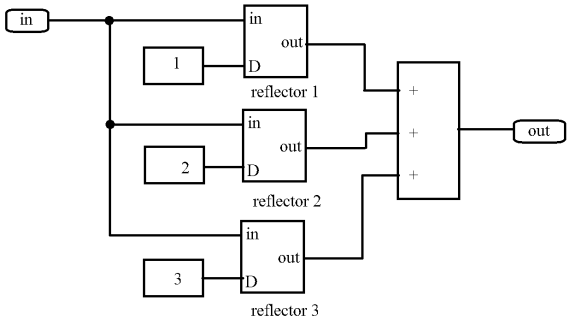

Fig. 4. Delay line with three reflectors

Model RFID system is shown in figure 5.

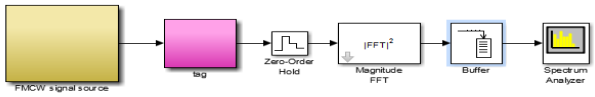

Fig. 5. Model RFID system

The signal obtained at the time the reader is shown in figure 6.

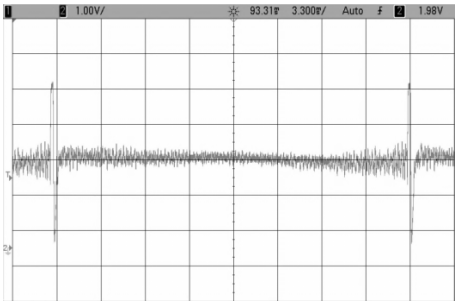

Fig. 6. The received signal from the tag reader

After the fast Fourier transform, signal in the frequency domain is supplied to the signal processor of the reader.

Figure 7 shows the input signal pulses and pulses of the response signal, delayed in time.

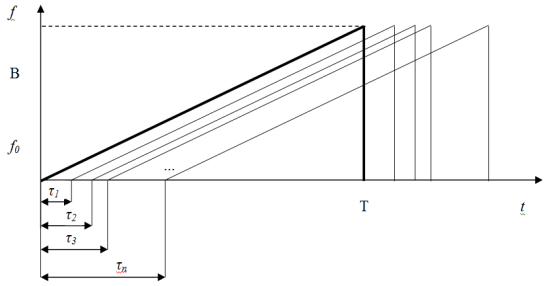

Fig. 7. Frequency signals in the time domain

III. CONCLUSION

During the study of passive SAW tags were considered basic design of SAW devices, their basic design elements, mathematical model. Consider the possibility of imitating models of tags. The study examined the simulated frequency signal emitted by the reader, and the delay line simulates tags work. As starting data used were the following:

- initial f0 = 2.4 GHz;
- signal bandwidth B = 80 MHz;
- signal duration T = 2 ms;
- power P = 20 dBm.

The resulting model confirms the possibility of RFID reader module assembly code indicator by chirped. The resulting model has a signal and noise and interference signals corresponding to real time. Moreover, at low signal-to-interference to achieve high reliability can be read response code by accumulating and processing the label data averaged. Based on the above results, the practical interest in further investigation of the response signal processing techniques tags.

IV. REFERENCES

[1] Surface Acoustic Wave RFID Tags S. Härmä and VP Plessky, Helsinki University of Technology, GVR Trade SA, Finland Switzerland, InTechOpen, Published on: 2009-01-01

[2] Morgan D. signal processing devices based on surface acoustic waves. Lane. from English. - M.: Radio and communication, 1990 - 416 p.

[3] V. Novikov , V. Dmitriev, Calculation reflector structures encoding RFID SAW Microelectronics and Microsystem , 2008, Special Issue ,66 -67 page

POLARIZATION CHARACTERISTICS OF THE PROPAGATION MEDIUM

Anna Vershinina

Saint-Petersburg State University of Aerospace Instrumentation,
Saint-Petersburg, Russia

avershinina1203@gmail.com

Abstract

Polarization transformations of electromagnetic signals in the propagation medium are investigated. Polarization spectra of vector signals are entered. The method of research is based on representation of polarization characteristics of a signal in the form of Jones vectors. Properties of the propagation medium transforming a polarization state, are described frequency depended Jones matrix by means of which the transfer constant of the propagation medium is defined.

I. INTRODUCTION

Problems of extraction, transfer and processing of information are primary for many areas of science and equipment, such as optics, communication, automatic control, a radiolocation and radio navigation, radiophysics, etc. The main physical data carrier in the called areas of science and equipment are electromagnetic (EM) waves. EM wave has vector character, and for its complete description it is necessary to specify wave polarization in addition to amplitude, frequencies and phases.

The polarization state is additional information parameter which isn't considered in the information theory and in the theory of signals where model of dynamic signals is scalar function of time $s(t)$ [1 – 4]. This oscillation compare with EM wave, which have constant polarization state both by transmission and at recept, i.e. EM radiation is completely described by a wave vector and further will be transformed to a scalar signal. Some information on characteristics of observed objects is thus lost. For obtaining the maximum information capacity of EM wave it is necessary to maintain its polarization properties that is reached by application of vector procedure of processing of received signals.

In general present methods of extraction of information transferred by EM wave are based on the analysis of its energy characteristics and considerably exhausted potentialities. Therefore use of information put in the polarization properties of EM wave, and in statistical parameters of its polarization characteristics gives additional opportunities for improvement of procedure of extraction of information.

Research of polarization distortions in the propagation medium of electromagnetic waves demands equipment creation for measurement of these distortions and, probably, their automatic adaptive correction. The transfer constant was chosen as the parameter which characterizes polarization properties of the propagation medium. The purpose of work is determination of transfer constant within the chosen description of polarization characteristics of EM signal.

II. VECTOR MODEL OF THE DYNAMIC SIGNAL. POLARIZATION SPECTRUM

The polarization state of EM wave and its polarization transformations are described, proceeding from a plane wave, for example [5]. The same wave is supposed at establishment of the vector model of EM signal, also this wave is supposed uniform.

Spectral components of a signal propagate in the linear propagation medium independently from each other. The behavior of a scalar wave is given by superposition of harmonious waves of infinitesimal amplitude.

$$s(z,t) = \frac{1}{2\pi}\int_{-\infty}^{\infty} S(\omega)\exp[i(\omega t - kz)]d\omega, \qquad (1)$$

where $k = \omega/c$ – the wave number, c – speed of light.

The vector model of a signal [6] assumes what it is possible to present both horizontal and vertical components of a plane electromagnetic field in the equation (1):

$$\mathbf{s}(t,z) = \mathbf{i}\frac{1}{2\pi}\int_{-\infty}^{\infty} \dot{S}_x(\omega)\exp[i(\omega t - kz)]d\omega + \\ + \mathbf{j}\frac{1}{2\pi}\int_{-\infty}^{\infty} \dot{S}_y(\omega)\exp[i(\omega t - kz)]d\omega. \qquad (2)$$

In this equation it is supposed that each pair infinitesimal spectral wave component with angular frequency ω'

$$\dot{S}_x(\omega')\exp[i(\omega' t - k'z)]d\omega', \qquad (3)$$

$$\dot{S}_y(\omega')\exp[i(\omega' t - k'z)]d\omega'$$

has the individual condition of polarization. In aggregate these components make a vector signal (2) with one or another polarization state: from complete polarization to its total absence.

Just as the scalar ratio (1) is superposition of infinitesimal scalar oscillations, expression (2) represents superposition of infinitesimal vector oscillations (1) [7].

Pair of waves (2) can be written down in the form of column vector

$$\begin{bmatrix} \dot{S}_x(\omega) \\ \dot{S}_y(\omega) \end{bmatrix} = \begin{bmatrix} |S_x(\omega)| \cdot \exp i[\varphi_x(\omega)] \\ |S_y(\omega)| \cdot \exp i[\varphi_y(\omega)] \end{bmatrix}, \quad (4)$$

which is quite similar to a column vector describing a plane monochromatic electromagnetic field, extending along the axis z [5]

$$\begin{bmatrix} \dot{E}_x \\ \dot{E}_y \end{bmatrix} = \begin{bmatrix} H \exp i\varphi_x \\ V \exp i\varphi_y \end{bmatrix} \cdot \exp[i(\omega t - kz)]. \quad (5)$$

In Eq. (5) variable in time $\dot{E}_x$ and $\dot{E}_y$ describe complex oscillations horizontal and vertical component of an electromagnetic field, values H and V – amplitudes of these oscillations, and values φ_x and φ_y – their initial phases. The column vector in the right part of Eq. (5) is called the Jones vector of monochromatic plane wave [5]. Therefore, the column vector in Eq. (4) forms a continued set of Jones vectors which is called polarization spectrum [8]:

$$\mathbf{J}(\omega) = \begin{bmatrix} \dot{S}_x(\omega) \\ \dot{S}_y(\omega) \end{bmatrix}. \quad (6)$$

Here the polarization spectrum is considered as most a general characteristic of a vector electromagnetic signal. From a polarization spectrum by the corresponding transformations it is possible to receive all other characteristics and parameters of this signal.

The Whittaker interpolation theorem defines properties of Fourier transform compact function. This theorem allows to transform continued spectral set (6) to bounded countable set

$$\{S(\omega_n)\} = \left\{ S\left(\frac{n\pi}{T}\right) \right\}, \quad (7)$$

which contains all information about spectral structure of a pulse signal. To set (7) corresponds a bounded countable set of Jones vectors [9]

$$\{\mathbf{J}(\omega_n)\} = \left\{ \begin{bmatrix} \dot{S}_x(\omega_n) \\ \dot{S}_y(\omega_n) \end{bmatrix} \right\} = \left\{ \begin{bmatrix} |S_x(\omega_n)| \cdot \exp i[\varphi_x(\omega_n)] \\ |S_y(\omega_n)| \cdot \exp i[\varphi_y(\omega_n)] \end{bmatrix} \right\}, \quad (8)$$

which forms generally stochastic collective consisting of vector, with a corresponding probability mass. The set (8) can be determinative, for example, at taking into account of Faraday effect on change of polarization characteristics of signals in the form of EM field.

Thus, polarization characteristics of any dynamic signal are described by a bounded countable set of Jones vectors, whose elements characterizes polarization state of monochromatic components, being a spectral bandwidth of signal (figure 1).

III. POLARIZATION TRANSFORMATIONS OF ELECTROMAGNETIC SIGNAL

In this work the propagation medium of EM wave is represented polarization system, by interaction of incident wave with it at the exit of system there are one or several modified plane waves [10].

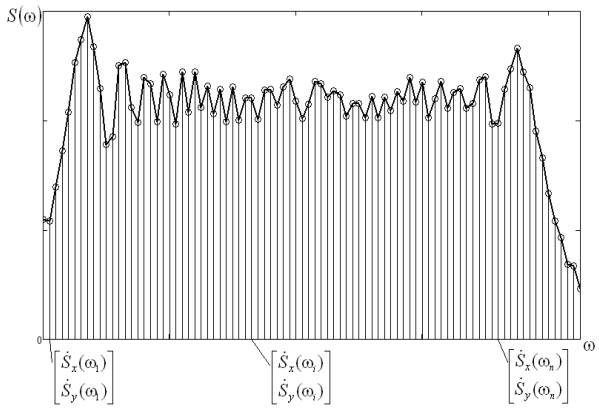

Fig. 1. Polarization spectrum of electromagnetic signal

According to Jones's method, frequency dependent polarization properties of such system 2x2 look are described by a countable set of Jones matrixes [11]:

$$\mathbf{I}(\omega) = \begin{bmatrix} I_{11}(\omega) & I_{12}(\omega) \\ I_{21}(\omega) & I_{22}(\omega) \end{bmatrix}. \quad (9)$$

If polarization state of an input signal are described by a bounded countable set of Jones vectors (6) and characteristics of polarization system are described by a bounded countable set of Jones matrixes (9), polarization characteristics of an output signal will write down in the following form:

$$\mathbf{J}_2(\omega) = \mathbf{I}(\omega) \cdot \mathbf{J}_1(\omega). \quad (10)$$

In an expanded form

$$\begin{bmatrix} \dot{S}_{2x}(\omega) \\ \dot{S}_{2y}(\omega) \end{bmatrix} = \begin{bmatrix} I_{11}(\omega) & I_{12}(\omega) \\ I_{21}(\omega) & I_{22}(\omega) \end{bmatrix} \cdot \begin{bmatrix} \dot{S}_{1x}(\omega) \\ \dot{S}_{1y}(\omega) \end{bmatrix}. \quad (11)$$

The Eq. (10) can be rewritten in the form:

$$\dot{S}_{2x}(\omega) = I_{11}(\omega) \cdot \dot{S}_{1x}(\omega) + I_{12}(\omega) \cdot \dot{S}_{1y}(\omega); \quad (12)$$

$$\dot{S}_{2y}(\omega) = I_{21}(\omega) \cdot \dot{S}_{1x}(\omega) + I_{22}(\omega) \cdot \dot{S}_{1y}(\omega). \quad (13)$$

The Eq. (2) can be presented the following expression:

$$\mathbf{s}_2(t,z) = \frac{1}{2\pi} \int_{-\infty}^{\infty} \mathbf{J}_2(\omega) \exp[i(\omega t - kz)] d\omega = \frac{1}{2\pi} \int_{-\infty}^{\infty} \mathbf{I}(\omega) \cdot \mathbf{J}_1(\omega) \exp[i(\omega t - kz)] d\omega \quad (14)$$

IV. TRANSFER CONSTANT OF THE PROPAGATION MEDIUM

At propagation of signals through the propagation medium its polarization characteristics randomly change, eventually this process affects quality of signal recept. Determination of transfer constant of the propagation medium gives its exhaustive characteristics in frequency domain.

The continued set of Jones vectors (4) contains full information about amplitudes S(ω) and absolute phases φ(ω) of spectral component of uniform plane EM wave. When the initial wave interacts with polarizing system these characteristics of EM wave change.

Application of the two-port networks theory allows to write down transfer constant of horizontal component of a plane electromagnetic field

$$\dot{K}_x(\omega) = \frac{\dot{S}_{2x}(\omega)}{\dot{S}_{1x}(\omega)}, \tag{15}$$

where $\dot{S}_{1x}(\omega)$ and $\dot{S}_{2x}(\omega)$ are spectral horizontal wave components of a signal on an input and a output two-port network.

Similarly, the transfer constant of vertical component of a plane electromagnetic field is defined as

$$\dot{K}_y(\omega) = \frac{\dot{S}_{2y}(\omega)}{\dot{S}_{1y}(\omega)}, \tag{16}$$

where $\dot{S}_{1y}(\omega)$ and $\dot{S}_{2y}(\omega)$ are spectral vertical wave components of a signal on an input and a output two-port network.

Eq. (12) and Eq. (13) allow to transform Eq. (14) and Eq. (15) to the following forms:

$$\dot{K}_x(\omega) = I_{11}(\omega) + I_{12}(\omega)\frac{\dot{S}_{1y}(\omega)}{\dot{S}_{1x}(\omega)}, \tag{17}$$

$$\dot{K}_y(\omega) = I_{22}(\omega) + I_{21}(\omega)\cdot\frac{\dot{S}_{1x}(\omega)}{\dot{S}_{1y}(\omega)}. \tag{18}$$

If polarization spectrum of input signal and transfer constants of vertical and horizontal spectral components of the signal which has passed through the propagation medium are known, it is possible to define an output signal:

$$\mathbf{s}_2(t,z) = \mathbf{i}\frac{1}{2\pi}\int_{-\infty}^{\infty}\left[\begin{array}{l}\dot{S}_{1x}(\omega)\dot{K}_x(\omega)\times\\ \times\exp[i(\omega t - kz)]\end{array}\right]d\omega + \\ + \mathbf{j}\frac{1}{2\pi}\int_{-\infty}^{\infty}\left[\begin{array}{l}\dot{S}_{1y}(\omega)\dot{K}_y(\omega)\times\\ \times\exp[i(\omega t - kz)]\end{array}\right]d\omega. \tag{19}$$

Determination of transfer constants of the propagation medium by means of the description of polarization characteristics of EM wave Jones's method will allow to solve a problem of correction of brought polarization distortions of a transmitted signal.

V. CONCLUSION

Researches of polarization transformations of signals leaned on vector model of a signal, polarization spectrum and the Jones matrixes defining polarization properties of the propagation medium of the electromagnetic wave. In general elements of these matrixes are complex functions of frequency.

Research of polarization distortions in the propagation medium of electromagnetic waves demands equipment creation for measurement of these distortions and, probably, their automatic adaptive correction. As parameters which characterize polarization properties of the propagation medium transfer were defined transfer constants of vertical and horizontal spectral components of the transmitted signal.

VI. REFERENCES

[1] Тарасенко, Ф. П. Введение в курс теории информации / Ф. П. Тарасенко. Томск: Изд-во Томского ун-та. 1963. 240 с.

[2] Шеннон, К. Теория информации. В кн.:Работы по теории информации и кибернетике / К. Шеннон, пер. с англ. М.: ИИЛ. 1983. С. 243-666.

[3] Френкс, Л. Теория сигналов / Л. Френкс, пер. с англ. М.: Советское радио. 1974. 344 с.

[4] Фано, Р. Теория информации. Статистическая теория связи / Р. Фано, пер. с англ. М.: Мир. 1965. 437 с.

[5] Джеррард, А., Берч Дж.М. Введение с матричную оптику / Джеррард А., Берч Дж.М., пер. с англ. М.: Мир. 1978. 341 с.

[6] Москалец, О. Д. Модель сигнала при обработке векторных стохастических полей / О. Д. Москалец // Всесоюзная конференция по статистическим методам обработки данных дистанционного зондирования окружающей среды. Рига, 1986. С. 54.

[7] Вершинина, А.С. Поляризационные преобразования зондирующих и отраженных сигналов радиочастотной идентификации / А. С. Вершинина, С. В. Кулаков, О. Д. Москалец // Информационно-управляющие системы.-2013.-№2.- С. 2-6.

[8] Vershinina A. Polarization transformation of spectral characteristics of the outgoing and echo radio frequency identification signals /A. Vershinina// XIV International Forum «Modern information society formation - problems, perspectives, innovation approaches»: Proceeding of the Forum. St. Petersburg, 2–6 June/ SUAI, SPb., 2013.– p. 75-78.

[9] O.D. Moskaletz, A.S. Vershinina Mathematical model of polarization spectrum of the outgoing and echo radio signals of radio frequency identification systems /O.D. Moskaletz, A.S. Vershinina// XV International Conference «Wave electronics and its applications in the information and telecommunication systems». Preliminary program and abstracts, Saint-Petersburg, 05 –10 September, 2012. – p. 49.

[10] Козлов, А.И. Поляризация радиоволн. Поляризационная структура радиолокационных сигналов / А.И. Козлов, А.И. Логвин, В.А. Сарычев.М.: Радиотехника, 2005. – 704 с.

[11] O.D. Moskaletz, A.S. Vershinina Polarization transformations of pulse electromagnetic signals/O.D. Moskaletz, A.S. Vershinina// XVI International Conference «Wave electronics and its applications in the information and telecommunication systems». Preliminary program and abstracts, Saint-Petersburg, 2–6 June, 2013.

COTENTS

The scientific edition

ФОРМИРОВАНИЕ СОВРЕМЕННОГО ИНФОРМАЦИОННОГО ОБЩЕСТВА – ПРОБЛЕМЫ, ПЕРСПЕКТИВЫ, ИННОВАЦИОННЫЕ ПОДХОДЫ

XV Международный форум
1 – 5 июня 2014 года

MODERN INFORMATION SOCIETY FORMATION – PROBLEMS, PERSPECTIVES, INNOVATION APPROACHES

XV INTERNATIONAL FORUM
1 – 5 June, 2014

PROCEEDINGS OF THE FORUM
Volume 3

Computer imposition *V. N. Sokolova*
Papers are published in author's edition

Сдано в набор 14.04.14. Подписано к печати 26.04.14. Формат 60×84 1/8.
Бумага офсетная. Усл. печ. л. 8,37. Тираж 150 экз. Заказ № 192.

Редакционно-издательский центр ГУАП
190000, Санкт-Петербург, Б. Морская ул., 67

Department of operative polygraphy
SUAI
190000, St. Petersburg, st. B. Morskaya, 67